UNCLASSIFIED

AD 424413

DEFENSE DOCUMENTATION CENTER

FOR

SCIENTIFIC AND TECHNICAL INFORMATION

CAMERON STATION, ALEXANDRIA, VIRGINIA

UNCLASSIFIED

NOTICE: When government or other drawings, specifications or other data are used for any purpose other than in connection with a definitely related government procurement operation, the U. S. Government thereby incurs no responsibility, nor any obligation whatsoever; and the fact that the Government may have formulated, furnished, or in any way supplied the said drawings, specifications, or other data is not to be regarded by implication or otherwise as in any manner licensing the holder or any other person or corporation, or conveying any rights or permission to manufacture, use or sell any patented invention that may in any way be related thereto.

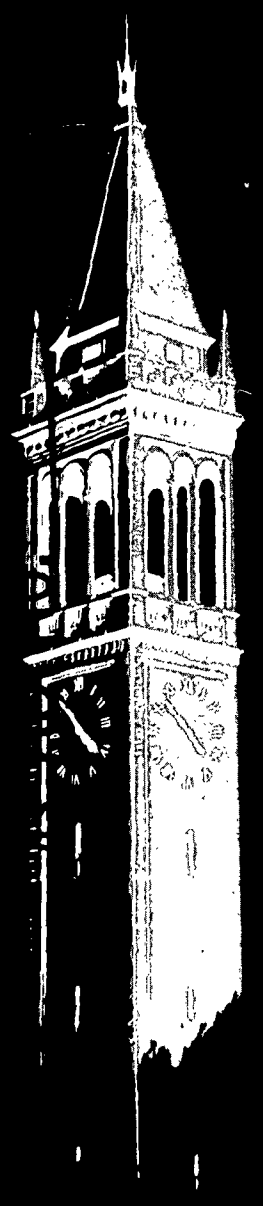

Electron Beam in the Cold-Cathode Magnetron

by

M. Chamran

Series No. 60, Issue No. 453

Contract No. AF 19(628)–324

June 15, 1962

ELECTRONICS RESEARCH LABORATORY

UNIVERSITY OF CALIFORNIA

BERKELEY, CALIFORNIA

Requests for additional copies by Agencies of the Department of Defense, their contractors, and other Government agencies should be directed to the:

DEFENSE DOCUMENTATION CENTER (DDC)
Arlington Hall Station
Arlington 12, Virginia

Department of Defense contractors must be established for DDC services or have their 'need-to-know' certified by the cognizant military agency of their project or contract.

All other persons and organizations should apply to the:

U.S. DEPARTMENT OF COMMERCE
OFFICE OF TECHNICAL SERVICES
WASHINGTON 25, D.C.

AFCRL-63-396

Electronics Research Laboratory
University of California
Berkeley, California

ELECTRON BEAM IN THE COLD-CATHODE MAGNETRON

by

M. Chamran

Institute of Engineering Research
Series No. 60, Issue No. 453

Contract No. AF 19(628)-324
Project No. 5634
Task No. 563402

Scientific Report No. 18

June 15, 1962

Prepared for
Air Force Cambridge Research Laboratories
Office of Aerospace Research
United States Air Force
Bedford, Massachusetts

ACKNOWLEDGMENTS

The author wishes to express his profound gratitude to Professor D. H. Sloan for his guidance and help, to Dr. Y. Ikeda and Dr. C. W. Hartman for their many valuable suggestions and helpful discussions, to Professor J. R. Woodyard and Professor W. B. Kunkel for their many corrections and valuable suggestions, and to Mr. O. B. Westwick for his technical assistance.

SUMMARY

The cold-cathode magnetron with various cathode materials is examined. The kinetic energy of electrons in the direction of the magnetic field is found. The anode current and cathode back bombardment are formulated on the basis of statistical mechanics. Noise and bunching are studied. It is shown here for the first time that the space charge starts to bunch most easily when the length of a useful bunch is equal to the distance between cathode and anode in both smooth-anode magnetrons and in magnetrons with a slow-wave rf anode structure. Several rf anode configurations are discussed, and the results are given. It is found why the easiest starting configuration has the wavelength of the slow-wave structure equal to double the spacing between cathode and anode, and why the minimum starting value of magnetic field makes the cyclotron frequency equal to double the frequency of the slow-wave structure, when a specific energy of back bombardment is demanded by the cold-cathode secondary emitter.

TABLE OF CONTENTS

		Page
I.	INTRODUCTION	1
	A. Statement of the Problem	1
	B. Historical Background	6
	C. Brillouin's Magnetron Theory	8
	D. Space-Charge-Distribution Results of Reverdin	10
	E. Space-Charge Distributions Obtained by Nedderman	13
	F. Statistical Approach to the Space-Charge Distribution	15
	G. Slipping-Stream Oscillations	17
	H. Space-Charge Distributions Obtained by Mathias	20
	J. Circulating-Current Measurement	23
	K. Anode-Current Measurement	25
	L. Conclusion	27
II.	SMOOTH-ANODE, COLD-CATHODE MAGNETRON	31
	A. Introduction	31
	B. Magnetron Assembly	33
	C. Electron Trajectories	36
	D. Characteristic Curves of the Cold-Cathode Magnetron	40
	E. Short Anodes	44
	F. Stainless-Steel and Graphite Cathodes	52
	G. Measurement of Voltage in Longitudinal Plasma Oscillators	56
	H. Cathode Surface	69

Page

III. DIFFUSION APPROACH TO MAGNETRON PROBLEMS 71

A. Introduction 71

B. Space-Charge Distribution 71

C. Anode Current 76

D. Circulating Current 80

E. Cathode Back Bombardment 82

IV. NOISE AND TURBULENCE 83

A. Introduction 83

B. End-to-End Oscillation 84

C. Relaxation Oscillation 84

D. Circumferential Oscillation 85

E. Cyclotron Frequency 88

F. Oscillation Due to the Space-Charge Current 88

G. Periodicity of Electron Bunch: Cyclotron Synchronism . . 89

H. Oscillations Due to the Presence of Ions 91

J. Slipping-Stream Oscillation 99

K. Plasma Oscillation 100

L. Minimum Starting Voltage and Cross-Field Space Charge . . 101

M. Bunch Size when Only a Limited Number of Electrons Are Available from Gas 105

V. RF STRUCTURES 107

A. Introduction 107

B. The 150-Mc Rf Anode 109

C. Variation of Efficiency with Magnetic Field 113

D. The 150-Mc Tube Used as a Probe 115

Page

V. RF STRUCTURES (Cont.)

E. The 105-Mc Rf Anode 116

F. The 400-Mc Rf Anode with Copper Cathode 118

G. The 400-Mc Anode with Magnesium Cathode 123

H. The 400-Mc Anode with Aluminum Cathode 125

J. The 160-Mc Anode with Aluminum Cathode 128

K. The 1240-Mc Anode 130

L. The 1160-Mc Anode with Aluminum Cathode 133

M. Space-Charge Bunching in Smooth and Rf Anodes 136

VI. CONCLUSIONS 145

REFERENCES 147

LIST OF ILLUSTRATIONS

Figure		Page
1.	Brillouin's Results: Space Charge ρ_0, Electric Field E, and Potential V, as Functions of Distance	9
2.	Radial-Field Distribution: $V_a = 45$ v, $r_c = 0.0125$ cm, (a) Space-Charge-Saturated Magnetron, (b) Temperature-Limited Magnetron	11
3.	Radial-Field Distribution: $V_a = 45$ v, $r_c = 0.1$ cm (Temperature-Limited Magnetron).	11
4.	Typical Space-Charge Distributions: (1) Typical Experimental Results, (2) Results of the Hull-Brillouin Theory, and (3) Occasionally Obtained by Experiment . .	12
5.	Computed Space-Charge-Density Distribution from Nedderman's Experiments. B = 1000 gauss	14
6.	Computed Space-Charge Distribution from Nedderman's Experiments. B = 600 gauss	14
7.	Variation of Potential Across the Interaction Space Computed from the Curves of Fig. 5	15
8.	Space-Charge Distribution for Two Different Voltages (after Hok)	16
9.	Planar Magnetron: Undulation Traveling Along Brillouin Beam	18
10.	A Growth in the Stream Lines	19
11.	Space-Charge Distribution by Mathias. $r_a/r_c = 2.53$, $r_c = 1.58$ mm, H = 416 gauss, $V_a = 293$ v.	21

Figure		Page

12. Space-Charge Distribution by Mathias. $r_a/r_c = 1.96$, $r_c = 2.04$ mm, H = 416 gauss, $v_a = 258$ v 22

13. Variation of Space Charge with Anode Voltage 22

14. Circulating and Anode Current vs Anode Potential 24

15. Normalized Anode Currents (from Hartman) 28

16. Schematic Diagram of Cold-Cathode Inverted Magnetron 32

17. Vacuum Chamber (left) and Aluminum Slotted Cathode Shown Before Assembly 35

18. Cycloidal Motion of the Electrons in a Planar Magnetron Without Space Charge. 36

19. Laminar Flow of Electron Beam in a Planar Magnetron with a Full Space Charge. 39

20. Typical Cold-Cathode Characteristic Curves 41

21. Characteristic Curves for Aluminum Cathode 45

22. Dc Characteristic Curves for Aluminum Cathode 46

23. Characteristic Curves with the Magnesium Cathode 47

24. Magnesium Cathode and Smooth Copper Anode 48

25. Short Copper Anode, Watercooled 48

26. Characteristic Curves with the Magnesium Cathode and Short Anode 49

27. Characteristic Curves with the Magnesium Cathode and Short Anode. Two Cathode Buffers Are Used to Accumulate the Space Charge 51

Figure		Page

28. Characteristic Curves with the Magnesium Cathode and Short Anode. One Cathode Buffer and an Anode Extension with Three Different Lengths Are Used 53

29. Characteristic Curves with the Stainless-Steel Cathode . . . 54

30. V_a—I_a Characteristic of Graphite Cathode Vacuum Was Spoiled Because of Lack of a Fast Pump. 55

31. Schematic Diagram of the Cup, Cathode, Anode, and Three Cathode Holes 58

32. Dc V_a—I_a Characteristics for Aluminum Cathode, Long Copper Anode 60

33. Variation of Cup Current with Respect to Anode Current for Different B 60

34. Collected Current in Cup 1 Against Bias Voltage at 156 gauss for Several Anode Currents 61

35. Collected Current in Cup 1 Against Bias Voltage. (Same as Fig. 34 but on Semilogarithmic Paper.) 63

36. Collected Current in Cup 1 Against Bias Voltage, for 310 gauss 64

37. Variation of the Average Electron Voltage with Anode Current. (Data from Fig. 35.). 66

38. Variation of the Average Electron Voltage with Anode Current. (Data from Fig. 36.). 66

39. Variation of V_{av} (peak) with Magnetic Field 67

40. Calculated V_{av} of Cups 2 and 3 with Respect to Cup 1 67

Figure		Page

41. V_a—I_a Characteristic Curves for Aluminum and Magnesium Cathodes 70

42. Distributions of Space Charge, Electric Field, and Potential Between the Cathode and Anode 74

43. Space-Charge Distribution Between Cathode and Anode 74

44. Sketch of the Anode Voltage and Cup Current Variations Against Time 86

45. Photograph of the Oscilloscope Screen 87

46. Electron Motion in the "Almost-Brillouin" Flow 90

47. Electron Trajectory with Four Fluctuations 90

48. Showing the Possibility of Accumulation of Ions and the Predicted Ion Charge Ripples 91

49. Three Distinct Regions of the V_a—I_a Characteristics . . . 92

50. The Anode Voltage Oscillation in the Top Part of Region 1 . 95

51. Variation of Frequency with Pressure in Region 1 96

52. Rising and Falling of the Anode Voltage Due to the Relaxation Oscillation 97

53. V_a—I_a Characteristics and MSV 102

54. Bunches in a Smooth Anode Configuration, where $\lambda \approx d$ . . . 104

55. Bunches in a Slow-Wave Structure Anode Configuration, where $\lambda \approx 2d$ 104

56. The Important Dimensions of the 150-Mc Anode 110

57. The 150-Mc Rf Anode 111

58. Arc from the Top of the 150-Mc Anode 111

Figure		Page

59. V_a—I_a Characteristic Curves of the 150-Mc rf Anode 112

60. The Variation of E_{eff}/E_{ave} with B. 117

61. Bars of the 105-Mc Anode when Separated from the Central Pipe 118

62. Dimensions of the 105-Mc Anode 119

63. The Rf Radiation of the 105-Mc Anode with Different Magnetic Fields. 120

64. The 400-Mc Anode 121

65. Dimensions of the 400-Mc Anode 122

66. V_a—I_a Characteristic Curve of 400-Mc Anode with Magnesium Cathode 123

67. Characteristic Curves of 400-Mc Anode with the 140 Aluminum Cathode 126

68. The 160-Mc Anode 129

69. The V_a—I_a Characteristic Curves and the Length of the Arc in the 160-Mc Anode 130

70. The 1240-Mc Anode 131

71. The 1240-Mc Anode Characteristics 132

72. The Top and Bottom Parts of the 1160-Mc Cavity 134

73. The 1160-Mc Anode 134

74. The Characteristic Curves of the 1160-Mc Anode with Aluminum Cathode 135

75. Trajectories Relative to a Square 136

76. Electron Cloud in a Bunch 138

Figure		Page
77.	Slipping Stream Instability	139
78.	Bunch-Fitting Square Spaces in 1160-Mc Anode	141
79.	Bunch Spacing in 150-Mc Anode	141

List of Tables

Table		Page
1.	Minimum Starting Voltage and Magnetic Field for Four Efficient Anodes	144

I. INTRODUCTION

A. STATEMENT OF THE PROBLEM

The magnetron and its fundamental theory were based on Hull's relation[1] in 1921. Since that time, the violation of Hull's cutoff relation has become a well-established phenomenon. Before World War II, much research[2-5] was directed toward magnetrons and better understanding of the physics of magnetrons. World War II and the increasing wartime needs of radar for communication changed the channel of research mostly to empirical methods. The first high-power, pulsed, 10-cm British magnetron[27] was built in 1940 at a peak power input of several hundred kilowatts. Their success with magnetrons led investigators to different types of crossed-field tubes, such as crossed-field amplifiers, wideband amplifiers, linear crossed-field amplifiers, rotating-plasma devices, and some types of magnetically confined plasmas. Crossed-field amplifiers such as platinotrons compete with the klystron and O-type traveling-wave tubes.

In recent years many papers have been concerned with understanding the physical picture of the magnetron and valuable experiments have been conducted to investigate the important parameters inside the magnetron. Outstanding among these experiments were those of Reverdin,[9] who used "the electron optical shadow method;" Peterson,[28] who used a beam of electrons parallel to the axis of the magnetron and observed its deflection by the radial field; Mathias,[23] who used a beam of neutral molecules and observed the scattering by ionization in the cloud; and

Nedderman,[13] who used helium atoms and observed the ionization radiation. All of these measurements showed that an abrupt radial discontinuity, as predicted by the Hull-Brillouin theory, does not exist in the electron cloud and that the space charge covers almost all the interaction space. These results guided the theoreticians into new areas. Statistical mechanics was applied to formulate equations of charge density and electric fields, and to explain the experimental results.[17,18] Some electrons were observed to have higher energy than could be possible from the emission energy or the potential. Therefore, some mechanism had to be postulated to explain this excess energy and the unexpected back bombardment of the cathode. Instability of plasma seemed the most probable. Many authors[19-22,31-34] developed methods for calculating the frequencies of the instability and its rate of growth, and found valuable information. At the present time, there are many theories about magnetron problems: Hull-Brillouin cutoff relation, maximum current boundary, anode current, cathode back bombardment, excess noise, and instability in plasma. Different and sometimes opposite ideas are held by various authors about these problems. Although much progress has been made, much work remains to be done.

Work at this Laboratory has been largely devoted to cold-cathode inverted magnetrons. Much information from this Laboratory, under the guidance of Prof. D. H. Sloan, has been published by Hoag[25] and Hartman,[26] and this report is a continuation of their work.

In the present report emphasis is on the smooth anode (static magnetron), because the fundamental phenomena are almost the same in all magnetrons. Moreover, the static magnetron is much easier to treat analytically. To be sure, analysis of the smooth-anode magnetron is by no means a simple problem, either theoretically or experimentally. The cold cathode has been used because of many advantages over hot cathodes. In cold cathodes, secondary emission is an essential source of electrons. The emitting cathode surface, then, can be much larger than regular cathode surfaces. A high peak power of multimegawatt rf can be obtained, with the cathode water cooled for still higher output powers. Also the cold cathode is just a metalic cylinder. It is inexpensive to create, is easy to work with, and may be used indefinitely. The secondary-emission coefficients for pure metals are very close to unity. A thin layer of oxide (e.g., Al_2O_3 on the surface of aluminum) is enough to increase the secondary-emission coefficient by a factor of 5 or more. Therefore, to increase the life of this oxidized layer (and thus the life of the tube), it is enough to provide a small leak of oxygen or air into the tube.

The inverted magnetron was used because of the resulting ease of experimentation. The magnetic field has a small curvature near the ends of the tube, and a magnetically confined potential well is made. If the anode were outside, then all electrons would go directly to the anode and no space charge would remain in the tube. The diameter of the anode (about 15 cm) is quite large with respect to the spacing (about 1 cm) between the cathode and anode. The inversion thus does not

actually change anything, and we may consider instead a plane magnetron.

Most theories for explaining the instability and growth rely on the laminar flow of Brillouin's theory. In fact, most of them use a perturbation on the Brillouin flow to find the instability. In a cold-cathode, smooth-anode magnetron, this assumption is questionable, because the secondary-emission process requires cathode back bombardment by relatively energetic electrons, to produce secondary electrons, and emits electrons having initial velocities. These phenomena do not agree with the laminarity of the Brillouin flow.

In our system, space charge builds up by the P.I.G. (Penning Ion Gage) discharge process. Electrons may go back and forth repeatedly in the magnetic well before colliding with the neutral gas molecules and liberating more electrons. The ions formed may bombard the cathode and possibly emit some more electrons. When the space charge builds up, some type of oscillation starts. This plasma oscillation, which might be similar to the Buneman's instability, makes for some type of collective collision between electrons and space-charge fluctuation. This collision causes a random displacement of electrons toward the anode or cathode, resulting in the anode current or the cathode back bombardment. This random-walk of electrons is the basis for our statistical approach; a simple diffusion process is assumed and a linear space-charge distribution is obtained.

In the experiments a cup is placed outside a cathode aperture to collect energetic electrons. From these measurements, the temperature of electrons is calculated and consequently an empirical relationship

between electron temperature and anode current is found.

From this diffusion, expressions for the anode current and the cathode back bombardment are formulated. In the magnetron, the diffusion coefficient is found to be proportional to $1/B$, where B is the magnetic field. In comparison to the diffusion ($1/B^2$) due to collision with atoms, electrons diffuse much faster with increased B in our case. The same situation may arise in crossed-field fusion devices. In this case, the electric field due to the charge separation, in the presence of the cross magnetic field, produces a diffusion proportional to $1/B$, which shortens the containment time.

In Sec. IV, noise is analyzed and bunching is examined. The space charge forms bunches within smooth anodes <u>or</u> slow-wave structures. If λ is the wavelength of the slow-wave structure and d is the spacing between the cathode and the anode, then the best configuration is $\lambda = 2d$. And if f_s is the frequency of the slow-wave structure and f_c is the cyclotron frequency, it is believed that optimum magnetic field obtains when $f_c = 2f_s$.

In Sec. V, many rf anodes are examined and their advantages and disadvantages are discussed. One of the rf anodes, the 150-Mc slow-wave structure, works very well, and a long arc of rf power is dissipated in air. Many of the rf anodes did not work satisfactorily, because of mode problems and multipactor effects, but valuable information was obtained.

B. HISTORICAL BACKGROUND

The first basic formula of a magnetron was reported by Hull[1] in 1921. Hull's magnetron was simply a cylindrical diode immersed in a magnetic field parallel to the axis. The cathode, a thin hot filament, was the source of electrons and was surrounded by a cylindrical anode. Emitted electrons from the cathode are subject to (1) an electric force between the anode and the cathode, $\bar{F}_e = e\bar{E}$, and (2) a magnetic force due to the magnetic field $\bar{B}$, $\bar{F}_m = e(\bar{v} \times \bar{B})$, where $\bar{v}$ is the velocity of the electron. Under these forces, electron trajectory is cycloidal and the frequency of rotation is $f_c = eB/2\pi m$. With an adequate voltage V_a between the anode and the cathode, electrons start from the cathode with a very low velocity (or zero velocity) and after a cycloidal trajectory come back to the cathode. If the anode voltage is increased, the orbit diameter of the electrons may increase until the electrons strike the anode and a large anode current occurs. The voltage at which the electrons reach the anode is called the Hull cutoff voltage, and in a cylindrical geometry is given by

$$V_H = \frac{eB^2}{8m} r_a^{\,2} \left[1 - (r_c/r_a)^2\right]^2 \tag{1.1}$$

where r_a and r_c are the anode and the cathode radii, respectively. For large anode and cathode radii, where r_a and r_c are much larger than the separation between the anode and the cathode, Eq. (1.1) may be approximated by

$$V_H = \frac{eB^2}{2m} d^2 \tag{1.2}$$

where $d \equiv |r_a - r_c|$ ("planar" magnetron).

The above theory implies that, for voltages below the Hull cutoff voltage, no electron should reach the anode. But many experiments have shown the contrary.

Later on, Harvey[2] carefully investigated the anode current below the cutoff voltage and considered the space charge in the interaction space to find the equation of motion of the electrons. He tested many magnetrons under various conditions and published the results of his experiments in 1943, showing that the departure from Hull's relation is a fundamental problem.

In 1939 the first British cavity magnetron was developed and a peak power input of several hundred kilowatts was observed, at voltages below the Hull cutoff voltage.

At this time, the possibility of some type of plasma oscillation was thought of, and the existence of cathode back bombardment and noise was observed. In 1938, Linder[3] had published the result of his experiments on the effect of high-energy electron random motion on the shape of the magnetron cutoff curve. He concluded that the space charge and the electron temperature are responsible for the anode current below cutoff voltage. In another paper, Linder[4] explained that a Maxwellian velocity distribution is superimposed on the orbital velocity of the electron, causing a random motion and gain of energy by some electrons, which then bombard the cathode. But up to this time, no satisfactory explanation of these phenomena existed. In the 1940's and later on, many useful experiments and suggestive theories were developed, and some of the important papers will be discussed here.

C. BRILLOUIN'S MAGNETRON THEORY

Before Brillouin, many authors neglected space charge or magnetic field to simplify their equations, which indicate the inaccuracy of their calculations. Brillouin[5-8] considered both the space charge and the magnetic field, but to simplify his calculations, he made the following assumptions.

(a) Electrons are emitted with zero velocity from the filament, and the cathode is at zero electric field.

(b) Conditions are static, i.e., the beam velocity does not depend on time.

(c) The speeds of electrons are such that at each point in the cloud, the Lorentz force cancels the electric force and electrons remain at the same equipotentials.

In a plane magnetron, the results of Brillouin's theory are shown in Fig. 1. A constant space-charge density $\rho_0 = (\epsilon_0 m/e)\omega_c^2$ is accumulated near the cathode up to a distance $t = eE_a/m\omega_c^2$, where $\omega_c = (e/m)B$ is the cyclotron frequency. Electric field is zero at the cathode and increases linearly to the maximum value at the distance t from the cathode, and beyond that to the anode is a constant. The potential distribution is a parabola between the cathode and the distance t, and a straight line from distance t to the anode. In Brillouin's analysis, each electron in the plasma moves with a velocity of $v_d = E/B$, where E varies from zero to E_a. Therefore, v_d is zero at the cathode and is maximum at $y = t$ and beyond. The Lorentz force,

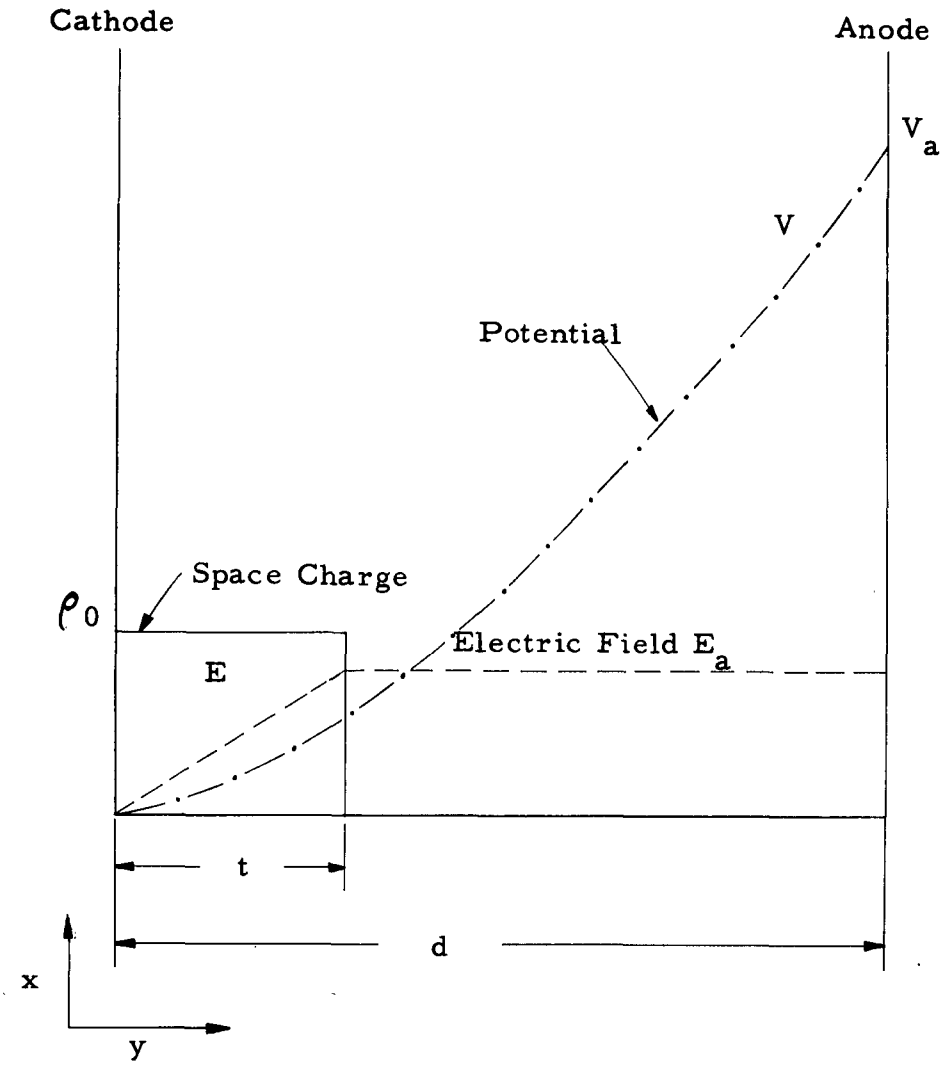

FIG. 1.—Brillouin's results: space charge ρ_0, electric field E, and potential V as functions of distance.

then, is

$$\bar{F}_m = e(\bar{E} + \bar{v}_d \times \bar{B})$$

$$= e\left(\bar{E} - \frac{\bar{E}}{B} \cdot \bar{B}\right) = 0$$

Thus, there would be no transverse force on the electrons and consequently the beam would be in a laminar-flow state. This state is a critical one, because there cannot be any electron emission and,

therefore, no anode current occurs. The important result of Brillouin's theory is the fact that the constant space-charge density ρ_0 is just that required to make the plasma frequency ω_p equal to the cyclotron frequency ω_c where $\omega_p \equiv (e\rho_0/me)^{\frac{1}{2}}$. Brillouin's theory was the first to explain magnetron operation, and though it is based on some unrealistic assumptions which are practically impossible, it still has great value and use because of its simplicity.

D. SPACE-CHARGE-DISTRIBUTION RESULTS OF REVERDIN

In 1950 Reverdin[9] published the results of his experiments for finding the electric-field and space-charge distributions. Before him Engbert[10] tried to measure the space-charge distribution directly by inserting a thin tungsten-wire probe into the magnetron. Although it is possible to measure the potential distribution by Engbert's method, the symmetry of the system may be disturbed. Reverdin's experiment was based on the optical method, called "the electron optical shadow method."[11] By this method, Reverdin found the electric-field distribution in a static cylindrical magnetron. It is worth noting that in a cylindrical situation, in the absence of space charge, the electric field E decreases as 1/r, where r is the radius of the beam. The results of Reverdin's experiments for electric-field distribution are shown in Figs. 2 and 3. Two cathodes of $r_c = 0.0125$ cm and $r_c = 0.1$ cm are used. In Fig. 2, the small-diameter cathode $r_c = 0.0125$ cm, and the anode voltage $V_a = 45$ v is used. Curve (a) is for a space-charge-saturated magnetron; curve (b) is for a temperature-limited magnetron.

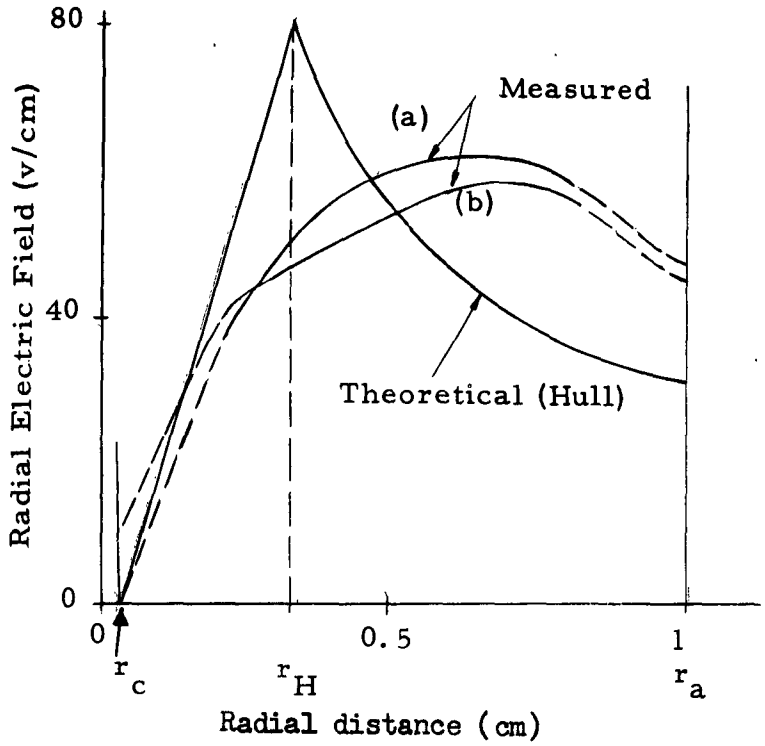

FIG. 2.—Radial-field distribution: $V_a = 45$ v, $r_c = 0.0125$ cm, (a) space-charge-saturated magnetron, (b) temperature-limited magnetron.

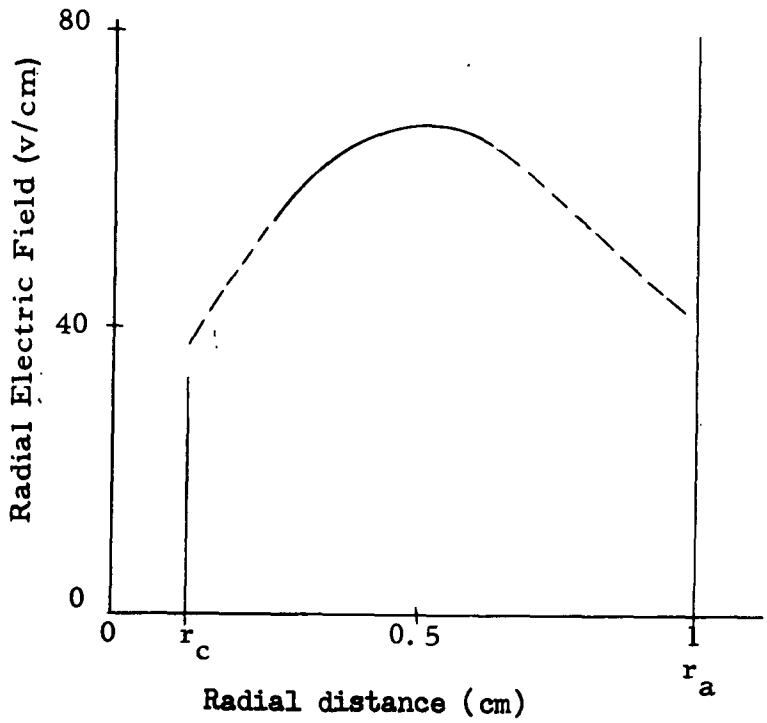

FIG. 3.—Radial-field distribution: $V_a = 45$ v, $r_c = 0.1$ cm (temperature-limited magnetron).

In Fig. 2, Hull's result for a cylindrical magnetron without space charge is drawn for comparison. In Fig. 3, the field distribution in a temperature-limited magnetron with a large cathode (r_c = 0.1 cm) is shown. Curves (a) and (b) contain measured points between r = 0.3 and r = 0.8 cm; the dotted lines are extrapolated.

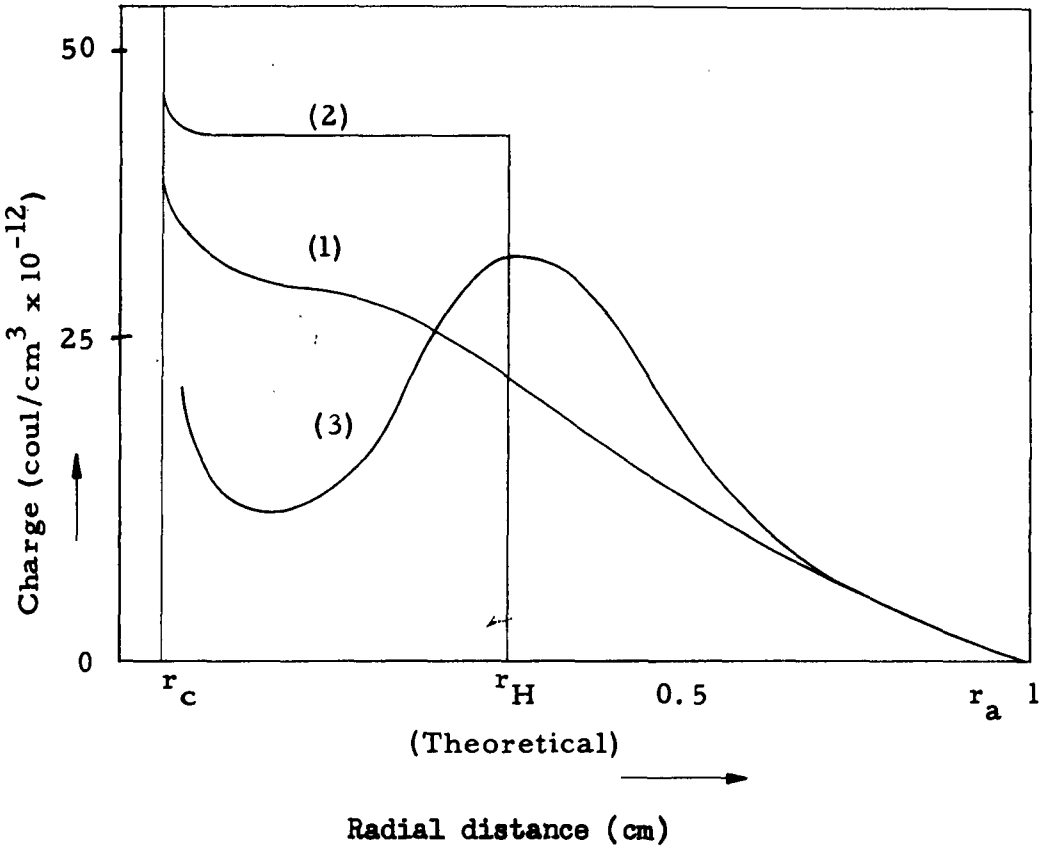

FIG. 4.—Typical space-charge distributions: (1) typical experimental results, (2) results of the Hull-Brillouin theory, and (3) occasionally obtained by experiment.

From the measured electric field, we may find the space-charge distribution. Curve (1) in Fig. 4 represents a typical space-charge-density distribution computed from the field curve in Fig. 2(a). Curve (3) in Fig. 4 is found sometimes, but is very difficult to reproduce. Because it is closer to the theoretical result of Page and Adams,[12]

it is shown here. Curve (2) in Fig. 4 represents the constant space-charge density given by the Hull and Brillouin theories. It is obvious that the charge never cuts off at Hull's radius as predicted in Brillouin's theory; rather, the charge decreases gradually to zero at the anode.

E. SPACE-CHARGE DISTRIBUTIONS OBTAINED BY NEDDERMAN

Nedderman[13] also tried to find the space-charge distribution in a static magnetron experimentally. His measurements are based on the radiation from atoms excited by electronic collisions at low pressure. The excitation cross sections are, of course, energy dependent, so that only an approximate interpretation of the experimental results directly in terms of space-charge density is possible. Furthermore, electrons below 20 ev are not detected at all. Therefore, the space-charge distribution close to the cathode is in doubt.

Figures 5 and 6 show a few curves of Nedderman's experimental results. It is obvious again that charge does not stop at the Hull radius; on the contrary, charge extends continuously from cathode to anode. The arrows in Fig. 5 indicate the edge of the cloud according to the Brillouin theory. It is thus clear that there is no connection between the Brillouin cutoff radii and the observed location of the space charge. In all cases a substantial fraction of space charge is outside the cutoff radius.

In Fig. 7, the potential distributions (from the curves of Fig. 5) are drawn. Except near the cathode, they look very realistic. The gradient at the cathode is nonzero owing to the exclusion of electrons

Curve No.	V_a	I_a
1	1500	0.200
2	1100	0.010
3	800	0.000
4	600	0.000

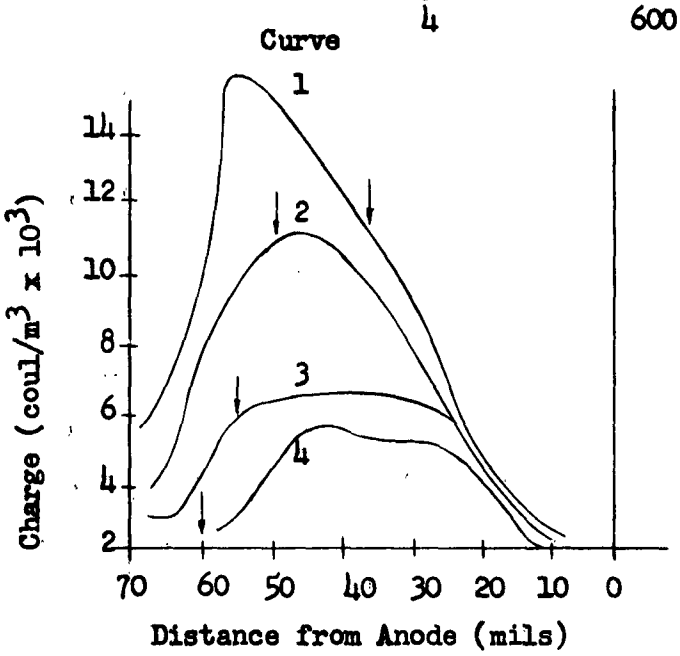

FIG. 5.—Computed space-charge-density distribution from Nedderman's experiments. Electrons with less than 20 ev are not included. b = 1000 gauss.

Curve No.	V_a	I_a
1	620	0.350
2	500	0.015
3	400	0.003
4	300	0.005

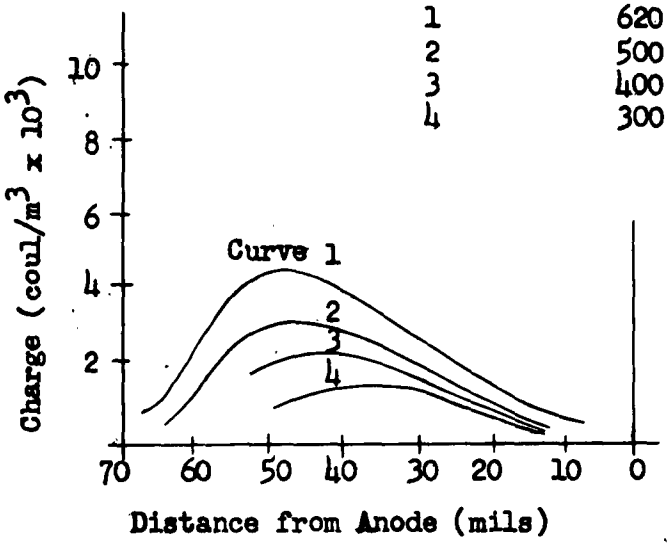

FIG. 6.—Computed space-charge distribution from Nedderman's experiments. Electrons with less than 20 ev are not included. B = 600 gauss.

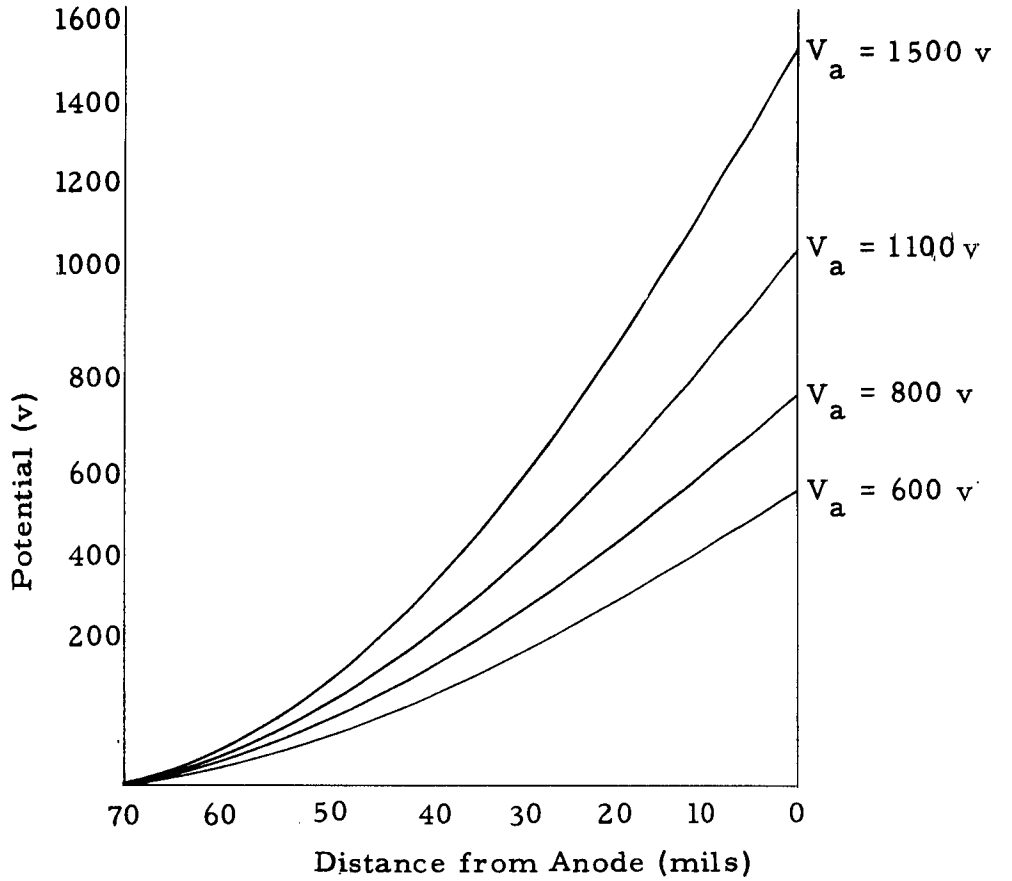

FIG. 7.—Variation of potential across the interaction space computed from the curves of Fig. 5.

of energy less than about 20 ev.

F. STATISTICAL APPROACH TO THE SPACE-CHARGE DISTRIBUTION

The results of Nedderman and Reverdin's experiments suggest the possibility of some kind of random motion in the interaction space. The electrons emitted from the cathode usually have a Maxwellian velocity distribution in all directions and the Brillouin mechanism practically never works. Somehow some electrons gain energy and diffuse across the magnetic field. These suggestions made many authors approach the problem on the basis of statistical mechanics.[14-17] Hok[17] works out carefully the statistical mechanics in the problem and considers

electron-electron scattering to find the steady drift of electrons to the anode. He emphasizes that this scattering is the cause of violation of the Hull and Brillouin theories. Hok[17] does not solve the equation of motion to find space-charge distribution, but later on[18] gives the result of his assumptions in some special cases. In Fig. 8, the space-charge distribution for two different voltages are shown.

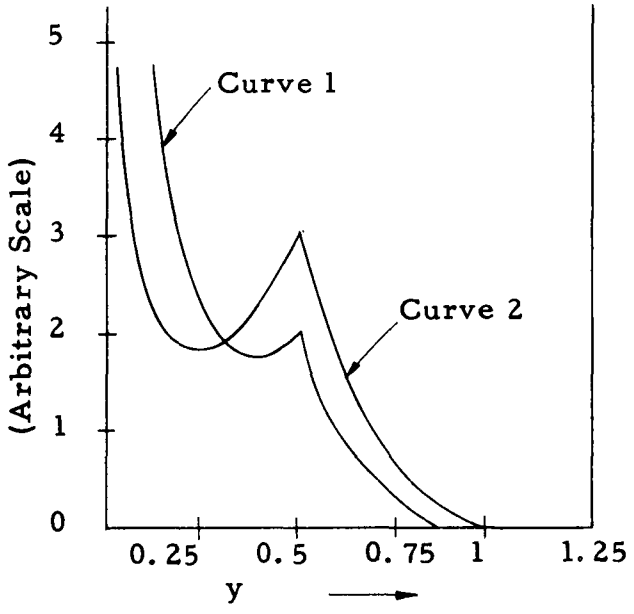

FIG. 8.—Space-charge distribution for two different voltages (after Hok, Ref. 18).

Hok's result is more realistic than Brillouin's but is still not wholly convincing, expecially as electron-electron interaction is negligible and cannot produce the experimental large anode currents.

G. SLIPPING-STREAM OSCILLATIONS

The violation of the Hull cutoff condition and of the Brillouin theory, the diffusion of electrons across the magnetic field, and the statistical approach to the magnetron problem all suggest some type of fluctuation or instability in the plasma in the interaction space. In 1948, Haeff[19] found a growth in a double stream by a perturbation method. Later on, MacFarlane and Hay[20] extended Haeff's method to a precise analytical calculation of the slipping-stream oscillations. They considered a beam in a crossed field, in which electrons move in parallel paths with a drift velocity that varies with distance transverse to the motion of electrons. Then the spectrum of frequencies that could be amplified by the slipping stream was found. Buneman[22] used the same method to develop his small-amplitude theory for the magnetron. He takes the Brillouin flow as the basis and treats the analysis as a perturbation on the Brillouin flow. He linearizes

(1) The equations of motion (Lorentz equations)

(2) Poisson's equation $\nabla^2 V = -\rho/\epsilon_0$

(3) Conservation of charge or continuity equation

$$\frac{\partial \rho}{\partial t} + \nabla \cdot (\rho \bar{v}) = 0$$

Then he assumes the rf quantities to vary like $\exp(j\omega t - j\beta x - j\gamma z)$, where β and γ are the propagation constants along x and z directions, respectively. (The coordinate system is shown in Fig. 9; the z-axis is perpendicular to the paper.) Here, ω will be allowed to acquire an imaginary part indicating growth or decay in time. For

$\lambda = 2\pi/\beta$, the wavelength of the perturbation, less than about four times the beam thickness a, ω is imaginary and we have a growth. This growth happens even in the absence of a circuit, just with a smooth anode. Thermal noise may serve as a trigger to the growth. The rate of growth depends on the wavelength λ of the perturbation. As the perturbation wavelength decreases the growth rate increases. For $\lambda \cong 3a$, the growth rate will be about $\exp(\omega_c t/20)$. The growth is shown in Fig. 10.

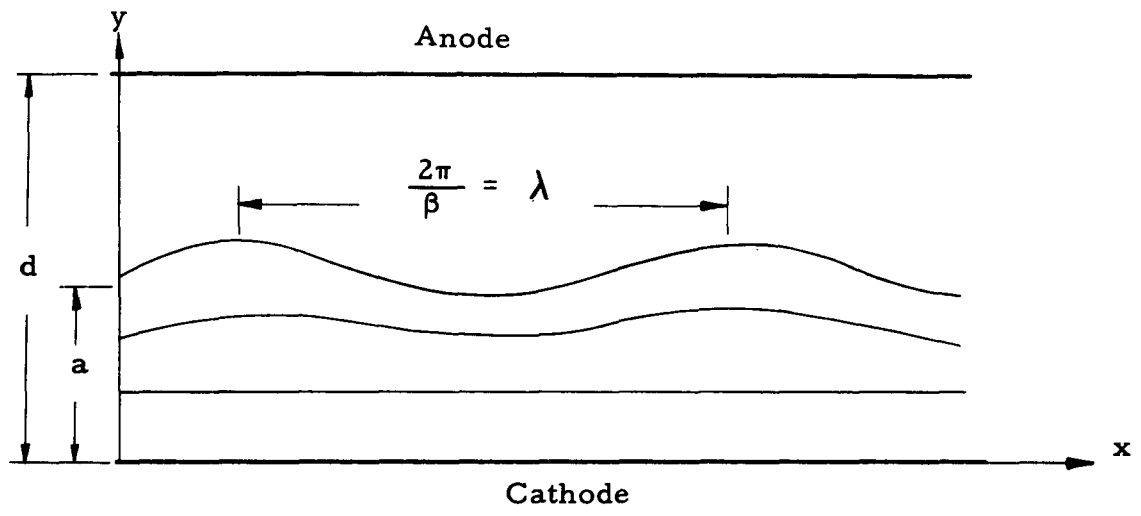

FIG. 9.—Planar magnetron: Undulation traveling along Brillouin beam.[22]

There is a stream line between the cathode and the cloud surface, at about y = a/2, which moves with the mean drift velocity $\omega_c a/s$; to an observer traveling with this stream, the cloud pattern appears stationary. The streams above this stream appear to move forward and those below it appear to move backward. Some electrons are trapped by the wave and just circulate. The growth of the beam, which is an instability, grows up to some limit where nonlinearity is reached and

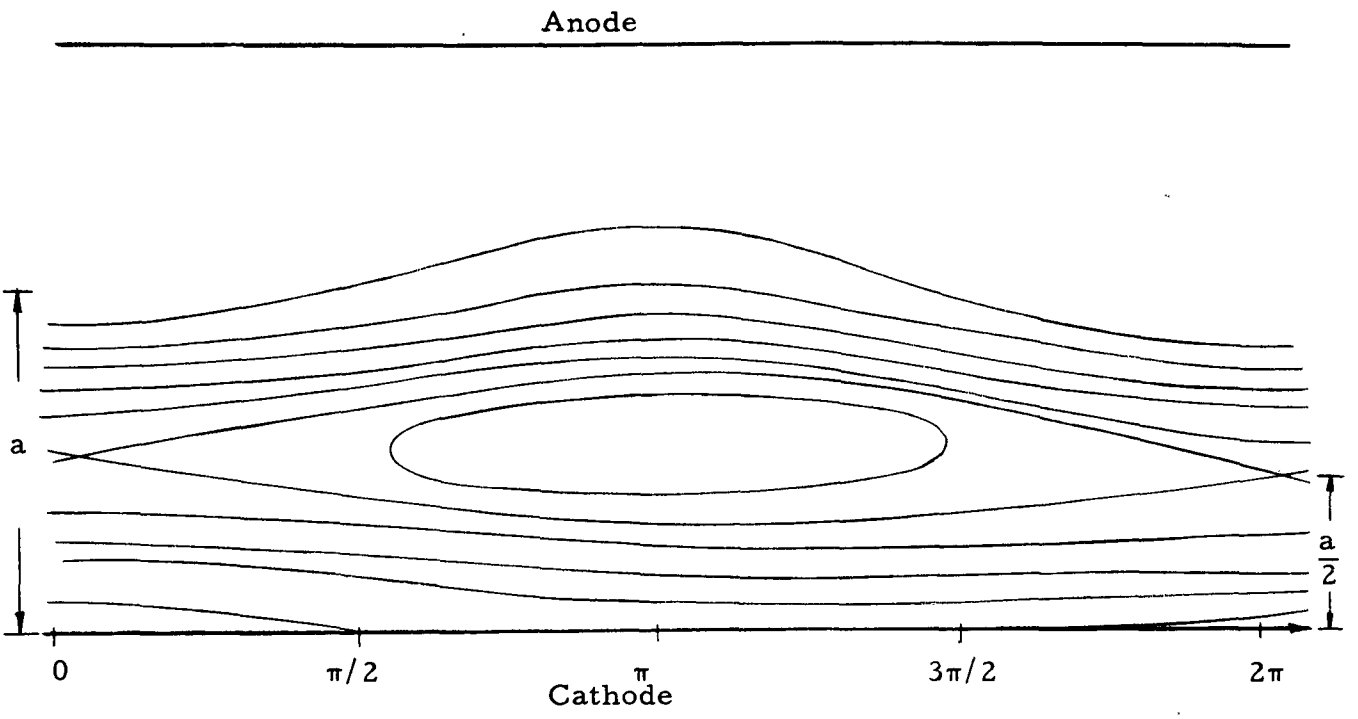

FIG. 10.—A growth in the stream lines.

the equations which led to growth do not not apply any longer. The instability causes some electrons to diffuse across the magnetic field and reach the anode; others return to the cathode. By this mechanism the problem of Hull cutoff violation is solved and the large cathode back bombardment is explained. The instability mechanism and the fluctuation of space charge result in some type of random-walk diffusion toward the anode and cathode. Statistical mechanics might be used in an attempt to calculate the anode current and the cathode back

bombardment on the basis of this instability mechanism.

H. SPACE-CHARGE DISTRIBUTIONS OBTAINED BY MATHIAS

Similar to the experiments of Reverdin and Nedderman, Mathias[23] used an experimental method to measure the space-charge density. Reverdin used electron-beam probes which, in the presence of electrostatic potential, are affected by stray and fringing electric fields. Mathias uses a molecular-beam probe to measure the average radial distribution of the space charge in a smooth-anode magnetron. This procedure gives a more direct measurement than the previous methods, and since the probe is electrically neutral, it does not affect the fields inside the magnetron. A beam of cesium bromide is sent parallel to the axis of the magnetron, through the space charge, where some of the molecules are ionized and removed from the beam by the cross electric field. The beam is collected by a detector which gives a reading proportional to the number of molecules arriving per second. Readings are taken with and without the space charge present, and the fractional decrease in the detector reading is determined. By knowing the number of ionized molecules, the cross sections of the molecules and electrons, and the drift velocity of electrons, it is possible to find the space-charge-density distribution.

The results of Mathias' experiments are shown in Figs. 11, 12, and 13. In Fig. 11, the space-charge distribution for two different voltages is given and the edge of the Brillouin cloud is marked for each voltage. In Fig. 12, the same experiment, for a different type

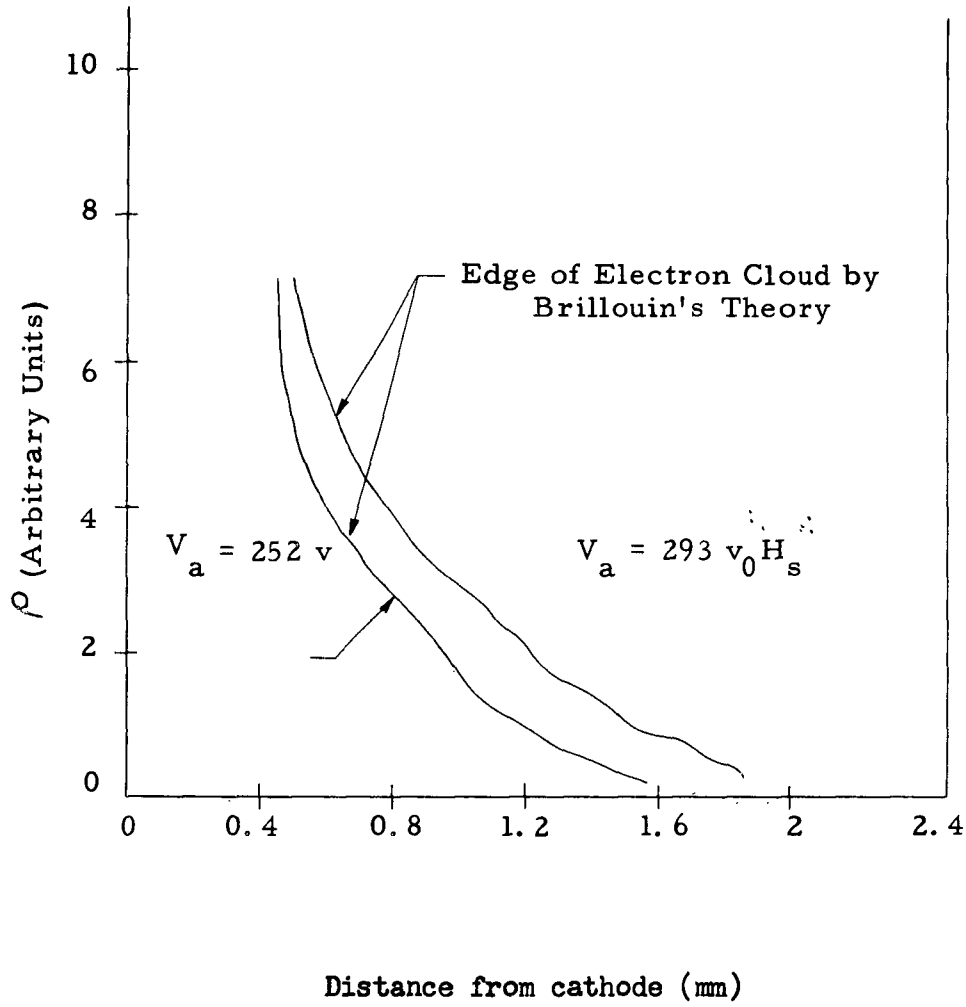

FIG. 11.—Space-charge distribution by Mathias. $r_a/r_c = 2.53$, $r_c = 1.58$ mm, $H = 416$ gauss, $V_a = 293$ v.

of magnetron, is repeated. Fig. 13 shows the increase of the space charge with respect to the increase of the anode voltage. As is clear from these results, the space-charge density does not stop at the edge of the electron cloud, calculated by Brillouin, but it covers all the interaction space and gradually goes to zero as the anode is approached.

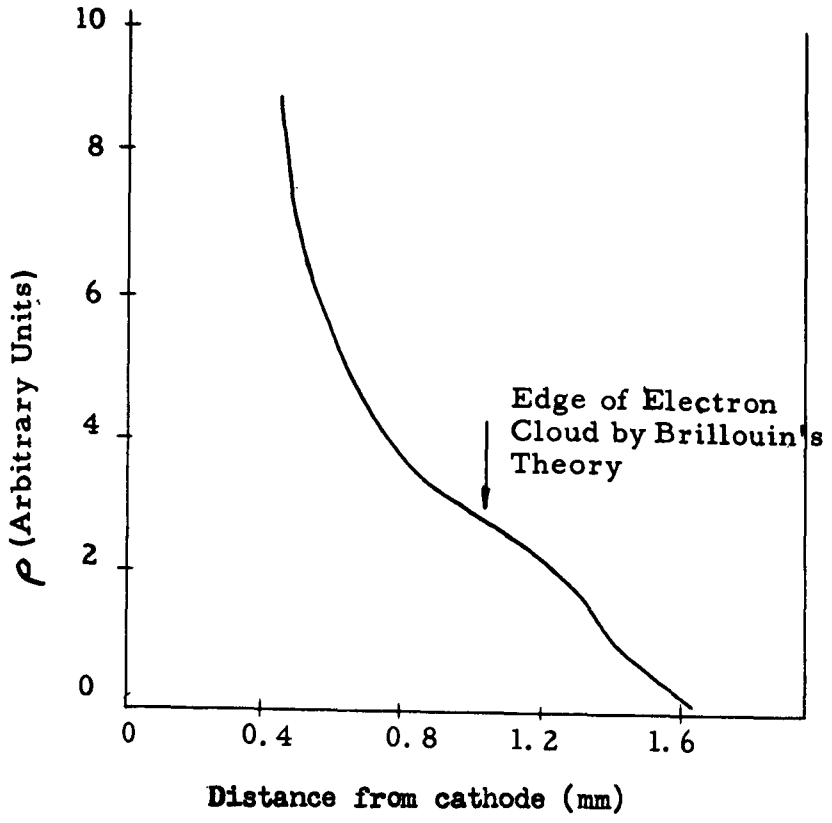

FIG. 12.—Space-Charge Distribution by Mathias. $r_a/r_c = 1.96$, $r_c = 2.04$ mm, H = 416 gauss, $V_a = 258$ v.

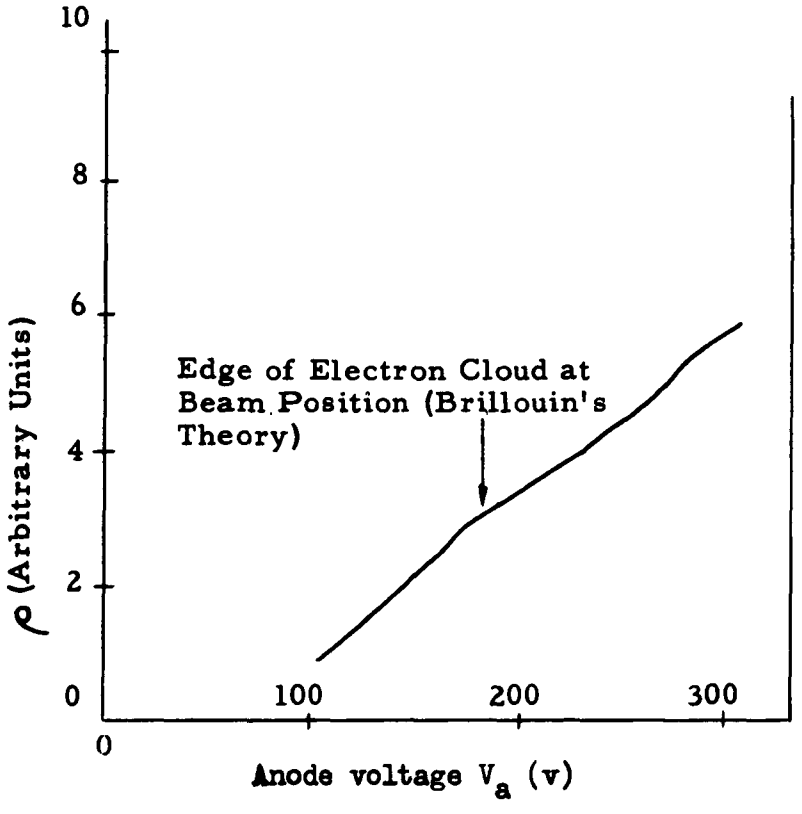

FIG. 13.—Variation of space charge with anode voltage: $r_a/r_c = 1.96$, $r_c = 2.04$ mm, H = 416 gauss, d = 0.65 mm.

J. CIRCULATING-CURRENT MEASUREMENT

Associated with the problem of space-charge distribution, the calculation of the anode current and the circulating current in a magnetron are important. The anode-current measurement and calculation will be given in the next section. Here the circulating current will be discussed. It is intuitively predictable that the circulating current is many times larger than the anode current. Lindsay[24] showed by his calculation that in a well-cutoff magnetron the circulating current may be several hundred times larger than the anode current. Thus, even slight imperfections in tube configuration may cause large contributions to the anode current from those electrons which nominally should only graze the anode.

Hoag at this Laboratory measured the circulating current by calibration of magnetic field.[25] The circulating current produces a magnetic field parallel to the axis of the anode that modifies the magnetic field of the magnetron. By measuring the changes in the total magnetic field, the circulating current is calculated. Two pick-up coils were placed on the axis of the magnetron, one at the center of the tube (where the influence of circulating current is maximum) and the other placed away from the beam but still in the main magnetic field. These coils were connected in series opposition in order to cancel out the main magnetic field but not that of the beam. A dc magnetic field and a pulsed voltage were applied. The results of the Hoag measurements are shown in Fig. 14. A smooth copper anode and an aluminum cathode with 0.87 cm spacing were used. The anode current and

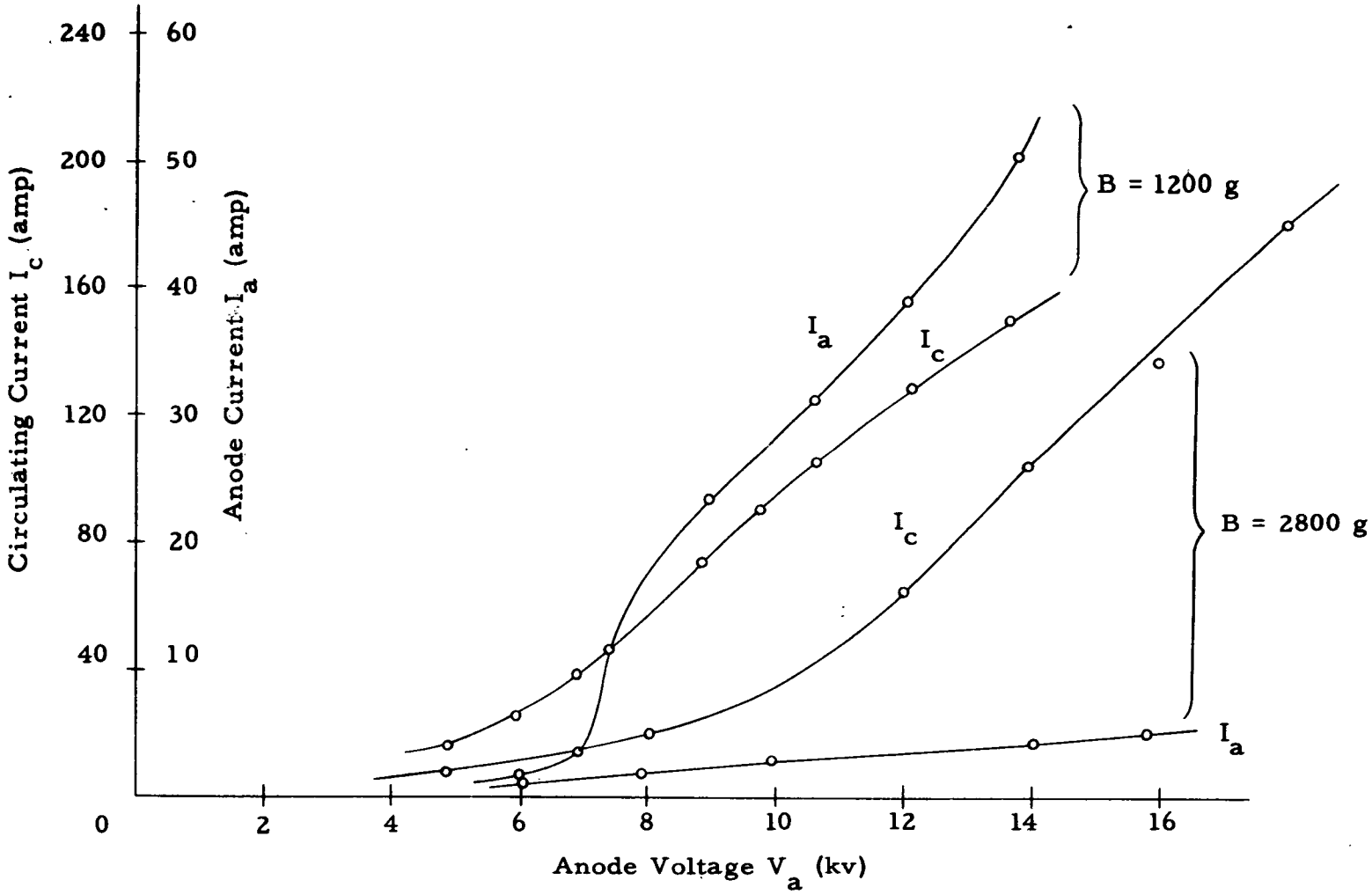

Fig. 14. Circulating and Anode Current vs. Anode potential: d = 0.87 cm. Pressure = 10^{-5} mm. of Hg.

the circulating current for two different magnetic fields are shown together. At the lower magnetic field the circulating current is about 4 times larger than the anode current. This means that an electron rotates 4 times around the anode before reaching the anode. At the higher magnetic field, the circulating current reaches 40 times larger than the anode current, i.e., an electron rotates more than 40 times around the anode before reaching it. In the case of larger spacing this ratio, of the circulating current to the anode current, may reach several hundred or more.

K. ANODE-CURRENT MEASUREMENT

The most valuable information regarding anode current has been obtained by Hartman at this Laboratory.[26] He uses Buneman's instability growth[21] as a basis for his calculation and then attacks the problem by the statistical method.

A model is assumed in which space charge accumulates near the cathode, within an electron-orbit diameter equal or proportional to $y_{max} = mE/eB^2$; the charge density in this region, as given by Brillouin, is $\rho_0 = (e\epsilon_0/m)B^2$. This laminar-flow Brillouin model is unstable and fluctuates.

The frequency or the time of this instability fluctuation is given by Buneman[22] as proportional to $\tau \approx 1/\omega_c$ where $\omega_c = (e/m)B$, the cyclotron frequency. It is assumed that after a space-charge instability each electron undergoes a collision with the space-charge bunch and then is assumed to undergo random displacements toward and away

from the anode. Each displacement is assumed to be a fraction ν of an orbit diameter y_{max}; $0 < \nu < 1$ and ν may be taken to be 1/2. If N is the number of encounters between the electron and the space-charge bunch necessary for the electron to travel the spacing or distance d (to reach the anode) by the random displacements of step size νy_{max}, then, by a simple random-walk consideration, the following relation holds:

$$d = N^{1/2}(\nu y_{max}) \tag{1.3}$$

Then

$$N \sim d^2/y_{max}{}^2 \sim d^2(B^2/E)^2$$

If n is the number of electrons per unit length near the cathode, in a layer of $y_{max} \sim E/B^2$, then

$$n \sim \rho_0 y_{max} \sim (e\epsilon_0/m)B^2(E/B^2) \sim E$$

An electron after each instability in Brillouin flow or in time $\tau \sim 1/\omega_c \sim 1/B$ makes a random displacement, and after N displacements reaches the anode; the anode current is

$$I_a \sim n/N\tau \tag{1.4}$$

Using the quantities of n, N, and τ from above we get:

$$I_a \sim \frac{E}{d^2(B^2/E)^2(1/B)} \sim (E/B)^3/d^2 \tag{1.5}$$

By using E as the average electric field $E = V_a/d$, we have

$$I_a \sim (V_a/dB)^3/d^2 = (V_a/B)^3/d^5 \tag{1.6}$$

The most important feature of Eq. (1.6) is the functional dependence of the anode current, distance, and the voltage and the magnetic

field. The (E/B) in Eq. (1.5) is the drift velocity, and it is seen that the anode current increases as cube of the drift velocity. Also it is shown that for a constant anode current, voltage and magnetic field are proportional. This equation is in good agreement with the experimental data.

Experimental results with an aluminum cathode, for various electrode spacings, and calculated values from Eq. (1.6) are plotted in Fig. 15.

L. CONCLUSION

A brief review of all papers, since 1921, shows that even for the simplest type of magnetron, the smooth anode, there is no consistent theory but rather a diversity of ideas and theories. The problems of the violation of Hull's cutoff condition, cathode back bombardment, space-charge distribution, and turbulence are the major subjects studied in plane magnetrons. There is at present no unanimity among authors about the magnetron problem. All papers may be divided into three periods of time: (1) papers before World War II, which deal mostly with static or smooth magnetrons; (2) works and research during World War II, mostly concerned with the production of high-frequency power for radar using empirical method (Collins[27] is the best product of this period); and (3) after World War II, in which the physical understanding of magnetrons is the chief concern.

The direct measurements of the space-charge distribution by Peterson,[28] Mathias,[23] Reverdin,[9] and Nedderman[13] were very valuable to guide the theoreticians into new areas. Hok[17] used a statistical method

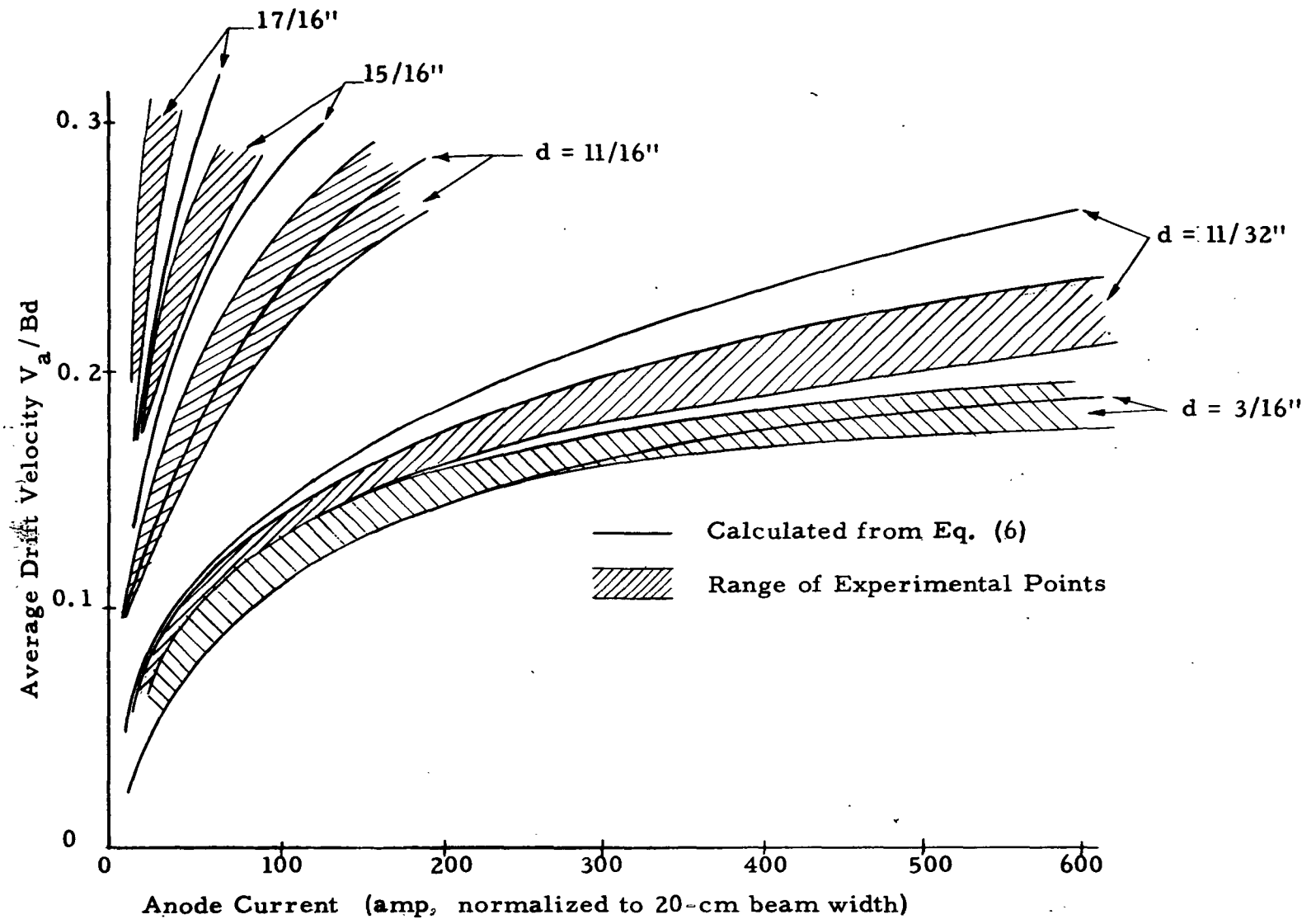

Fig. 15. -- Normalized Anode Currents (from Hartman, Ref. 26)

to prove the distribution of charge beyond the Hull-Brillouin radius. Fechner,[16] assuming a normal emission velocity for electrons, calculated the space-charge density, and found that most of the charge is located in a very thin ring of radius approximately the average of the Brillouin-Hull radius. Reverdin,[9] under some circumstances, observed a thin ring of space charge which confirmed the Fechner theory. Twiss[15,29] assumed a Maxwellian distribution of emission velocities and thoroughly calculated its effect on the steady-state situation. He found that, if the emission velocity is normal to the cathode, then a single stream exists and the space-charge distribution is close to that of Brillouin. But when a Maxwellian distribution of emission velocities is assumed, then a double stream or multistream exists, and the space-charge distribution still decreases very rapidly at a radius close to the Brillouin's radius. Lindsay[24] has also taken a Maxwellian emission-velocity distribution, and found no edge such as Brillouin's in the space-charge distribution.

Linder,[4] Harvey,[2] and the experiments at this Laboratory show that there are many electrons with much higher energy than that derived from the electric potential or initial emission velocity. A considerable number of electrons can be collected in a cage held negative with respect to the cathode. Thus a considerable portion of the electrons in the interaction space gain energy which is finally dissipated in cathode back bombardment[30] and other electrons reach the anode in violation of Hull's cutoff relation. The electron-electron collision

of Hok does not explain the gain or loss of energy by electrons. Therefore, some type of turbulence or collective collision seems necessary.

To find this turbulence or instability, MacFarlane and Hay,[20] Buneman,[21,22] Sime,[33] Gabor and Sims,[31,32] and Mourier[34] have used the perturbation method on the steady-state beam and found growth. Some of them, as Buneman, take a single stream as the basis of calculation; others, as Gabor and Sims, use the double stream as a model; but all of them work on the small-signal theory approximation which is not quite sufficient for the experiments, and the necessary large-signal calculations are still lacking. The statistical approach to the problem probably meets the practical case quite well, and it seems likely that any further attempts to formulate theories about magnetrons will be based on some sort of instability in the beam and statistical theory.

II. SMOOTH-ANODE, COLD-CATHODE MAGNETRON

A. INTRODUCTION

In the author's experiments, a smooth-bore-anode, cold-cathode, inverted magnetron was used. Slow-wave anode structures, for rf generation, are also designed and tested in this Laboratory, and will be discussed in Sec. V. Smooth-bore anodes are used usually for understanding of the essential problems of the magnetron, such as space-charge distribution, maximum current boundary, plasma instability, arcing, and relations between the anode voltage V_a, anode current I_a, magnetic field B, pressure p, and the geometrical construction.

Usually a long anode is used and, because the interaction space is long, it is difficult to make a straight parallel magnetic line throughout the volume. The configuration is such that the magnetic field diverges as it gets closer to the ends (Fig. 16). Electrons move easily along the magnetic lines and then strike the electrode at the ends. This configuration has forced us to use the outer electrode as the cathode. Still some electrons gain energy and strike the cathode at the ends and make serious problems as arcing or melting the cathode.

The inverted magnetron has been also used by others.[37] As mentioned previously, in large cathodes and smooth anodes there is not much difference between the inverted and regular magnetrons.

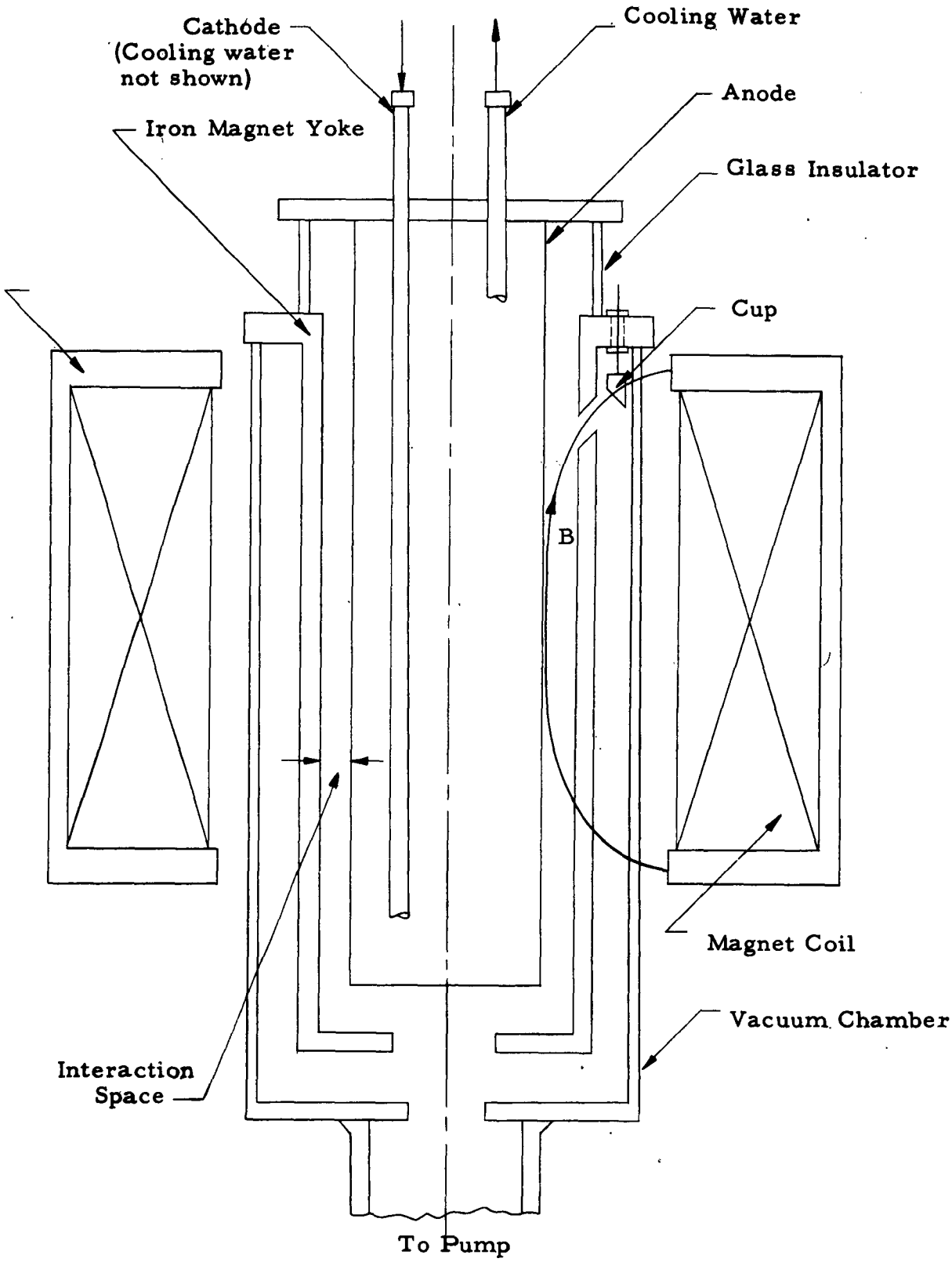

FIG. 16.—Schematic diagram of cold-cathode inverted magnetron.

Cold-cathode magnetrons also have been used previously by others.[38,39] Jepsen and Muller[30] have shown that the secondary emission is usually as much as 100 times the filament emission in regular magnetrons. This suggests the use of secondary emission as a source of electrons. For starting, an auxiliary filament or gas can be used. Cold-cathode magnetrons are important for their long life and the feasibility of large cathode surfaces.

B. MAGNETRON ASSEMBLY

The schematic diagram of the cold-cathode inverted magnetron is shown in Fig. 16. Anodes are copper pipes, watercooled, with various diameters around 5 in. Cathodes are watercooled pipes around 6 in. The spacings in different tubes range from a few millimeters to about 2.5 cm. The cathode material was especially important for secondary emission. Mostly aluminum was used, but graphite, copper, magnesium, and stainless-steel cathodes were also tried. Each material has some advantages and disadvantages. Aluminum and magnesium have high secondary-emission ratio (about 10), but for a high-velocity beam (large E/B), when the bombarding energy of electrons is large the vapor pressure of the aluminum and magnesium is so high that arcing takes place easily and stops operating. Copper and stainless steel have a lower vapor pressure and withstand a higher beam velocity, but their secondary-emission ratios are low (for copper $\delta = 1.3$).[36] The secondary-emission ratio of graphite is less than unity.[36] Graphite was used for producing a hot plasma by gas ionization, but because of

the high vapor pressure of graphite and lack of a fast pump, the experiment with graphite was not successful. Axial current in the cage is measured through a hole in the cathode (Fig. 16). For this purpose, a vacuum chamber surrounds the cathode.

The whole assembly (anode, cathode, and vacuum chamber) are centered in an iron-clad solenoid magnet which is aircooled. The dc magnetic field can be varied from zero to about 3000 gauss.

The vacuum chamber is connected to a diffusion pump and a mechanical pump, and a controlled leak is used to vary the pressure from 10^{-6} to 10^{-2} mm of Hg, with air, hydrogen, oxygen, and helium.

Usually at the beginning of operation, the cathode surface is covered by a thin film of oil from the diffusion pump. Also, in the case of aluminum and magnesium, a thin layer of oxide is necessary for a good secondary-emission ratio. Owing to the oil and the oxide layer, in the first few hours of operation, the characteristics are not reproducible and they change continuously. After a few hours of operation with an air leak, and the formation of an oxide layer, the operation is reproducible.

The high dc voltage, up to about 75 kv, is connected to the anode through a water resistance of about 5000 ohms. The water resistance is for protection in case of arcing in the tube, in order to reduce the current and to prevent any spot melting in the cathode or anode. The maximum available dc is about 10 amp. For higher currents and voltages, there are pulses available with 4-μsec pulses up to 100 amp at 80 kv and 230-μsec pulses up to 500 amp at 30 kv. The assembly is shown in Fig. 17.

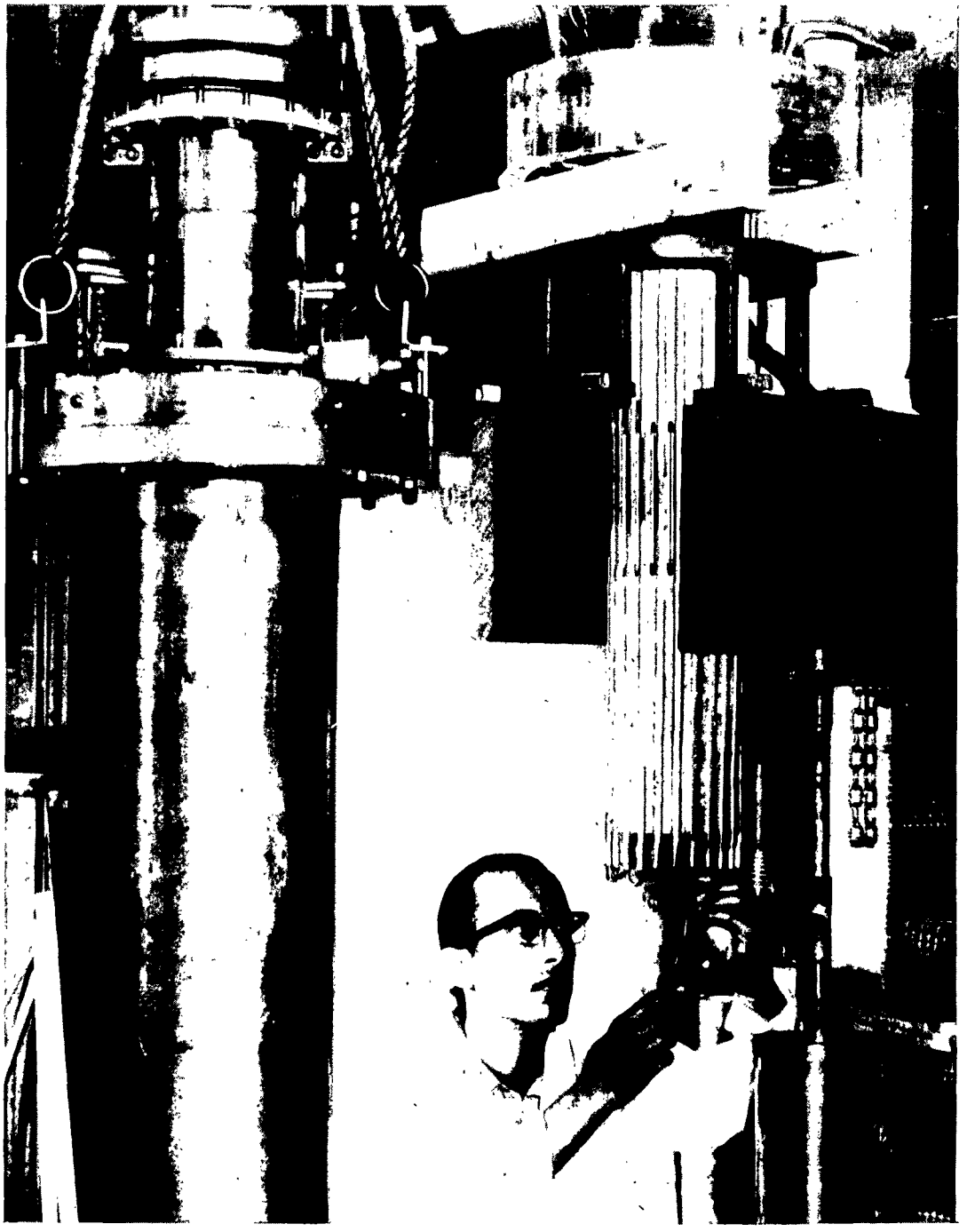

FIG. 17.—Vacuum chamber (left) and aluminum slotted cathode shown before assembly.

C. ELECTRON TRAJECTORIES

An ordinary magnetron works between two limiting cases, without space charge and fully space-charge limited.

1. ELECTRON TRAJECTORY WITHOUT SPACE CHARGE. In the magnetron configuration tested here, the spacing d is small compared to the cathode radius r_c ($r_c \approx 8d$) and it is convenient to assume that the configuration is a planar magnetron with the cathode at zero voltage and the anode at potential V_a. The schematic configuration of the magnetron and the coordinate axes are shown in Fig. 18.

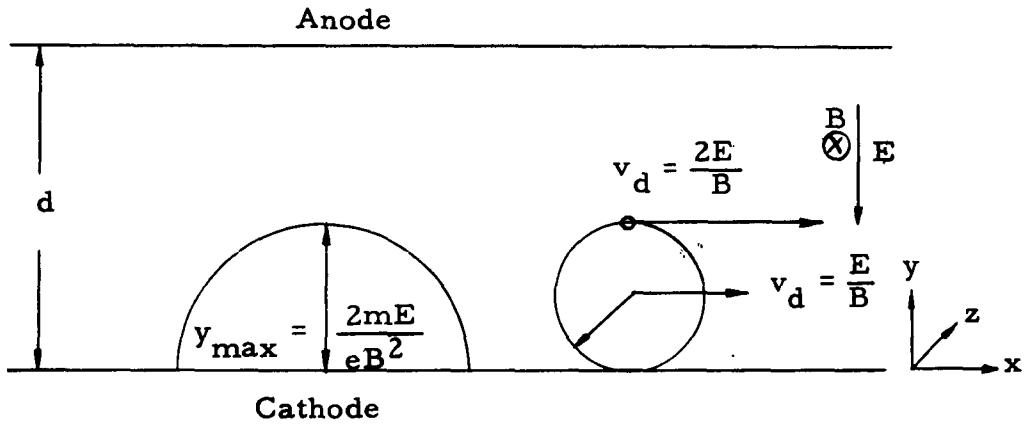

FIG.18.—Cycloidal motion of the electrons in a planar magnetron without space charge.

The electron motion is given by the differential equations

$$\ddot{y} = \frac{e}{m}(E - B\dot{x}) \tag{2.1}$$

$$\ddot{x} = \frac{e}{m} B\dot{y} \tag{2.2}$$

If we assume the electron starts from the cathode with zero initial velocity, (x, y, $\dot{y}$, and $\dot{x}$ are all zero at $t = 0$), and if we call $(e/m)B = \omega_c$ the cyclotron frequency, then Eq. (2.2) can be integrated with these boundary conditions to

$$\dot{x} = \omega_c y \tag{2.3}$$

Inserting $\dot{x}$ in Eq. (2.1) gives the oscillatory equation of electron motion in the y direction:

$$\ddot{y} + \omega_c^2 y = \frac{e}{m} E \tag{2.4}$$

The solutions of Eqs. (2.4) and (2.3) are as follows:

$$y = \frac{E}{\omega_c B}(1 - \cos \omega_c t) \tag{2.5}$$

$$x = \frac{E}{\omega_c B}(\omega_c t - \sin \omega_c t) \tag{2.6}$$

From Eq. (2.5), the maximum excursion of an electron from the cathode is

$$y_{max} = \frac{2E}{\omega_c B} = 2\,\frac{mE}{eB^2} \tag{2.7}$$

Eqs. (2.5) and (2.6) can be considered to be combined from two separate motions, (1) rotation and (2) translation, as follows:

$$\begin{aligned} y_{rot} &= \frac{-E}{\omega_c B} \cos \omega_c t \\ x_{rot} &= \frac{-E}{\omega_c B} \sin \omega_c t \end{aligned} \tag{2.8}$$

$$\begin{aligned} y_t &= \frac{E}{\omega_c B} \\ x_t &= \frac{E}{B}\, t \end{aligned} \tag{2.9}$$

From Eqs. (2.8), it is obvious that the electron rotates with frequency $f = \omega_c/2\pi$ and radius $E/\omega_c B$.

In Eqs. (2.9), it is shown that $y_t = E/\omega_c B = \text{const.}$ The point remains at a constant distance from the cathode and moves with a constant velocity $v_d = E/B$ parallel to the cathode. This velocity, which is called the drift velocity, is the average velocity of an electron in its motion. The velocity of an electron at the y_{max}, from Eqs. (2.3) and (2.7), is

$$v_{max} = \omega_c \frac{2E}{\omega_c B} = 2\frac{E}{B} \tag{2.10}$$

Then the maximum velocity is $2v_d$ and the velocity at the cathode is zero.

2. ELECTRON TRAJECTORY IN FULL SPACE CHARGE. The case of a full-space-charge configuration in a magnetron was first solved by Brillouin,[5] who considered the laminar-flow state in the magnetron. To solve the electron motion in the presence of space charge, Poisson's equation is used:

$$\nabla \cdot \bar{E} = -\frac{\rho}{\epsilon_0} \tag{2.11}$$

In the case of a plane magnetron (Fig. 18), Poisson's equation is

$$\frac{dE}{dy} = -\frac{\rho}{\epsilon_0} \tag{2.12}$$

or, in the case of zero electric field at the cathode,

$$E = -\frac{\rho}{\epsilon_0} y \tag{2.12a}$$

Then Eq. (2.1) is

$$\ddot{y} = \frac{e}{m}\left(-\frac{\rho}{\epsilon_0} y - B\dot{x}\right) \tag{2.13}$$

From Eq. (2.13), $\ddot{y} = 0$ if the following condition is satisfied:

$$\dot{x} = -\frac{\rho}{\epsilon_0 B} y \tag{2.14}$$

By equating Eqs. (2.3) and (2.14) we obtain

$$\rho = \frac{-e\,\epsilon_0}{m} B^2 = \frac{-\epsilon_0 m}{e} \omega_c^{\,2} \tag{2.15}$$

This means that, by choosing a proper value for the space charge, the acceleration in the y-direction is zero, electrons move in a laminar flow, and their drift velocities vary linearly from zero at the cathode to the maximum value at the edge of the electron beam (Eq. 2.14). This condition is shown in Fig. 19. The electric field E

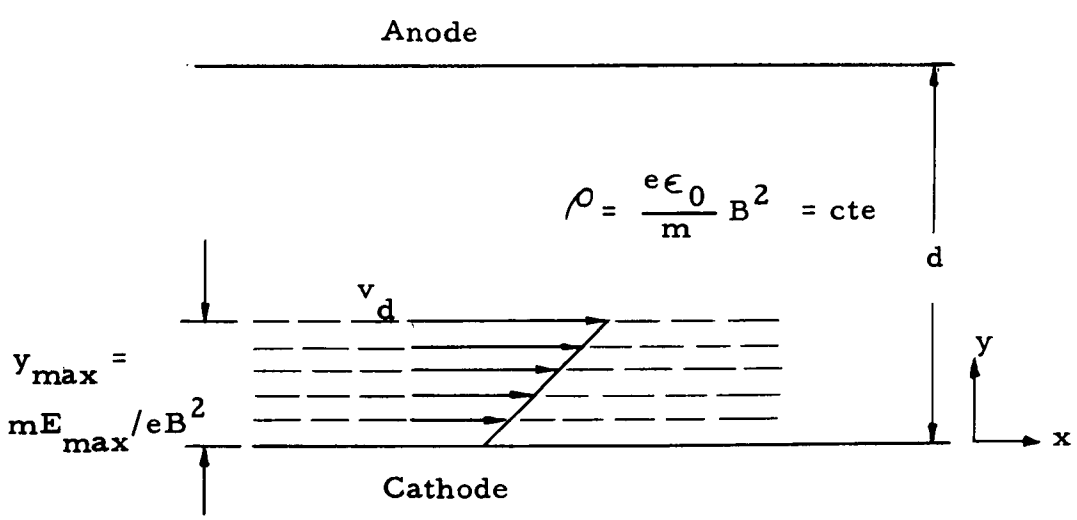

FIG. 19.—Laminar flow of electron beam in a planar magnetron with a full space charge.

also varies linearly with the distance from the cathode. From Eqs. (2.12) and (2.13), the maximum excursion of the electron beam is

$$t = y_{max} = \frac{mE_{max}}{eB^2} \tag{2.16}$$

where E_{max} is the electric field in the region free from space charge. In comparing Eqs. (2.16) and (2.17) it becomes clear that the maximum excursion of electrons in the case of no space charge is twice that of the case of full space charge, for the same E_{max}. However, with respect to the cathode the same potential exists at y_{max} in both cases.

An interesting coincidence in the case of the full space-charge state is that the plasma frequency $\omega_p = (e\rho/m\epsilon_0)^{1/2}$ is equal to the cyclotron frequency $\omega_c = (e/m)b$.

Laminar flow does not occur in the cold-cathode magnetron but it is quite useful to consider it as a limiting case.

D. CHARACTERISTIC CURVES OF THE COLD-CATHODE MAGNETRON

In this magnetron there is no emitting filament, not even an auxiliary filament. Starting is a remarkable process. The typical characteristic curves of the cold-cathode magnetron are shown in Fig. 20.

For a magnetic field of, say, 1000 gauss, the V_a—I_a curve in Fig. 20 is divided into three regions. In region 1, the voltage-current relationship is roughly linear and resembles the Penning Ion Gage (P.I.G.) discharge. There are always some free electrons in the

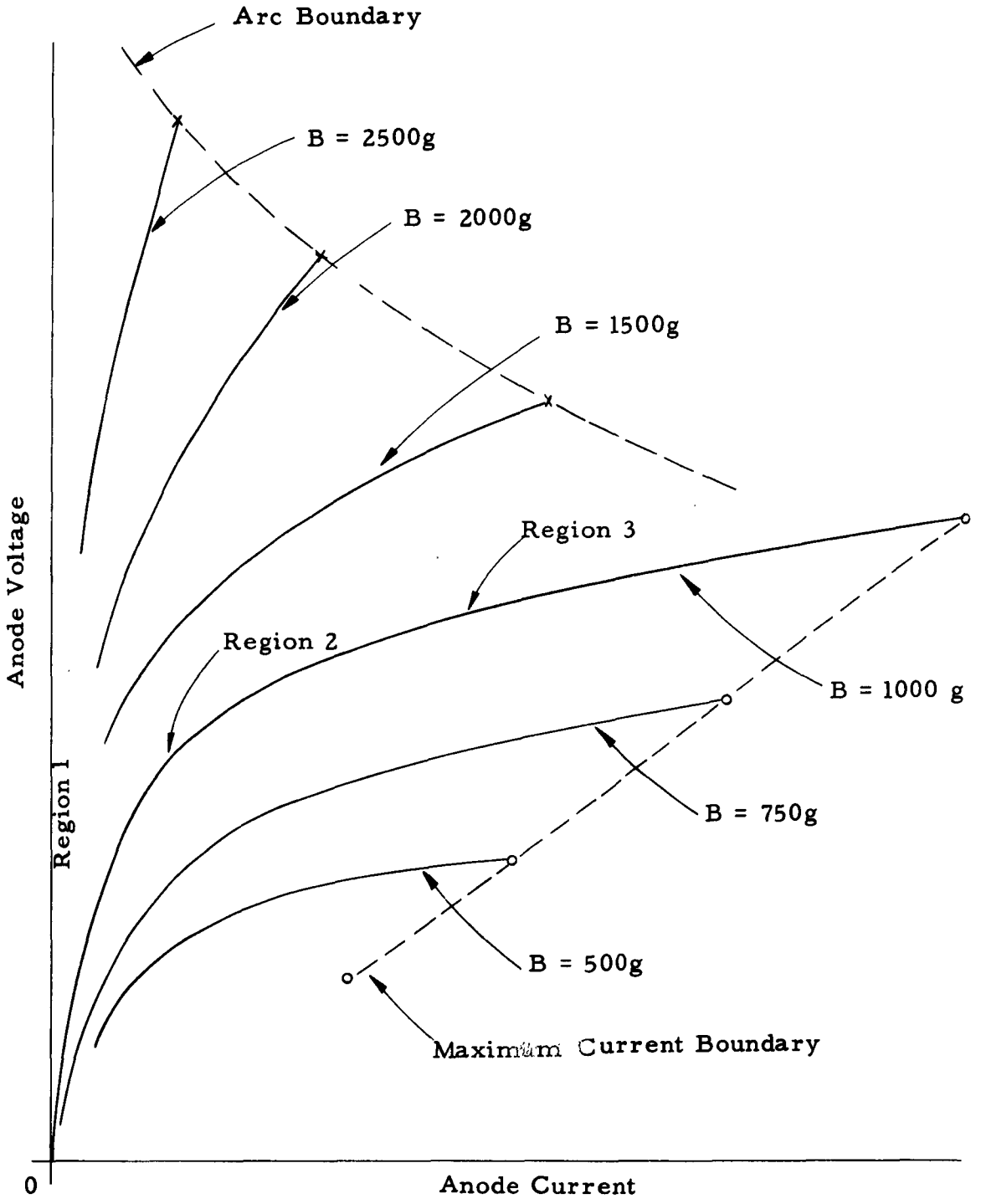

FIG. 20.—Typical cold-cathode characteristic curves.

interaction space, e.g., owing to cosmic rays, which are magnetically confined and trapped in the electrostatic potential well. These electrons move longitudinally back and forth, from one end to the other, as well as around the anode.

The collision of these electrons with gas molecules produces new electrons and ions and P.I.G. discharge occurs.[40] Because of this discharge the initial space charge builds up and the tube starts to run without any hot filament. When enough space charge is present in the tube, motion along B lines in opposite directions gives gain and oscillations, producing energetic electrons which hit the cathode at the ends, where the magnetic flux intersects with the cathode, and produce secondary emission. These excess electrons, produced by the secondary emission at the ends, generate more anode current (region 2 in Fig. 20). In region 3, the anode current is increasing rapidly, and it is assumed that this current is produced in the entire interaction area. In the upper part of this region the space charge is large enough to cause a second plasma instability.[21,22] This instability causes weak transverse turbulence in the plasma, which results in a random walk of electrons toward the anode and the cathode, which depletes the space charge and limits the turbulence.

Region 3 is reached when the transverse turbulence can be sustained strong enough to bombard the cathode with energy sufficient to release enough secondaries to increase the space charge and turbulence. This process produces more anode current and cathode back bombardment, which, in turn, produces more secondary emission. Therefore, the

anode current in region 3 increases rapidly with increasing voltage until the anode current exceeds the secondary-emission electrons, where the anode current cuts off. This cutoff point is called the maximum current boundary. The locus of these maximum current boundaries, for different magnetic fields, is almost a straight line (Fig. 20). The position and slope of the maximum current boundary is related to the secondary-emission ratio of the cathode material.[30]

As a result of the maximum current boundary, to increase the power, the magnetic field should be increased. For higher magnetic field, the tube arcs before reaching the maximum current boundary. At higher magnetic fields, it arcs at lower anode current, as shown in Fig. 20.

The reason for the arc boundary is thought to be due to the energetic back bombardment electrons which travel along B lines with greater ease when their cyclotron radii are small compared to d. This process yields a large number of secondary electrons which also travel along B lines, striking the ends and outgassing the cathode surface owing to spot heating.

At larger anode-cathode spacing d, the problem of the arc boundary is more serious, since it occurs at lower voltages and lower magnetic fields. An empirical relation Bd = constant was found, which holds cyclotron radii at a fixed fraction of d. This governs most phenomena in crossed fields. By this relationship, at larger spacing, a smaller magnetic field is required in order to operate successfully. With increased B or d the longitudinal motion of electrons from end to end is more effective, which causes high secondary emission at the

anode current in region 3 increases rapidly with increasing voltage until the anode current exceeds the secondary-emission electrons, where the anode current cuts off. This cutoff point is called the maximum current boundary. The locus of these maximum current boundaries, for different magnetic fields, is almost a straight line (Fig. 20). The position and slope of the maximum current boundary is related to the secondary-emission ratio of the cathode material.[30]

As a result of the maximum current boundary, to increase the power, the magnetic field should be increased. For higher magnetic field, the tube arcs before reaching the maximum current boundary. At higher magnetic fields, it arcs at lower anode current, as shown in Fig. 20.

The reason for the arc boundary is thought to be due to the energetic back bombardment electrons which travel along B lines with greater ease when their cyclotron radii are small compared to d. This process yields a large number of secondary electrons which also travel along B lines, striking the ends and outgassing the cathode surface owing to spot heating.

At larger anode-cathode spacing d, the problem of the arc boundary is more serious, since it occurs at lower voltages and lower magnetic fields. An empirical relation Bd = constant was found, which holds cyclotron radii at a fixed fraction of d. This governs most phenomena in crossed fields. By this relationship, at larger spacing, a smaller magnetic field is required in order to operate successfully. With increased B or d the longitudinal motion of electrons from end to end is more effective, which causes high secondary emission at the

ends and, as a result, hot spots occur at the ends.

Some experimentas results of aluminum, magnesium, copper, stainless-steel, and graphite cathodes are given in Figs. 21, 22, and 23. A photograph of the magnesium cathode electrode structure is shown in Fig. 24.

Most of the experiments were done at dc voltage, but some results of pulsed voltage are also included. In the case of pulsed voltage, usually a dc keep-alive voltage of a few kilovolts was maintaining the initial space charge in the tube. The use of pulses permits operation at much higher power before reaching the arc boundary.

E. SHORT ANODES

All the dc characteristics explained here are taken with the long anodes, unless it is indicated that the short anode is used. The short anode (Fig. 25) is important because it is of the size of the rf anodes tested at this Laboratory and will be explained later.

The characteristic curves of a long anode are different from those of a short anode (Figs. 23 and 26). To have the same anode current, the required anode voltage for a short anode (Fig. 26) is a few times larger than the required anode voltage for a long anode (Fig. 23). There is a possibility that in the case of a long anode, the edge of the magnesium cathode (12 cm diameter) is working as a new cathode with a smaller spacing (0.75 cm instead of 1.05 cm). This might be the reason for less anode voltage required. But in any

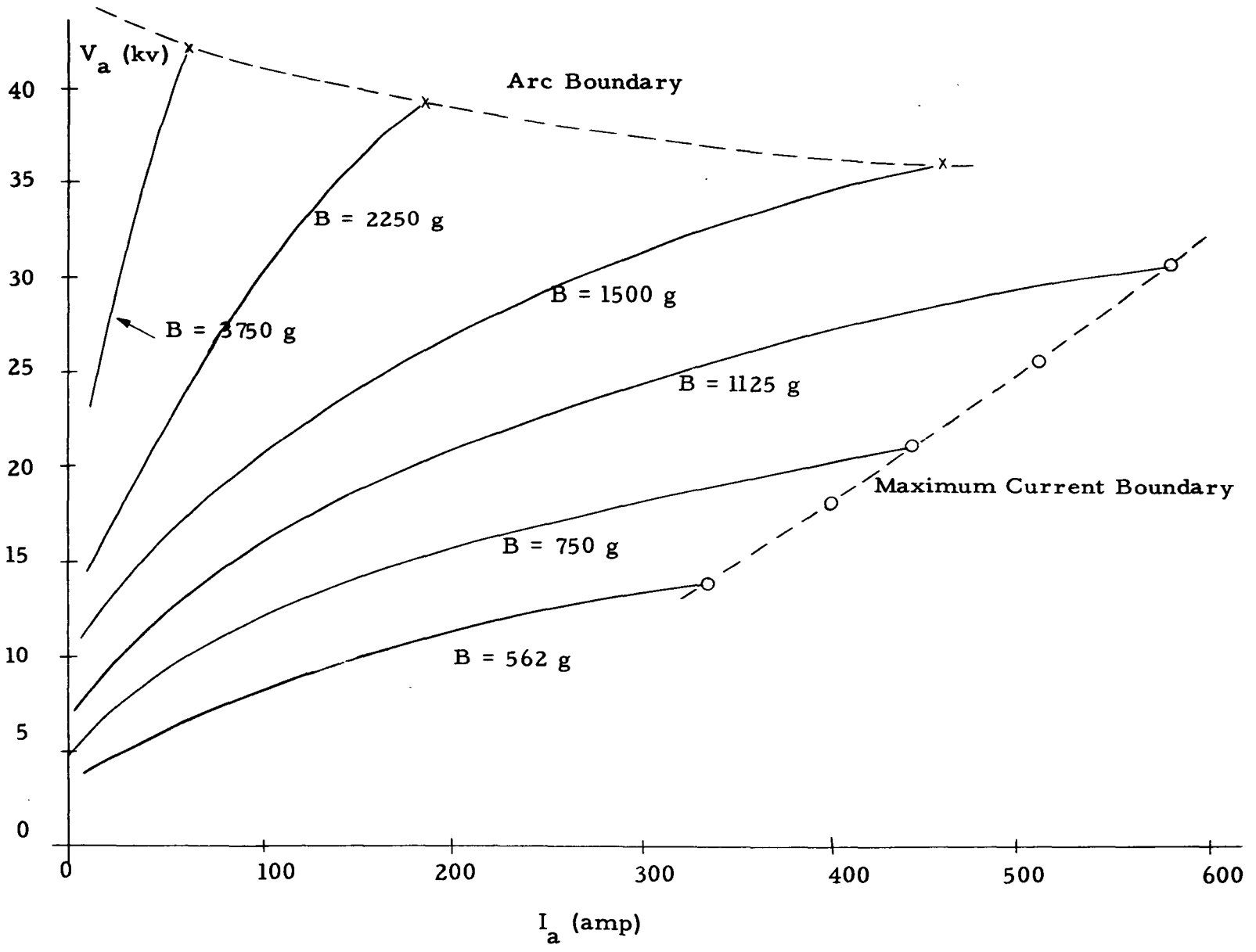

Fig. 21.-- Characteristic Curves for Aluminum Cathode: d = 0.88 cm, 4- and 230-μsec Pulses[26]

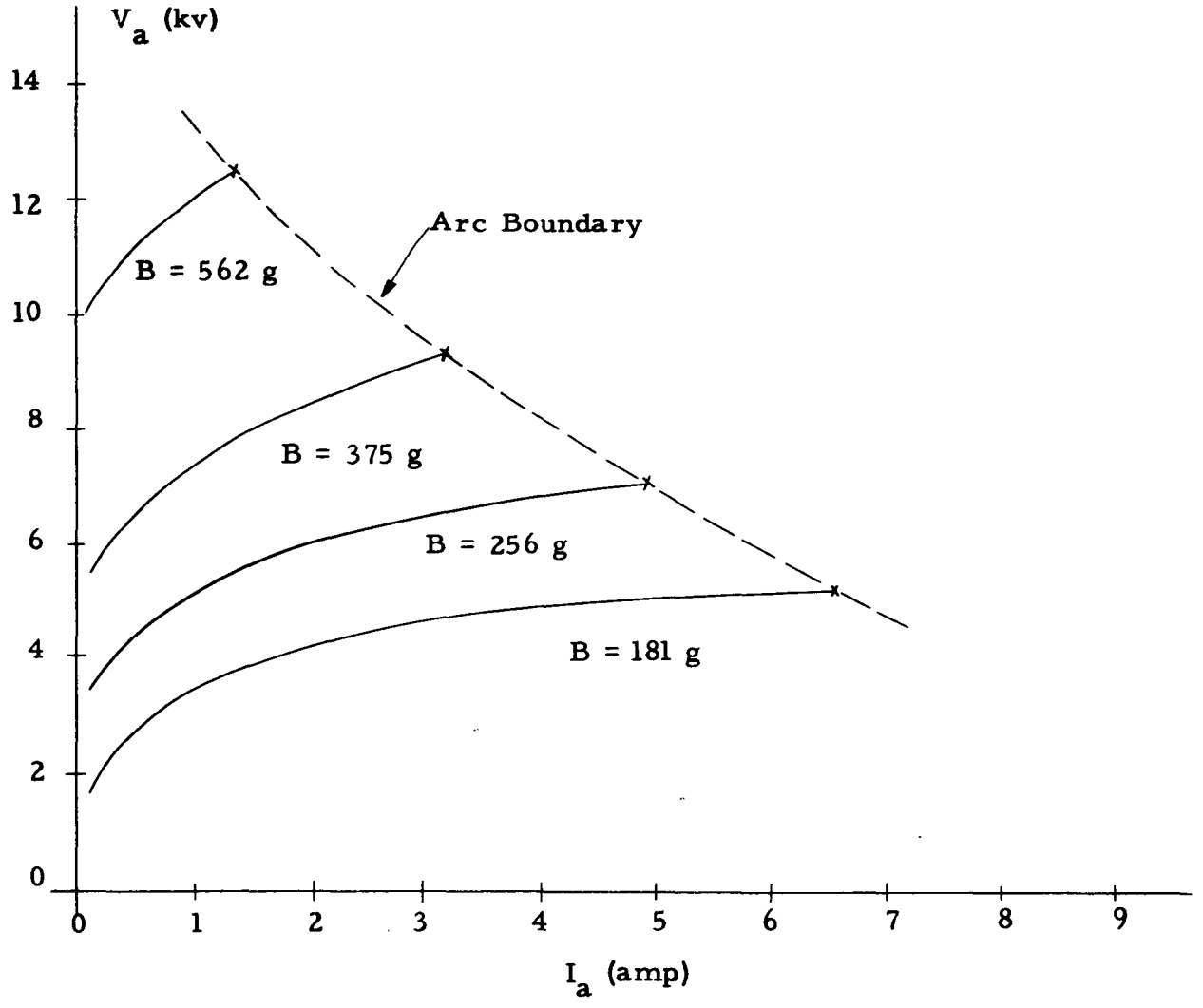

Fig. 22.-- Dc Characteristic Curves for Aluminum Cathode: d = 1.76 cm.[26]

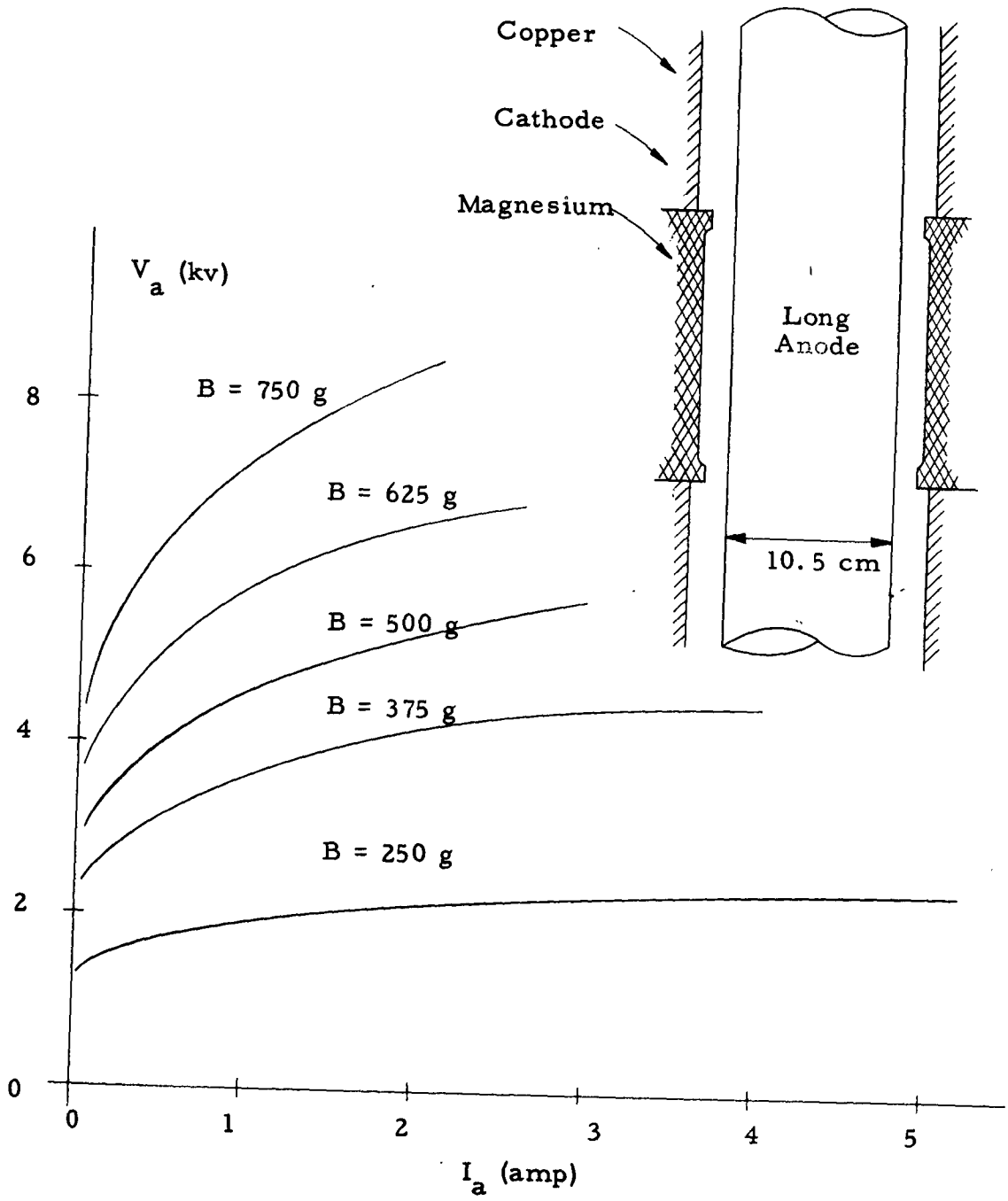

FIG. 23.—Characteristic curves with the magnesium cathode (dia. = 12.6 cm), long anode, 95.3 cm long (dia. = 10.5 cm), $p = 5 \times 10^{-5}$ mm of Hg, d = 1.05 cm.

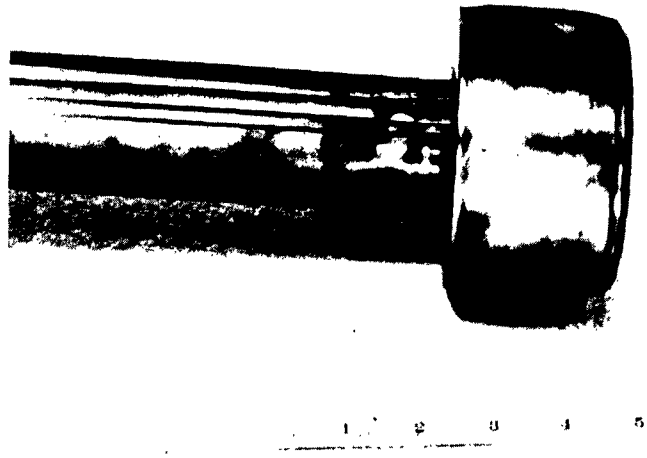

FIG. 24.—Magnesium cathode and smooth copper anode.

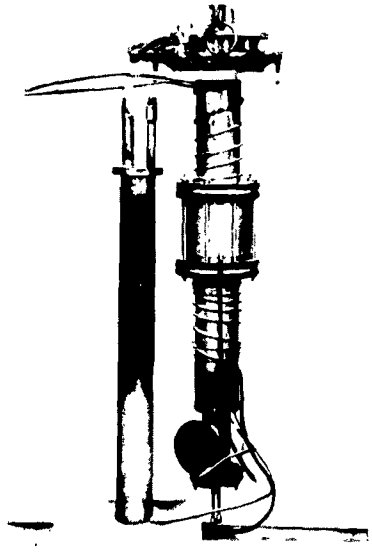

FIG. 25.—Short copper anode, watercooled.

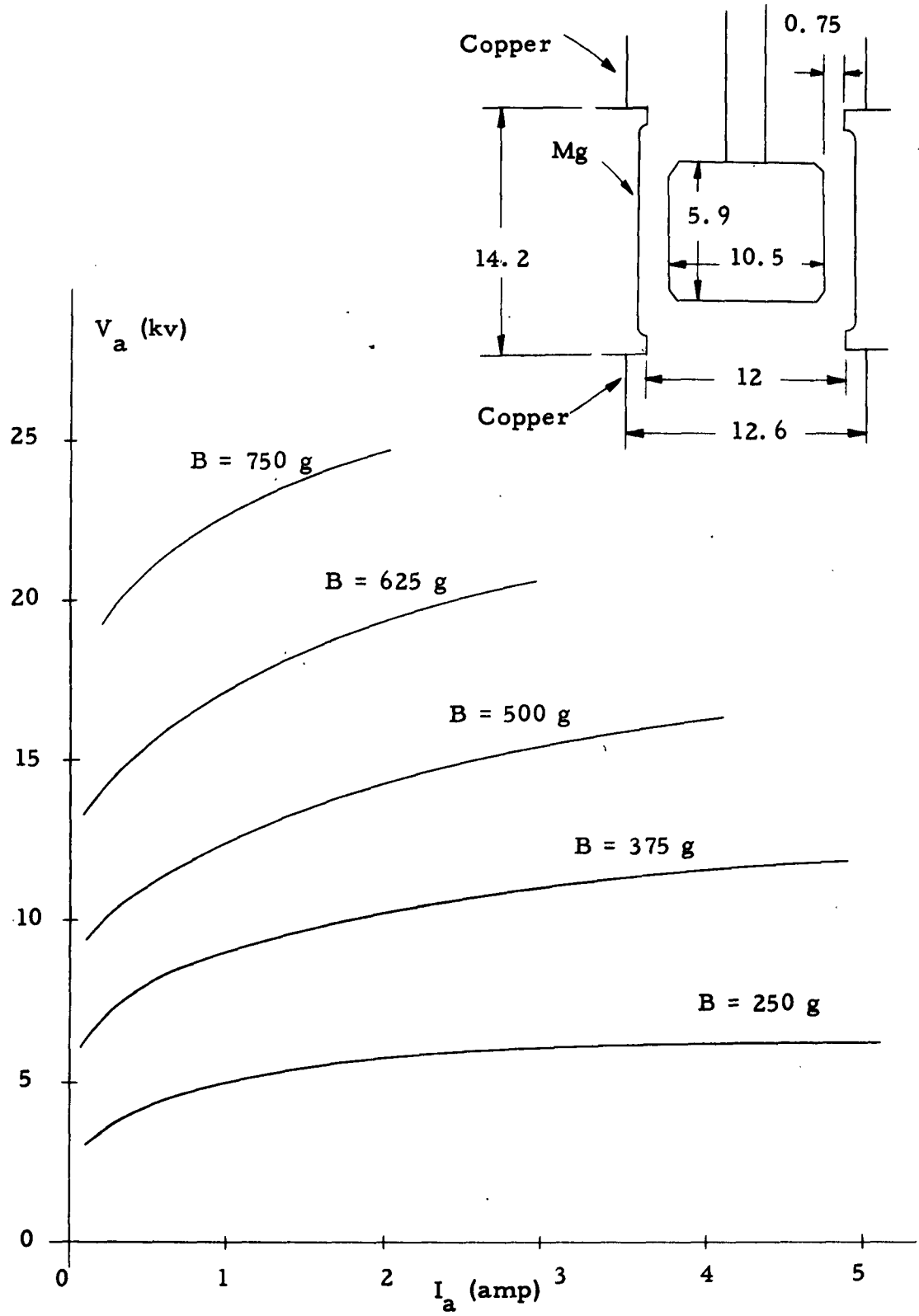

FIG. 26.—Characteristic curves with the magnesium cathode and short anode.

case, it is obvious that beside the effect of the cathode's edge, in general, the anode voltage decreases for a long anode much more than the change associated with changed current density. This fact is clearer if we compare Fig. 22 for a long anode and the aluminum cathode with Fig. 26 for a short anode and the magnesium cathode. There is no edge effect in any of these two cases, but the required voltage is higher in the short anode, considering that the magnesium-oxide (MgO) secondary emission ratio is higher than the aluminum-oxide (Al_2O_3) and the spacing in Fig. 25 is about 1 cm instead of 1.76 cm as in Fig. 22.

The reason for this difference between a short anode and a long one might be the difference in the space charge accumulated in the interaction space. In the long anode, the space-charge density in the interaction space might be greater than the charge density in the short-anode case. Therefore, the turbulences due to the space charge are greater in the long anode, which makes for a larger anode current and a stronger cathode back bombardment.

To investigate this problem further, two cathode "end hats" (actually collars or buffers) were made from 1/4-in. copper pipe, in the form of two circles, and installed at the edges of the magnesium cathode, as shown in Fig. 27. These buffers surrounded the space charge to keep the charge inside the interaction space. By this method the charge density was increased and more turbulence occurred. The required anode voltage in this case, then, was less than the previous one (compare Figs. 26 and 27).

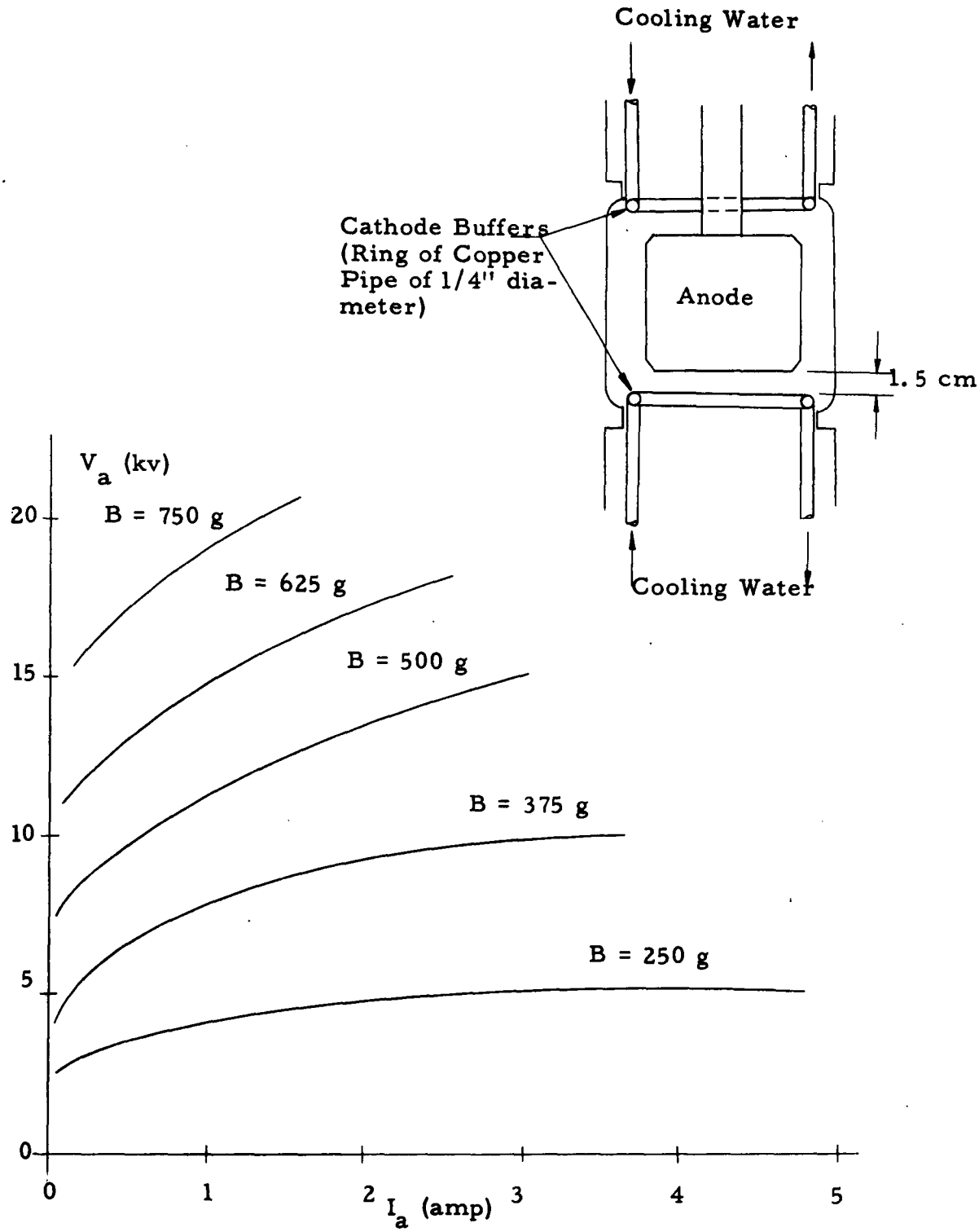

FIG. 27.—Characteristic curves with the magnesium cathode and short anode. Two cathode buffers are used to accumulate the space charge.

Another experiment was conducted to show the effect of the anode length. A copper pipe, diameter 8.8 cm, smaller than the anode diameter of 10.5 cm, was used as an extension for the anode, and its effect on the characteristic curves was observed. Three different lengths of the anode extension (2.3, 5, and 10 cm) were tested. The results are shown in Fig. 28. It is shown that as the length of the anode extension increases, the required anode voltage decreases. It is believed that the interaction space is limited to the magnesium area and though the anode length is more than the length of the magnesium cathode, the outer parts of the magnesium cathode are copper, which has a secondary-emission ratio much smaller than magnesium. The secondary emission from the copper parts of the cathode should be negligible.

F. STAINLESS-STEEL AND GRAPHITE CATHODES

In contrast with aluminum and magnesium cathodes, which have a high secondary-emission ratio, stainless-steel and graphite cathodes, which have secondary-emission ratios of unity or less, were also used. The aim of these tests was mostly to investigate noise and plasma temperatures, which are higher than in the case of aluminum or magnesium cathodes.

In Fig. 29, the characteristic curves of a stainless-steel cathode, with the spacing d = 2.5 cm, are shown. It is clear that, because of a small secondary-emission ratio, the anode current is very small, even for as high an anode voltage as 40 kv. Most of the current is

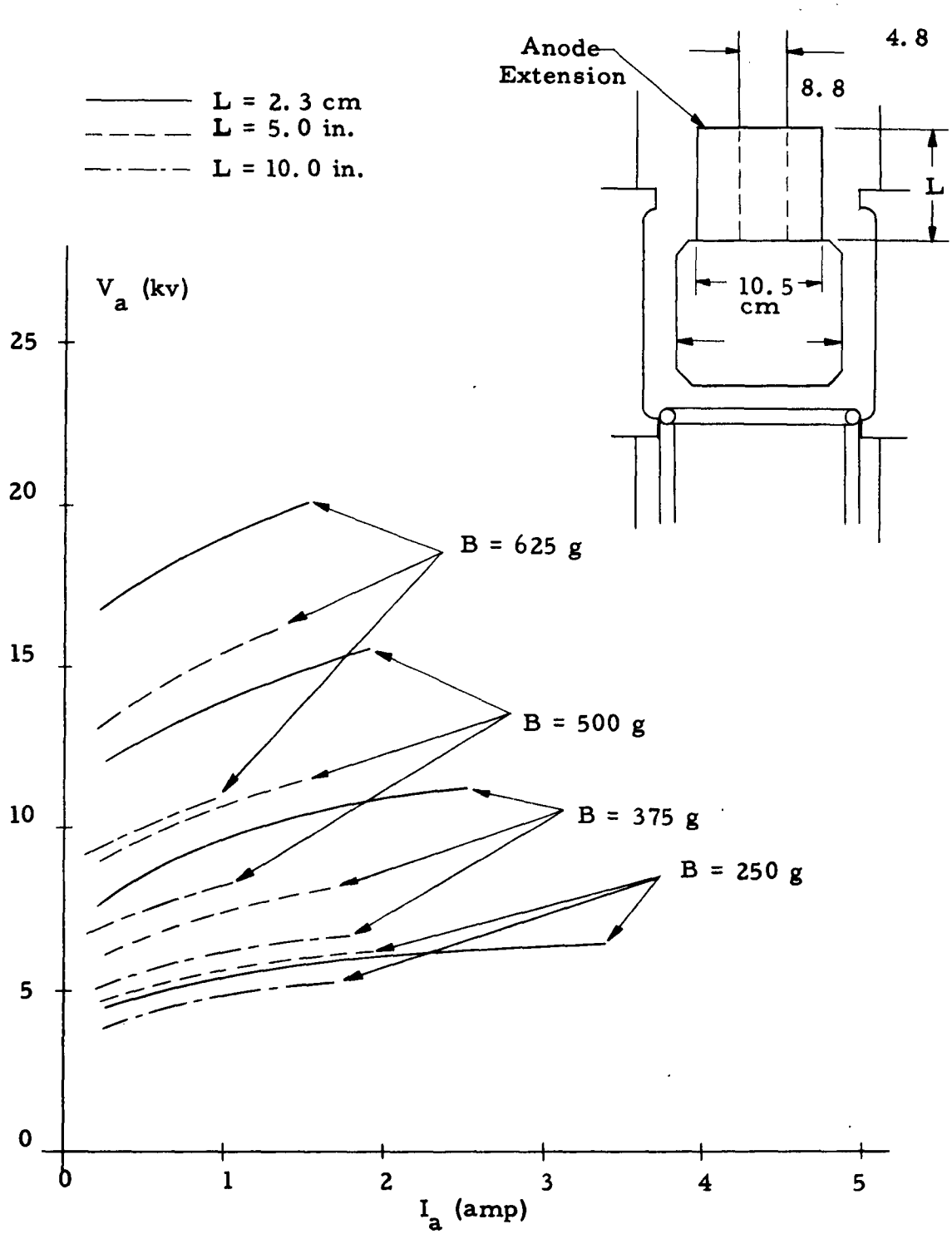

FIG. 28.—Characteristic curves with the magnesium cathode and short anode. One cathode buffer and an anode extension with three different lengths are used.

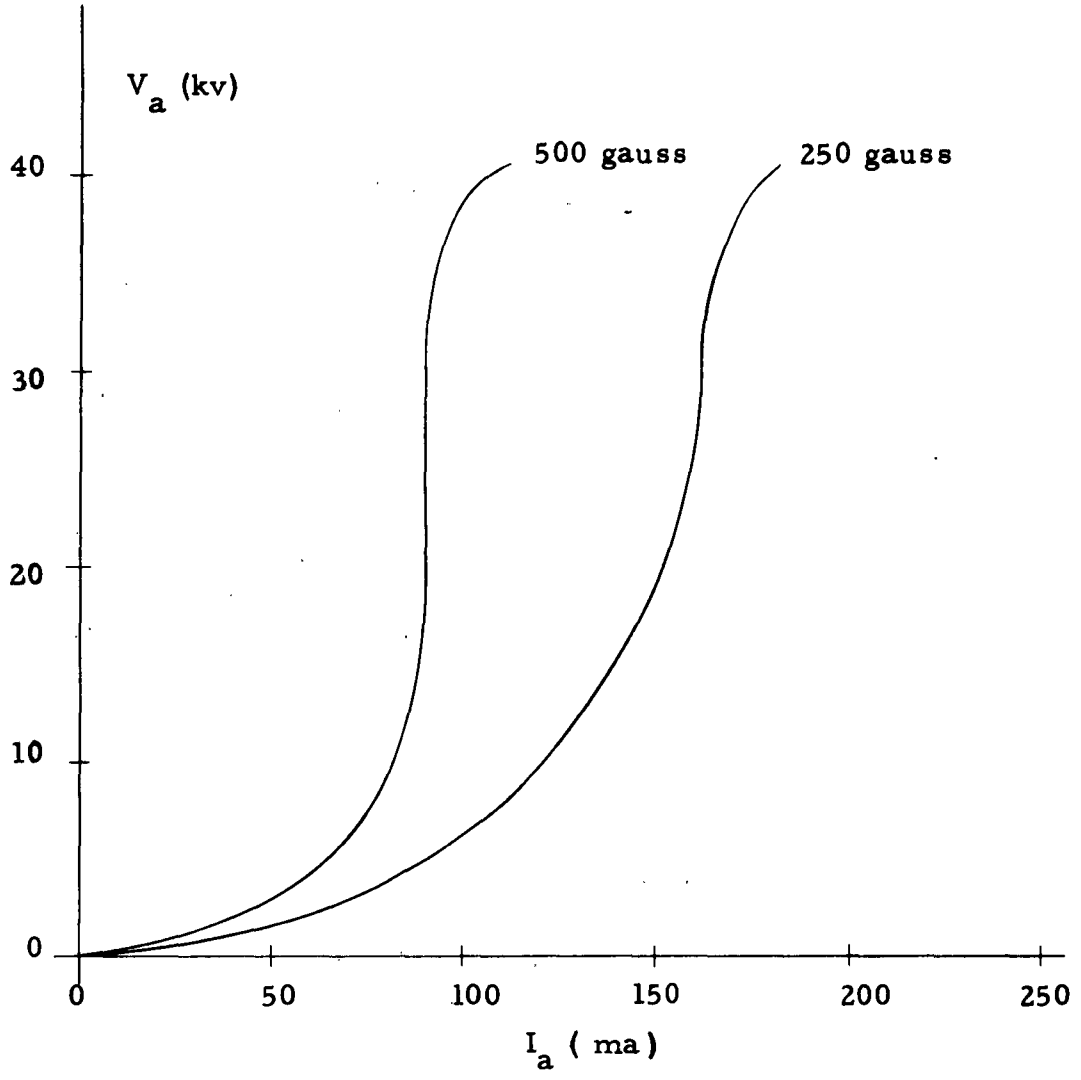

FIG. 29.—Characteristic curves with the stainless-steel cathode: $d = 2.5$ cm, $p = 2 \times 10^{-4}$ mm of Hg.

drawn from the gas ionization and P.I.G. discharge.

Figure 30 shows the schematic diagram of the graphite cathode and its characteristic curve. The anode is outside, with a diameter about 15 cm and more than 100 cm long. The graphite cathodes are in the form of disks located at the ends of the anode. The electrons move back and forth, along the magnetic lines, collide with the gas molecules, and produce electrons and ions which are collected by the cathodes. Therefore, an electron plasma is created between the two

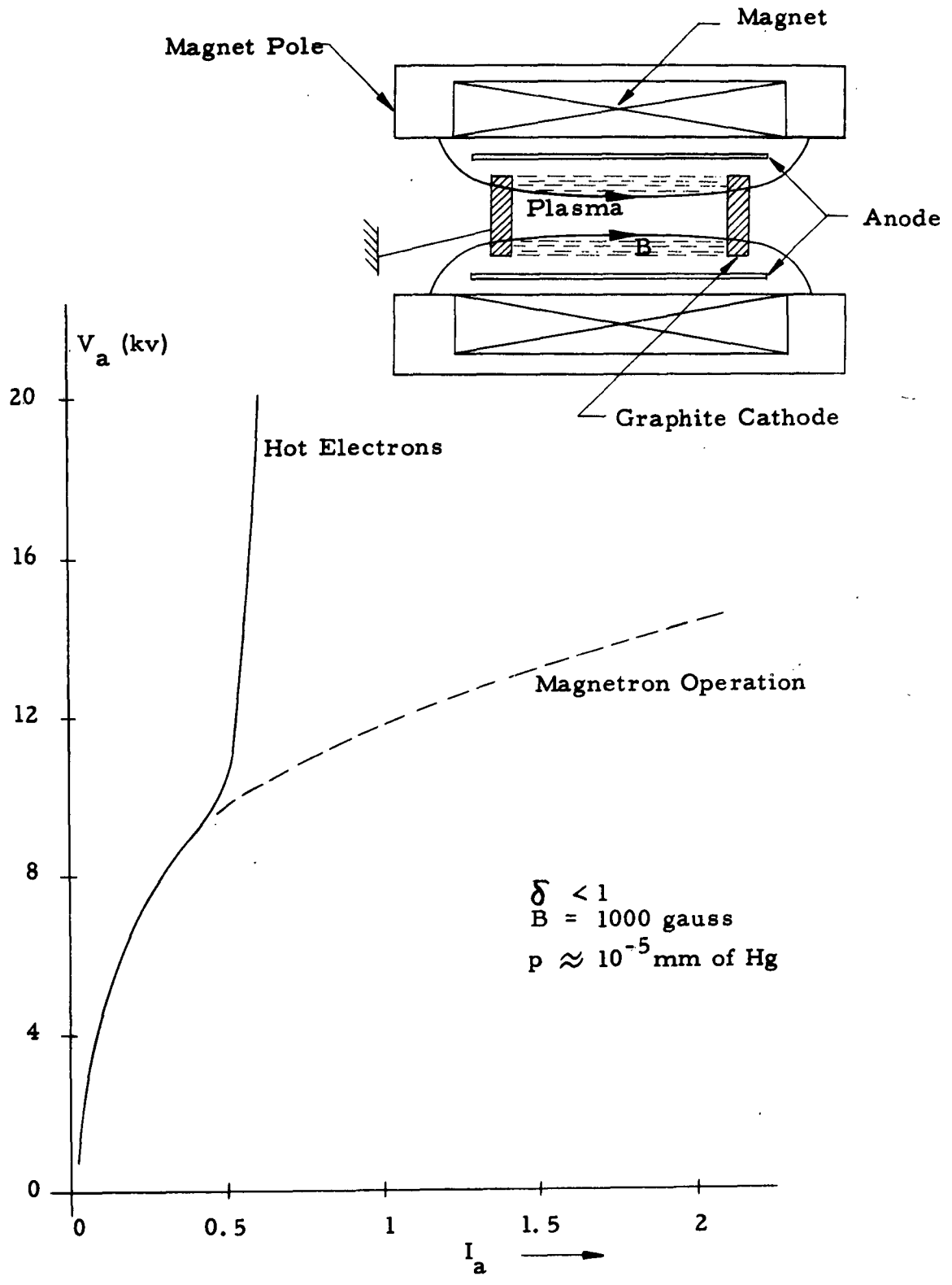

FIG. 30.—V_a-I_a characteristic of graphite cathode vacuum was spoiled because of lack of a fast pump.

cathodes. The column of plasma acts as a cylindrical cathode similar to the metallic cathodes in the previous cases. Then we may assume that the same type of static magnetron exists with the graphite cathodes.

The characteristic curve of Fig. 30 shows that the beginning of the curve is the same as in the other static magnetrons, but suddenly the anode voltage increases with almost a constant anode current. This phenomenon takes place because the turbulence in space charge evidently does not produce secondary emission, so that the anode current remains constant. The vacuum, at higher voltages, was spoiled because of the high gas pressure of the graphite and lack of a fast pump.

Usually the temperature of plasma or the amount of noise is proportional to the anode voltage, a circumstance that may prove to be important in the production of hot electrons or ions in a high voltage and a high magnetic field.

G. MEASUREMENT OF VOLTAGE IN LONGITUDINAL PLASMA OSCILLATORS

The electrons, beside the cycloidal motion and drift around the anode, have longitudinal motion from end to end. Each time an electron passes through the space charge, it loses or gains energy according to the phase of the plasma oscillations. Therefore, some electrons reach the ends of the cathode with a relatively high energy and strike the cathode at the ends, causing secondary emission. In the interaction space there are in effect many small oscillators,

and electrons passing through these oscillators are accelerated or decelerated according to their relative phases. This random acceleration gives the electrons a distribution of velocities corresponding to voltages ranging from zero to the sum of all the oscillators. This electron velocity distribution is found experimentally to be almost Maxwellian.

To measure the electron velocity, three holes were made in the cathode and three cups were installed outside the holes, such that the magnetic field lines passing through the holes would reach into the cups. Three cups were used in order to find the velocity of electrons from different places in the interaction space. Figures 16 and 31 show the schematic diagram of the cup and holes. These three cups and associated holes are labeled 1, 2, and 3, where hole 3 is the closest one to the center of the interaction space. The measurements were made with the aluminum and the stainless-steel cathode, which are basically the same.

The dc characteristic curves of the aluminum cathode, tested for the velocity measurements, are given in Fig. 32.

The cup is connected to a bias voltage V_b, usually negative, and its collected electrons are measured by a dc meter. The cups are installed at the end, in order to receive only electrons. The ions have very large radii, 1800 times greater than electrons; ions go to the cathode almost in a straight line and do not reach the ends of the tube, but electrons, which have a small radius, follow the flux lines to the cup.

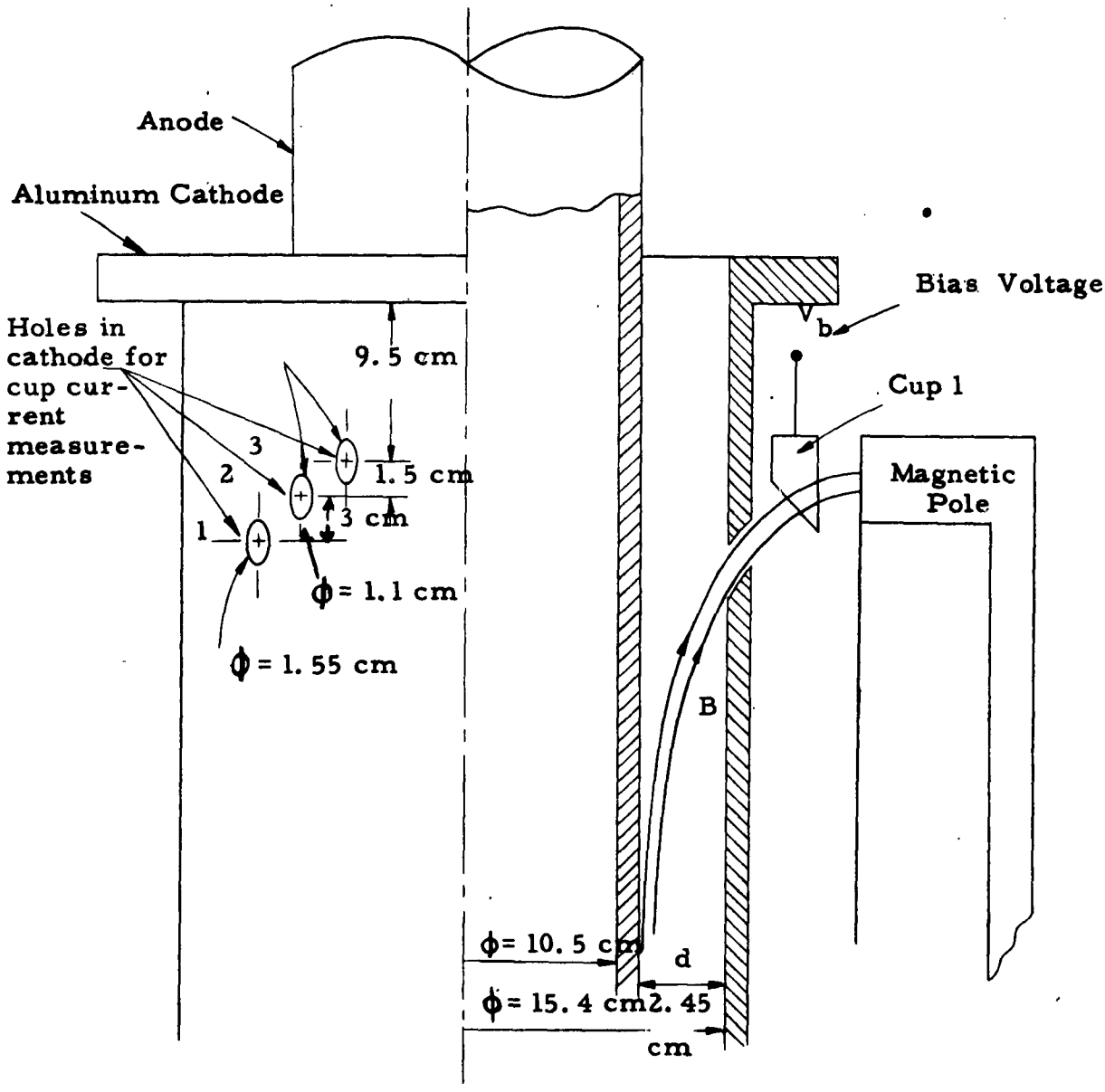

FIG. 31.—Schematic diagram of the cup, cathode, anode, and three cathode holes.

Figure 33 shows the collected current in the cup No. 1, with a zero bias voltage. When the anode current increases, the cup current first increases to a maximum and then decreases. The collected cup current is very sensitive to the magnetic field, but the form of these curves is typically the same.

The reason for this type of configuration might be explained as follows: At the beginning when the anode current is small, most of the electrons are created by the P.I.G. discharge and by the collision of electrons, in their longitudinal motion, with the gas molecules. In this case the longitudinal electron motion is an important process in the tube, setting up double-stream amplification and oscillations that extract energy from some electrons and give energy to other electrons, some of which travel against dc fields to reach the cathode ends, so that large cup current is observed. But when there is enough electric field and space charge in the tube, transverse or slipping-stream turbulence starts and most of the electrons are produced by secondary emission from the cathode at the center of the tube where this interaction takes place. In other words, the electron drift around the anode is more important than the longitudinal motion of the electrons, the anode current increases due to the increased circular drift motion, and the collected cup current decreases. When the magnetic field is increased, the longitudinal motion of electrons will be more effective and, as is clear from Fig. 33, the maximum of the cup current occurs at a higher anode current.

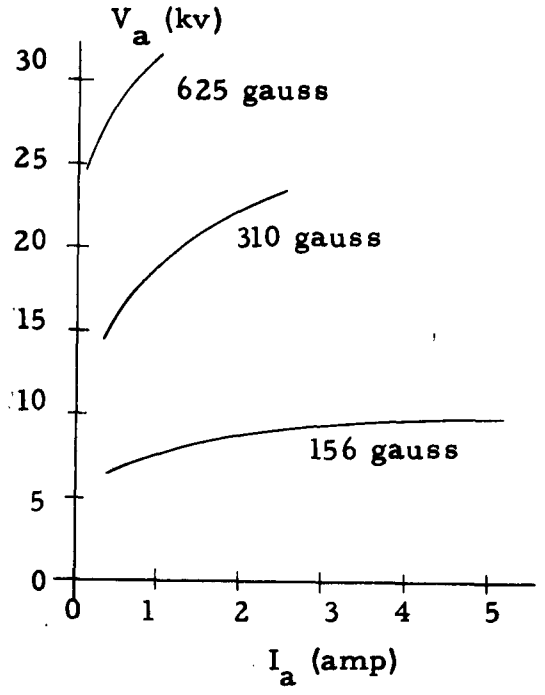

FIG. 32.—Dc V_a-I_a characteristics for aluminum cathode, long copper anode: d = 2.45 cm, $p \approx 10^{-5}$ mm of Hg.

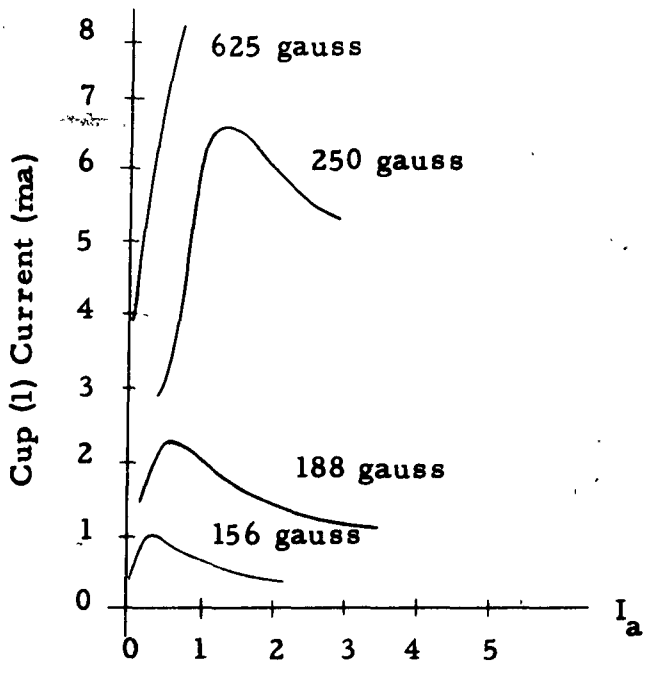

FIG. 33.—Variation of cup current with respect to anode current for different B. Aluminum cathode, long copper anode at zero bias voltage, d = 2.45 cm.

Strong longitudinal motion leads to concentration and arc formation at ends, if B or d is large, and voltage is applied for a time longer than a few microseconds. Strong circular drift current and turbulent diffusion current across B lines do not lead to concentrated arc formation, but heat both anode and cathode electrodes uniformly in the large area of the middle of the tube, so that much greater power can be carried than by the longitudinal process.

Figure 34 shows the collected current in cup No. 1, for 156 gauss but different anode currents, with respect to the bias voltage V_b. As is seen in this figure, there are some energetic electrons of over 500 ev. This measurement is for B = 156 gauss; for higher magnetic fields, this energy is much higher.

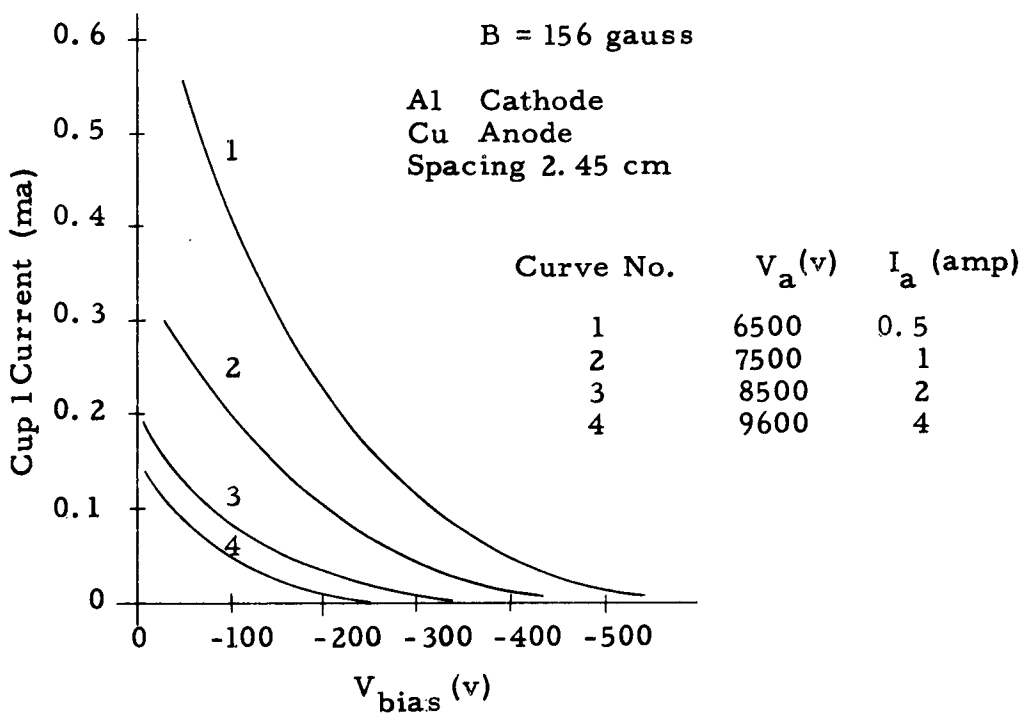

FIG. 34.—Collected current in cup 1 against bias voltage at 156 gauss for several anode currents. Aluminum cathode, long copper anode, d = 2.45 cm.

The curves of Fig. 34 show almost Maxwellian distribution; on a semilogarithmic paper, these curves are almost straight lines (Fig. 35).

Figure 36 shows the variation of collected current in cup No. 1 with bias voltage for B = 310 gauss. It is clear that the energy of electrons is greater in this case, and there are some electrons of over 2000 ev when the anode voltage is 19,800 v. This shows that the energetic electrons may reach an energy equal to 10 per cent of the applied anode voltage.

This type of velocity distribution suggests a similarity between this distribution and a Maxwellian distribution due to temperature. To be sure, the above distribution is not due to an equilibrium temperature. This similarity is also mentioned by other authors.[42]

Because of the observed Maxwellian distribution of velocities, in comparison to a Maxwellian energy distribution due to the temperature $e^{-w/kT}$, we may express out distribution in terms of an average voltage of the plasma oscillators V_{av}. Therefore, it is possible to formulate the collected current to the cup by the following expression:

$$i_{cage} = i_0 e^{-V_b/V_{av}} \tag{2.17}$$

where V_b is the bias voltage applied to the cup and i_0 is the maximum collected current at zero bias voltage. Equation (2.17) can be written as:

$$\log i_c = \log i_0 - V_b/V_{av} \tag{2.18}$$

The graphs of Eq. (2.18) are straight lines (Fig. 35). The experimental results agree quite well with a Maxwellian distribution and

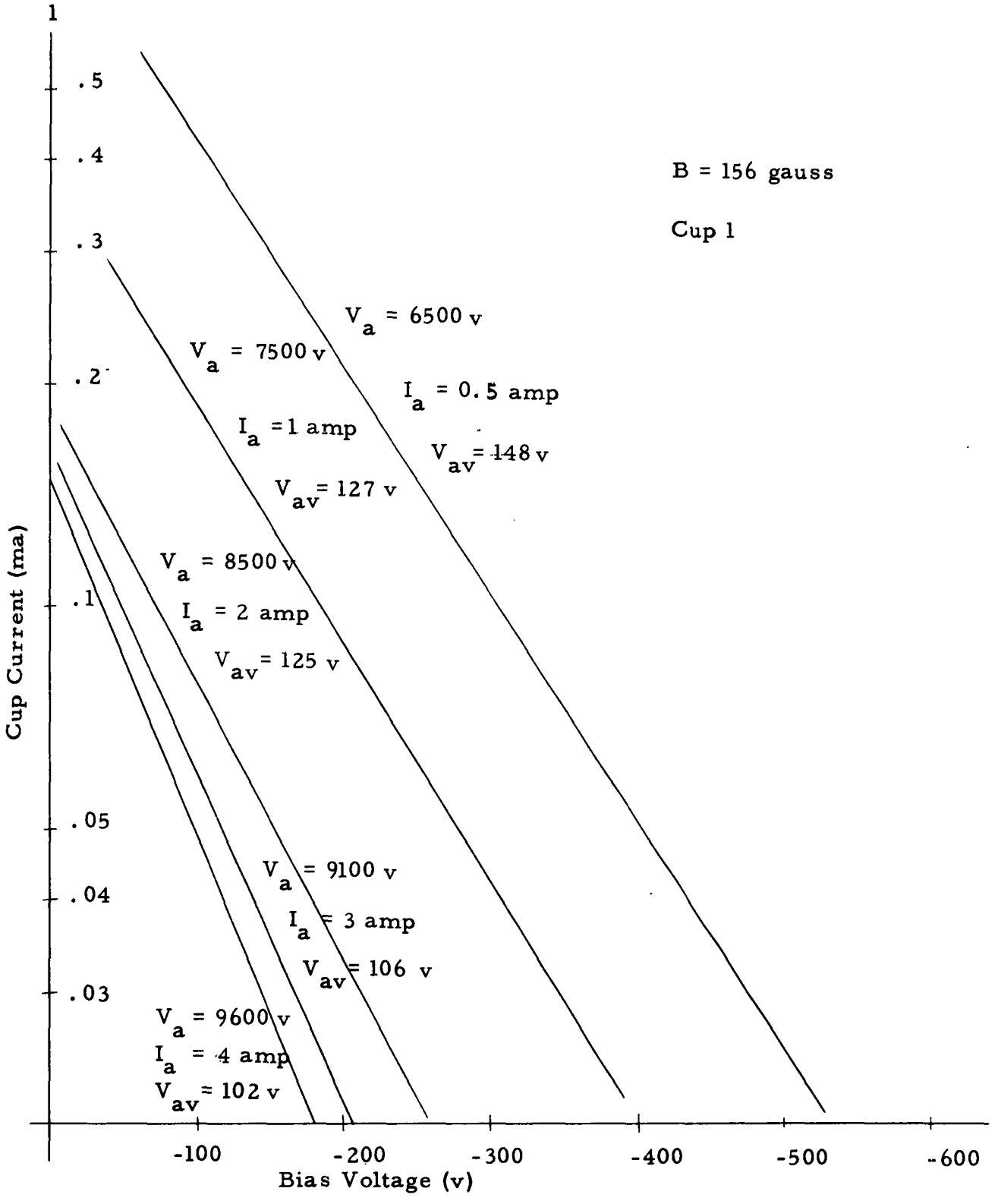

FIG. 35.—Collected current in cup 1 against bias voltage. This curve is the same as Fig. 34 but on a semilogarithmic paper.

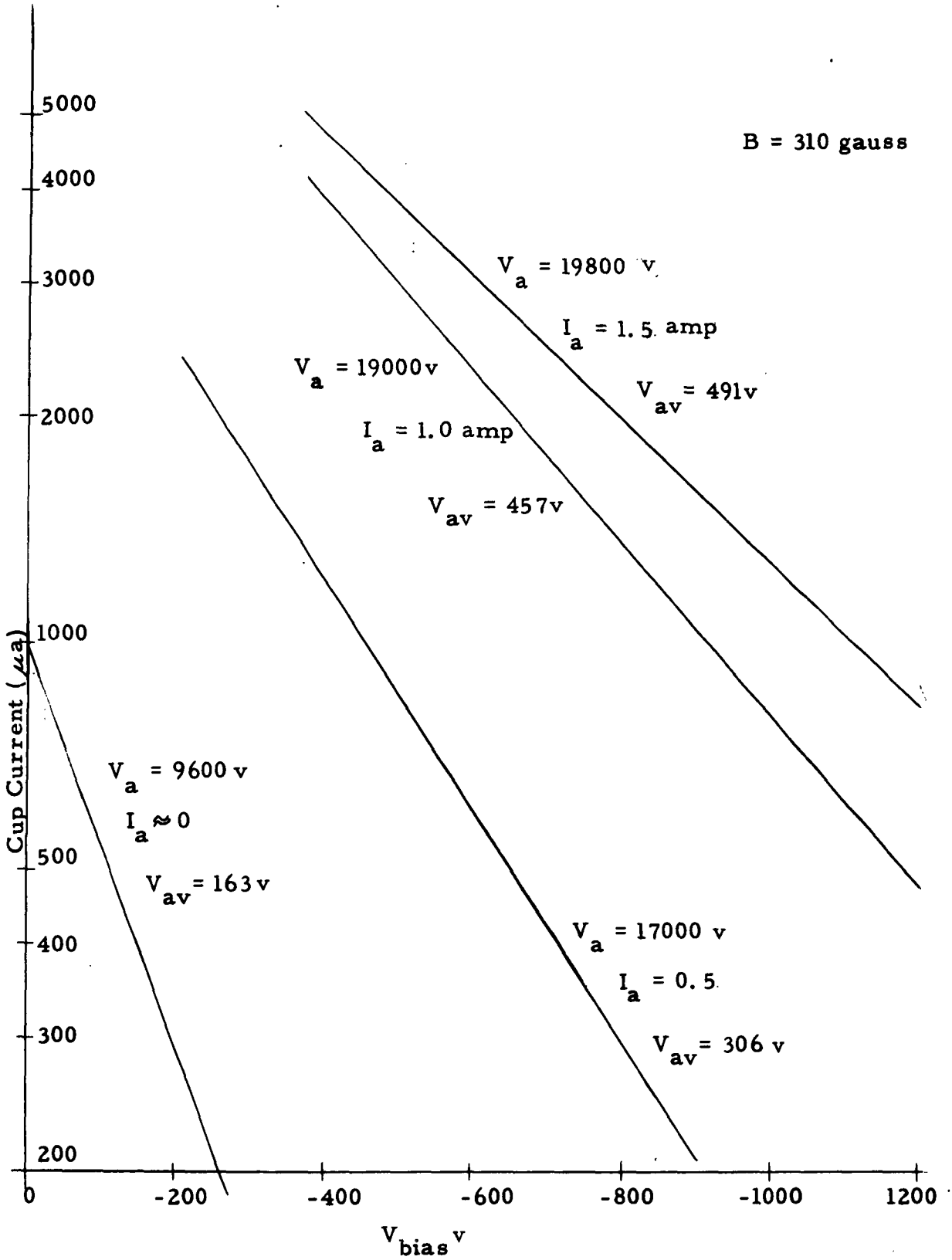

FIG. 36.—Collected current in cup 1 against bias voltage, for 310 gauss.

with Eqs. (2.17) and (2.18). In Figs. 35 and 36, the slope of the lines is, from Eq. (1.18), proportional to $1/V_{av}$. When V_{av} is large, the slope of the i—V_b curves is small and the maximum average voltage is obtained when the slope of the i—V_b line is a minimum. From the slopes of the curves drawn in Figs. 35 and 36 we may find V_{av}, the average voltage of the plasma oscillators. For example, we show the calculation for finding V_{av} in the curves of $V_a = 9600$ v, $V_b = 260$ v, $i_c = 200$ μa, and $i_0 = 1000$ μa,

$$V_{av} = 260 \frac{1}{\log \frac{1000}{2000}} = \frac{260}{\log 5} = 163 \text{ v}$$

The average voltage of other lines is also indicated in Figs. 35 and 36.

These average electron voltages V_{av} of Figs. 35 and 36 are drawn in Figs. 37 and 38 against anode voltage for two values of magnetic fields. In these figures, the V_a—I_a curves are also shown. It is clear from these curves that the variation is different for the beginning of the V_a—I_a curves and their flat parts. As was explained previously, at the beginning of the V_a—I_a curves it is mostly the P.I.G. type of discharge that causes the initial space-charge buildup, where the longitudinal electron motion is very important. In this region, V_{av} increases roughly linearly with anode current. In the flat part of V_a—I_a curves, where instability and turbulence occur in the plasma and the circular drift of the electron cloud around the anode is the major factor of the operation, V_{av} decreases almost inversely proportionally to the anode current. In the regime of

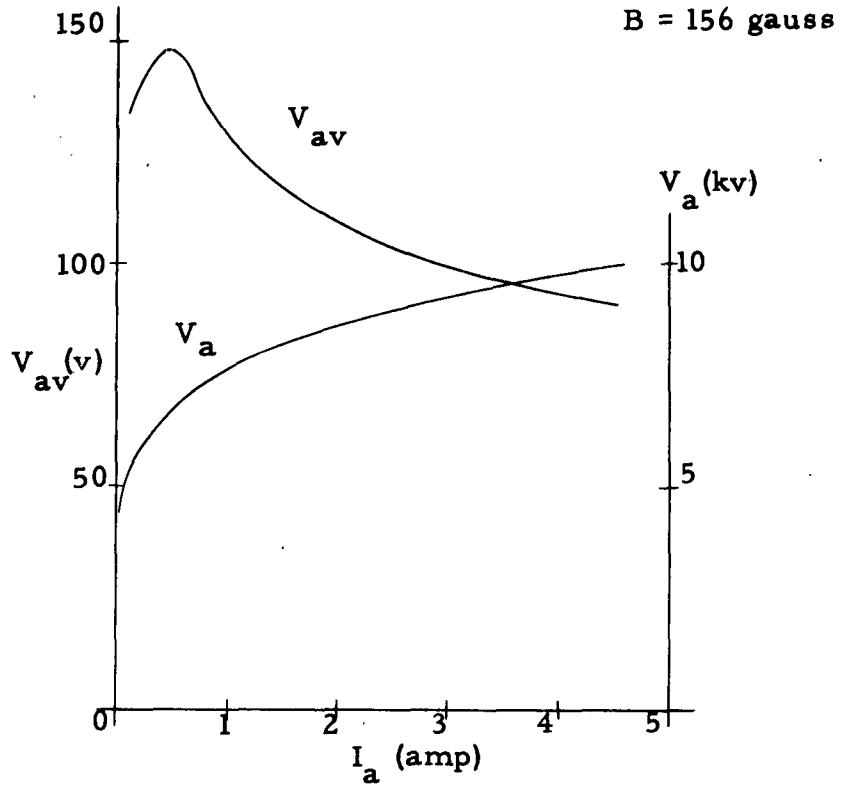

FIG. 37.—Variation of the average electron voltage with anode current. The data are taken from Fig. 35, aluminum cathode, d = 2.45 cm (as in Fig. 34).

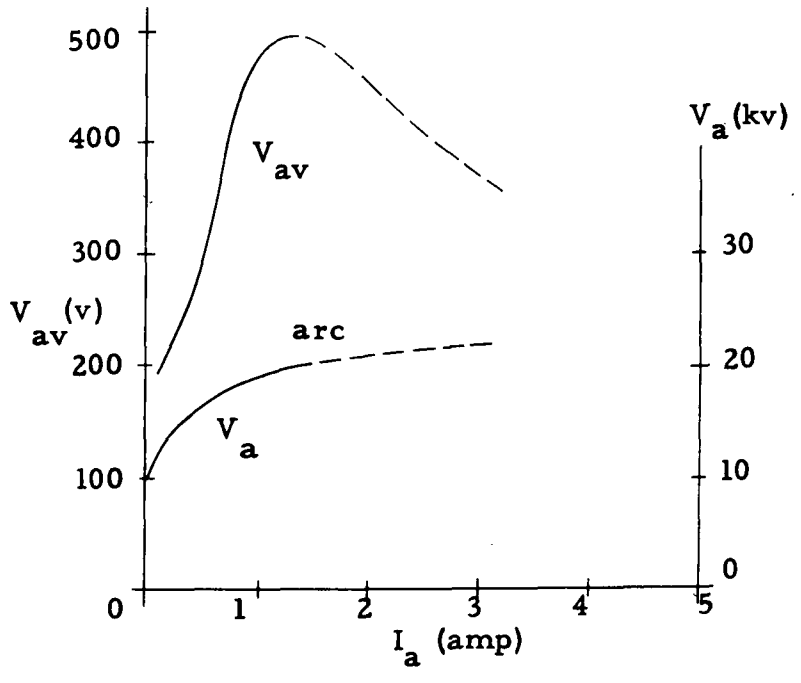

FIG. 38.—Variation of the average electron voltage with anode current. The data are taken from Fig. 36, aluminum cathode (diameter 15.4 cm), long smooth anode (diameter 10.5 cm), d = 2.45 cm.

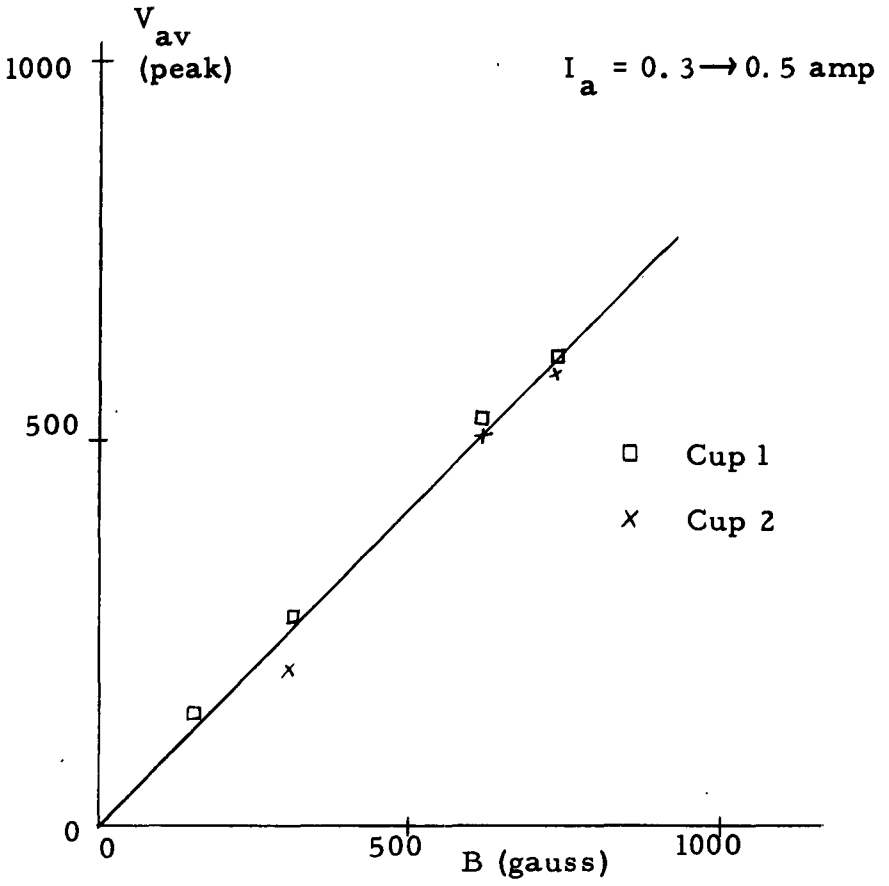

FIG. 39.—Variation of V_{av} (peak) with magnetic field. Tube is the same as in Fig. 34.

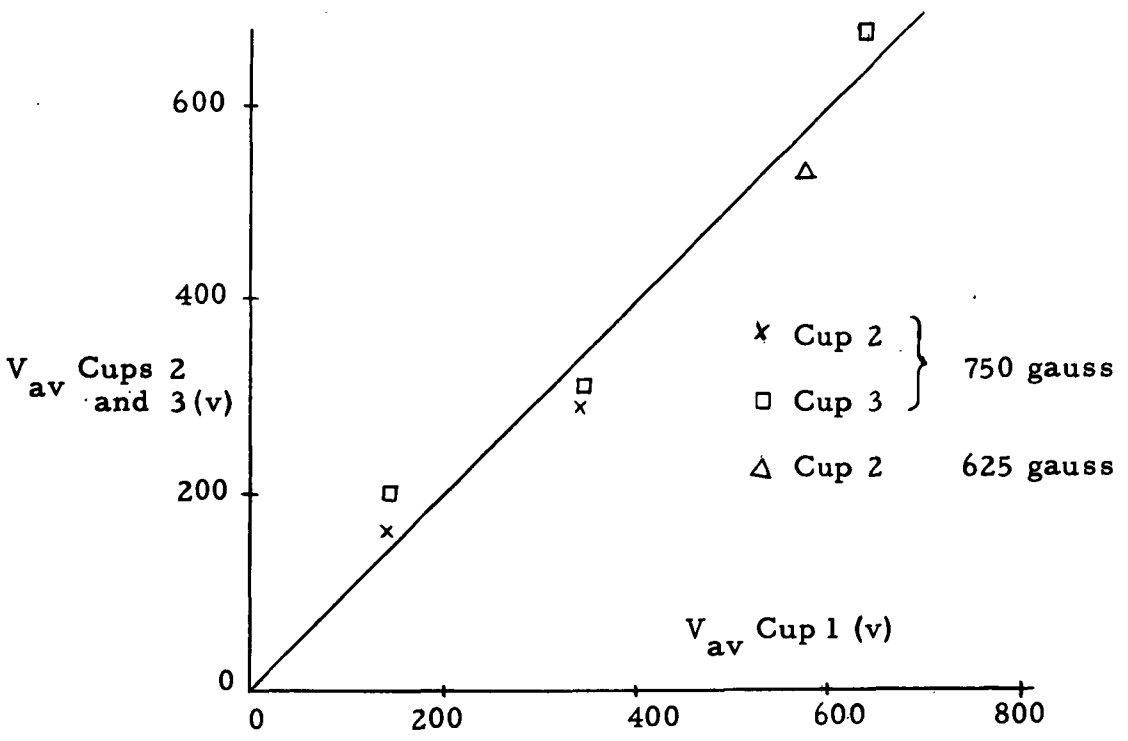

FIG. 40.—Calculated V_{av} of cup 2 and 3 with respect to cup 1.

ordinary magnetron operation, where the anode current is relatively large with respect to the P.I.G. current, V_{av} decreases continuously and the first part of the V_{av} curve may be neglected. Unfortunately, the arc boundary did not permit going to higher anode currents in these observations.

From Figs. 37 and 38, it is obvious that the peak of the V_{av}—I_a curve increases with magnetic field B. This fact is clearer in Fig. 39, where the variation of the peak values of V_{av} are drawn with respect to the magnetic field for cups 1 and 2. Figure 39 shows that the variation of the average voltage of electrons V_{av} is linear with respect to the magnetic field.

Figure 40 shows that the average voltage of electrons due to the postulated many oscillators of random phases is almost the same at all points of the interaction space. The holes of the three cups are placed at different places and three different groups of electrons are collected in these cups. Figure 40 shows that the V_{av} calculated from collected current by cup 1 is the same as those of cups 2 and 3. Thus the equivalent plasma temperature of the electrons appears to be homogeneous throughout the plasma.

It is worthwhile to note that the maximum sum of the average voltage gain by many randomly phased oscillators, along the same magnetic field lines or surface, has V_a/Bd such that the space-charge-free height of a cycloid is d/π. This is observed as the maximum temperature of electrons which enter the cups, when the secondary emission is too low to make appreciable turbulence.

H. CATHODE SURFACE

In a cold-cathode magnetron the state of the cathode surface is very important, because the secondary emission of the cathode is the major source of electrons. The cathode surface is also important for long-life operation. In our experiments, magnesium, stainless-steel, copper, graphite, and (chiefly) aluminum cathodes were used. The magnesium and aluminum cathodes were best for high secondary-emission ratios. The secondary-emission ratios of pure aluminum and pure magnesium are less than unity,[36] but a thin layer of oxide on the cathode surface increases the secondary emission ratios to about 10. Therefore, maintaining the oxide layer, in aluminum and magnesium cathodes, is of major importance in obtaining high secondary emission. At the beginning of operation, the cathode surface is covered by pump oil or other contaminants. After 15 min to 1 hr of operation, the surface is cleaned by ion bombardment.

Because of the importance of the oxide layer, the percentage of oxygen in the gas mixture is very important. After prolonged operation it is found that the proportion of oxygen in air is satisfactory for the aluminum and magnesium cathodes. If the amount of oxygen is increased, the anode voltage falls and the tube arcs or makes a glow discharge. If the percentage of oxygen is decreased, the secondary-emission ratio decreases too, and a higher anode voltage is required to produce secondary electrons. Figure 41 indicates the increase of the anode voltage, with the removal of the oxide layer from aluminum, by putting helium in the tube. In a few minutes, after letting helium

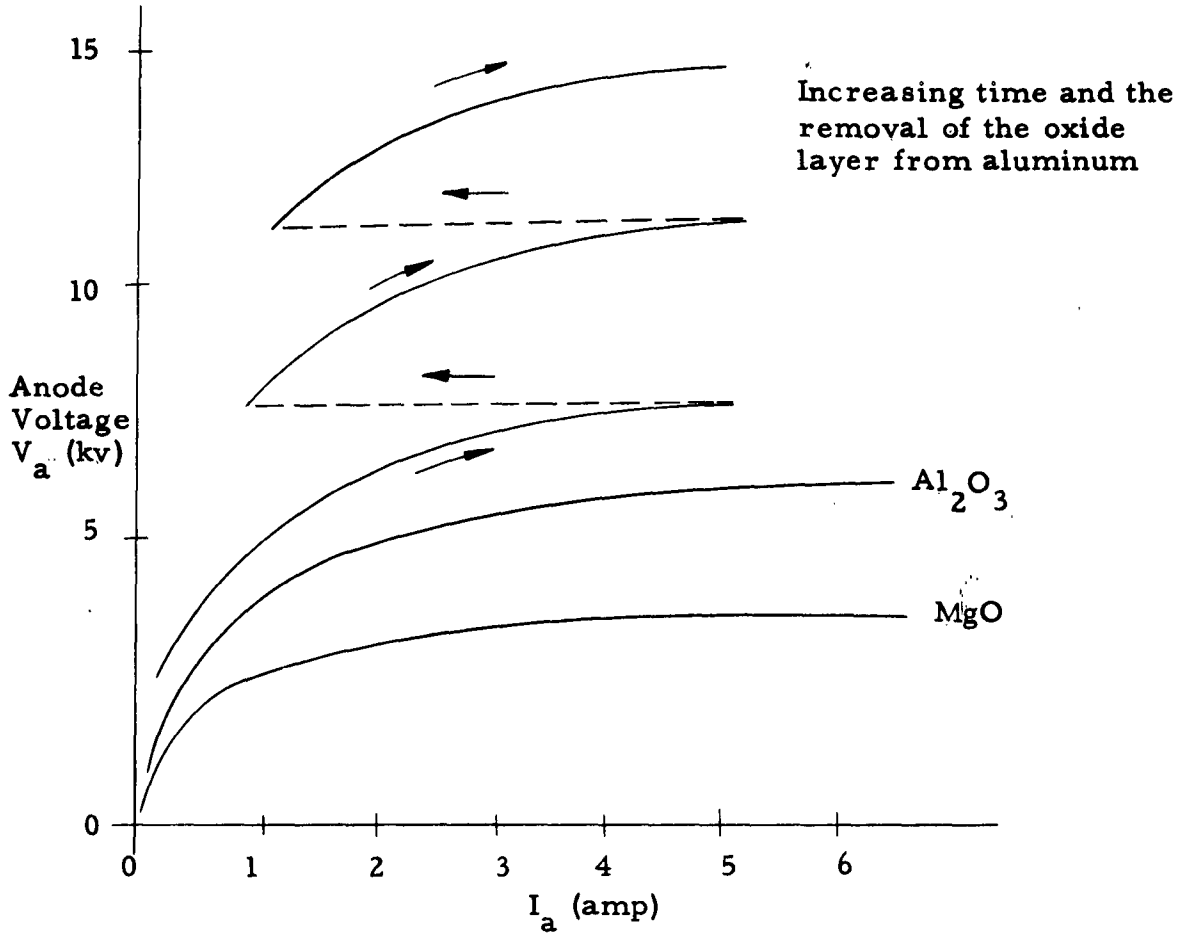

FIG. 41.—V_a—I_a characteristic curves for the aluminum and magnesium cathodes, $B \approx 1000$ gauss, spacing $d \approx 1$ cm, showing the increase of the anode voltage with removal of the oxide layer.

in, the anode voltage increases by about 2. In this case, the beam velocity increases and the aluminum cathode is more similar to copper and tungsten. By again letting oxygen into the tube, the anode voltage decreases again. The general conclusion of these experiments is that the oxygen mixture in the air is satisfactory for the aluminum and magnesium cathodes in cold-cathode magnetrons.

III. DIFFUSION APPROACH TO MAGNETRON PROBLEMS

A. INTRODUCTION

In Sec. I, the works of many authors are outlined. The most important theoretical work is the small-signal theory of Buneman[21,22] based on Brillouin laminar flow.[5] The most extensive experimental works are reported by Nedderman,[13] Reverdin,[9] and Mathias.[23] The experimental results are that the space charge extends well beyond the Brillouin radius, and the space charge has no definite edge.

The most important problems of the static magnetron are: the space-charge distribution, the anode current beyond cutoff, and the cathode back bombardment. Excess noise is also an important phenomenon in a static magnetron and will be discussed later. In this section, a statistical method is used to find the space-charge distribution and the anode current. The results of this method agree with the experimental data better than the previous work discussed in Sec. I.

B. SPACE-CHARGE DISTRIBUTION

Most of the previous theoretical approach to the magnetron problem is based on a small-signal theory which is not usually valid under experimental conditions. Most of the analyses given by the authors mentioned in Sec. I are at least partially valid, although none of them explains the magnetron problem completely; however, each one sheds light on some phase of the problem. Brillouin laminar flow

is the simplest approach to start with. The small-signal theory of Buneman, who applied perturbation methods to the static Brillouin space-charge distribution, is the most adequate approach to the problem. We believe the plasma oscillation explanation of MacFarlane and Hay or Buneman to be at least partially true. In any event some turbulence occurs in the electron cloud. This turbulence causes electrons to move randomly to the anode or to the cathode. The random walk of electrons is the best explanation of anode current or cathode back bombardment. If so, the statistical approach is the best method of attack. Statistical mechanics is used for many types of diffusion in the kinetic theory of gases: heat conduction and transfer of mass and energy through a gas. Random walk of electrons may be explained by the diffusion equation

$$\frac{\partial \rho}{\partial t} = D \frac{\partial^2 \rho}{\partial x^2} + \frac{\partial^2 \rho}{\partial y^2} + \frac{\partial^2 \rho}{\partial z^2} \tag{3.1}$$

where D is the diffusion coefficient, and is the charge density between the cathode and anode. In our magnetron configuration spacing d is small with respect to the anode radius. The configuration approximates parallel plates, and the derivatives with respect to x and z are zero. If we assume steady state, then the derivative with respect to time is zero, too; therefore

$$\frac{d^2 \rho}{dy^2} = 0 \tag{3.2}$$

$$\frac{d\rho}{dy} = C \tag{3.3}$$

where C is a constant. If we integrate Eq. (3.3), we find

$$\rho = Cy + C' \tag{3.4}$$

where C' is another constant. Equation (3.4) shows that the space-charge distribution between the cathode and the anode is a linear function of y. Considering the Brillouin laminar-flow space-charge distribution[5] and the experimental results of Mathias,[23] Reverdin,[9] and Nedderman,[13] we find that the best theoretical distribution close to the experimental results is the linear one, which is almost the average of the different distributions given by the above authors.

To find the constants C and C' in Eq. (3.4) we assume that the space-charge density falls to zero at the anode; then ρ can be written as

$$\rho = C(y - d) \tag{3.5}$$

where d is the distance from the cathode to the anode, and the cathode is assumed to be at zero abscissa (Fig. 42).

To find the electric-field distribution, Eq. (3.5) should be integrated with respect to y, using Poisson's equation. As a boundary condition to Poisson's equation, we assume the electric field is zero at the cathode. This assumption might be true for a hot cathode but not for a secondary-emission cold cathode; however, the difference is probably small and will be neglected.

From

$$\nabla \cdot \bar{E} = \frac{-\rho}{\epsilon_0}$$

and assuming variation in the y-direction only, we obtain

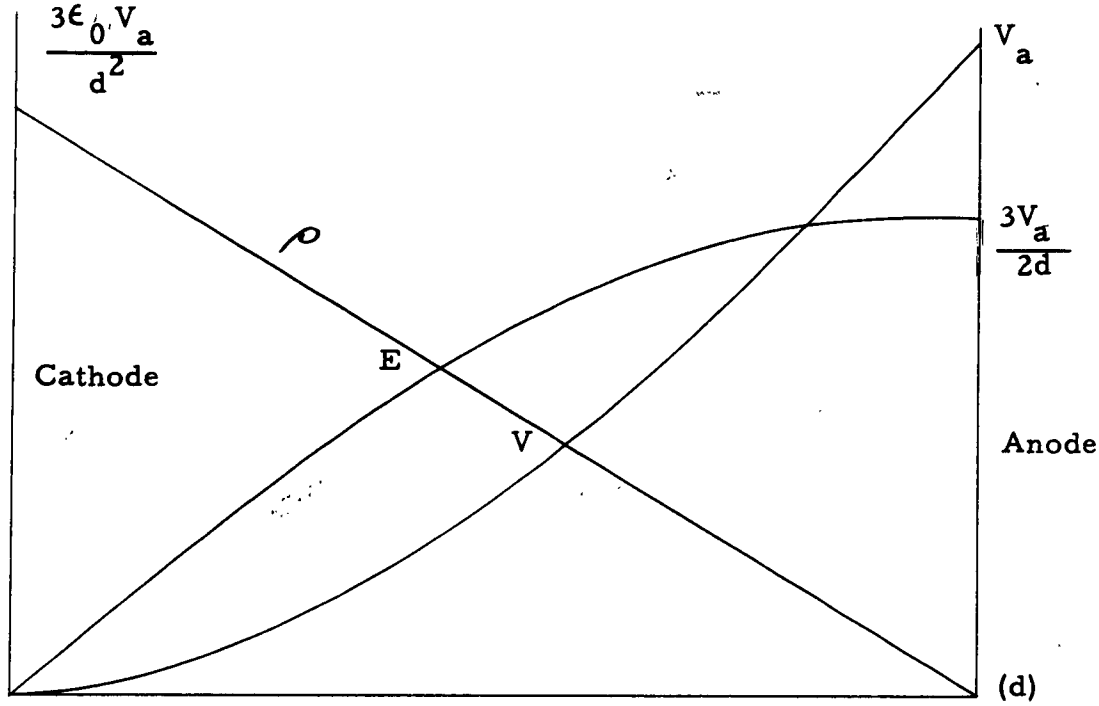

FIG. 42.—Distributions of space charge, electric field, and potential between the cathode and anode.

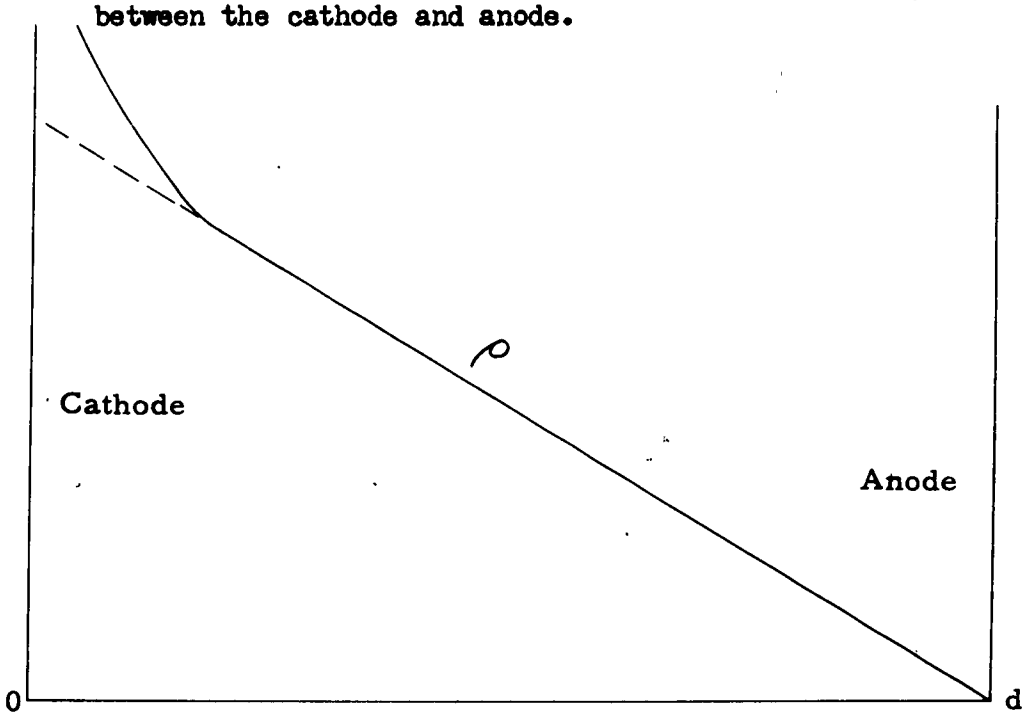

FIG. 43.—Space-charge distribution between cathode and anode, modified by decreased rate near cathode.

$$\frac{dE}{dy} = \frac{-\rho}{\epsilon_0} = \frac{-1}{\epsilon_0} C(y - d) \tag{3.6}$$

$$E = \frac{-C}{\epsilon_0}\left(\frac{1}{2} y^2 - dy\right) + C'' \tag{3.7}$$

But $C'' = 0$ on the assumption of zero electric field at the cathode.

The potential distribution follows from the integration of Eq. (3.7):

$$V = -\int E\, dy = + \frac{C}{\epsilon_0}\left(\frac{1}{6} y^3 - \frac{d}{2} y^2\right) + C''' \tag{3.8}$$

where $C''' = 0$, because voltage is zero at the cathode. Then,

$$V_a = + \frac{C}{\epsilon_0}\left(\frac{1}{6} d^3 - \frac{d}{2} d^2\right) = \frac{-C}{3\epsilon_0} d^3 \tag{3.9}$$

From Eq. (3.9) we may find the constant C:

$$C = \frac{-3\epsilon_0 V_a}{d^3} \tag{3.10}$$

Then the space-charge, electric-field, and voltage distributions will be as follows:

$$\rho = - \frac{-3\epsilon_0 V_a}{d^3} (y - d) \tag{3.11}$$

$$E = \frac{3V_a}{d^3}\left(\frac{1}{2} y^2 - dy\right) \tag{3.12}$$

$$V = - \frac{3V_a}{d^3}\left(\frac{1}{6} y^3 - \frac{d}{2} y^2\right) \tag{3.13}$$

Figure 42 shows the graphs of these distributions.

C. ANODE CURRENT

A well-known problem of the magnetron is the violation of the cutoff relation first derived by Hull[1] in a static magnetron. Harvey[2] and Linder[3] made careful measurements to show the existence of anode current and cathode back bombardment at magnetic fields beyond cutoff to prove the violation of Hull cutoff relation. More recently, the departure of Hull relation and anode current under cutoff conditions have become accepted phenomena. At the present time there is little doubt that some sort of plasma oscillation causes these phenomena. Several experiments on noise measurement prove turbulence in the electron cloud in the interaction space. Plasma oscillation or instability in plasma create turbulence which causes electron diffusion across the magnetic field. The turbulence explanation of Buneman[21] or MacFarlane and Hay[20] slipping-stream oscillations may be used in this analysis. However, it is not necessary to confine oneself to these types of oscillations; any other type of turbulence proportional to B gives rise to the same result. A bunch in the cloud encounters electrons moving faster or slower than the bunch and as a result makes them move randomly toward the anode or toward the cathode. Electrons that finally reach the anode, after many steps, result in anode current; those reaching the cathode result in back bombardment of the cathode. Measurements of the energy dissipation shows that almost half of the kinetic energy taken from the dc field by electrons reaching the anode goes to the cathode, carried back by very many more electrons than the small number that reach the anode. The cathode is

struck by low-energy electrons, but very energetic electrons predominate at the anode. Most of the secondary electrons do not travel very far from the cathode, but randomly wander back and are lost.

To find the anode current, we simply use the diffusion equation (3.1) which is based on the random walk of electrons due to the encounter between charge density fluctuations. The anode current density, by diffusion theory, is

$$J_a = D \frac{d\rho}{dy} \tag{3.14}$$

The distribution of ρ is found in Eq. (3.11) and the diffusion coefficient D is related to the number of encounters and electrons and to the average distance randomly walked by an electron after each encounter.

The time τ between two successive encounters is usually the lifetime of a bunch in the electron cloud; i.e., each bunch, between building up and dispersal, collides just once with an electron. Time τ is inversely proportional to the cyclotron frequency or simply the magnetic field B.

The step Δy walked by an electron after each encounter is a fraction of cycloidal diameter $2mE/eB^2$, found in Eq. (2.7),

$$\Delta y = \nu \, (2mE/eB^2)$$

where $0 < \nu \leqslant 1$.

Electric field E is not constant in the interaction space. It increases from cathode to anode, in addition to its fluctuations. Moreover, ν is not constant, i.e., near the bunch ν is large, close to

unity; farther from the bunch, ν gets smaller so that it decreases roughly from cathode to the anode. For simplicity we may assume that the systematic variation of ν and E cancel each other, or the step Δy is a constant proportional to $1/B^2$.

The diffusion coefficient D, by definition is[41]

$$D = \frac{\langle \Delta y \rangle^2}{\tau} \tag{3.15}$$

or

$$D \sim \frac{E^2/B^4}{B}$$

where $E = V_a/d$ is the average electric field between the cathode and the anode, V_a is the anode voltage, and d is the distance between the cathode and the anode. Then

$$D = C \frac{V_a^{\ 2}}{d^2 B^3} \tag{3.16}$$

where C is a constant. The anode current, by using Eqs. (3.11), (3.14), and (3.16), is

$$J_a = D \frac{d\rho}{dy} = C \frac{V_a^{\ 2}}{d^2 B^3} \frac{3\epsilon_0 V_a}{d^3}$$

$$J_a = C' \frac{1}{d^2} \left(\frac{V_a}{Bd} \right)^3 \tag{3.17}$$

where C' is a constant. This equation is similar to Hartman's anode current.[26] He calculated J_a in the case of Brillouin space-charge distribution where space charge exists only near the cathode.

Equation (3.17), which is based on the linear distribution of space charge between the cathode and the anode, is a more accurate analysis and agrees equally well with experimental data.[26]

The region of most intense oscillation occurs at about a sixth of the distance from cathode to anode. Between this region and the cathode, both ν and E diminish together, and their changes do not compensate each other as was assumed prior to the derivation of Eq. (3.15). This will modify the distribution of ρ, shown linear in Fig. 42, to some new form suggested in Fig. 43.

It is interesting to show the similarity between the anode current in a magnetron, Eq. (3.17), and the three-halves power law in a diode (Langmuir-Child law). Eq. (3.17) can be written as:

$$J_a \sim \frac{1}{d^2}\left(\frac{E}{B}\right)^3 = \frac{1}{d^2}\, v_d^{\,3} \tag{3.17a}$$

where $E = V_a/d$ is the average electric field in the interaction space and $v_d = E/B$ is the drift velocity of electrons around the anode. In high-vacuum diodes, the electron velocity is given by the relation below:

$$eV_a = \frac{1}{2}\, mv_d^{\,2}$$

or

$$v_d \sim V_a^{\,1/2} \tag{3.17b}$$

so that

$$J_a \sim \frac{1}{d^2}\, V_a^{\,3/2} \tag{3.17c}$$

The equation (3.17c) is the three-halves power law in diodes, and it shows that the anode currents in magnetrons and diodes are analogous.

This analogy can be better shown directly from Eq. (3.17) by a different assumption. The radius of an electron in its cycloidal motion was found in Eq. (2.16) to be $r = mE/eB^2$ or $r = mV_a/edB^2$. For

a constant electron radius and a fixed spacing d, then, the value of V_a/B^2 is a constant, or $B \sim V_a^{1/2}$. If we put this relation into Eq. (3.17), we obtain

$$J_a \sim (V_a/V_a^{1/2})^3 = V_a^{3/2} \tag{3.17d}$$

Equation (3.17d) also expresses the three-halves power law by maintaining unchanged ratios of r/d at each point and B is changed so that the ratios are unchanged as voltage changes.

D. CIRCULATING CURRENT

It is a well-known fact that the tangential component or the circulating current in a magnetron is usually much more than the perpendicular component or the anode current.[15,24] Hoag[25] measured the circulating current under various conditions. He tried to find a theory to agree with the results of his experiments. The available theory with which he compared his results was the theory of Buneman on the basis of the static Brillouin space-charge distribution. In this theory, the space charge is constant from the cathode to a distance $t \cong V_a/Bd\,\omega_c$ from the cathode, and is zero the rest of the way to the anode. Electric field, in the Buneman theory, varies from zero at the cathode to the maximum value at the edge of the space charge at distance t, and it is constant from distance t to the anode. Circulating current on the Buneman assumption is

$$I_c = \frac{\epsilon_0 V_a^2}{2Bd^2} \tag{3.18}$$

But Hoag himself has indicated that the circulating current by Buneman's theory is lower, almost by a factor of 3, than the experimental result.[25]

We next try to compare the results of the linear space-charge distribution explained in this paper with the experimental results given by Hoag.

The space-charge distribution from Eq. (3.11) is

$$\rho = -\frac{3\epsilon_0 V_a}{d^3}(y - d)$$

The drift velocity of the electrons is E/B and with the use of Eq. (3.12) becomes:

$$v_d = \frac{E}{B} = \frac{3V_a}{d^3 B}\left(\frac{1}{2}y^2 - dy\right)$$

To find the circulating current, we integrate ρv_d from the cathode to the anode:

$$I_c = \int_0^d \rho v_d dy$$

$$= -\frac{3\epsilon_0 V_a}{d^3}\frac{3V_a}{d^3 B}\int_0^d (y - d)\left(\frac{1}{2}y^2 - dy\right)dy$$

Then

$$I_c = \frac{9\epsilon_0 V_a^2}{8Bd^2} \tag{3.19}$$

By comparing Eq. (3.19) with Buneman circulating current (3.18), we find that the circulating current in the case of the linear space-charge distribution is 9/4 times that of the Buneman result, which more nearly agrees with Hoag's experimental results.

E. CATHODE BACK BOMBARDMENT

Back bombardment of the cathode has been observed by many investigators. Jepsen and Muller[30] have used pure metal cathodes to investigate the secondary emission of the cathode and the maximum current boundaries. In thermionic magnetrons, it is believed that the secondary emission is sometimes as high as 100 times the thermionic emission. These phenomena indicate the existence of a large cathode back-bombardment current. Secondary emission is the principal source of emission in cold-cathode magnetrons used extensively at this Laboratory. In our experiments, P.I.G. action provides the first electrons to start the operation of longitudinal waves and end bombardment. Then in the presence of space charge sufficient for strong turbulence, the back-bombardment electrons produce enough secondary emission to sustain the space charge when drawing large current to the anode.

Most of the secondary electrons return to the cathode quickly, without traveling far into the turbulent region, and their bombarding energy is not great. Unless assisted by ion bombardment, or by injected electrons, or by coherent rf in addition to turbulent fields, the bombarding energy has not been found to be sufficient to cause pure-metal cold cathodes to operate, presumably because for them $\delta < 2$. Metal oxide cathodes with large δ produce sufficient secondaries so that many travel into strong-turbulence regions before returning to strike the cathode. Most of these electrons retain considerable energy when they wander back and strike the cathode. A much smaller number reach the anode, but they have such great energy that the anode heating exceeds that of the cathode.

IV. NOISE AND TURBULENCE

A. INTRODUCTION

The noise problem in magnetrons is one of the most essential. In general, in crossed electric and magnetic field devices, there is usually an excess noise over shot noise and Johnson noise. Some authors[42] have tried to analyze the noise problem in a simple configuration, the planar, beam-type, nonreentrant cross-field device. But even in the simplest case there is no agreement about the noise problem between various authors. Our case, a cold-cathode magnetron, is a more complicated one. The beam does not flow laminarly. There is secondary emission, which depends upon turbulence; and the beam is circulating around the anode. Therefore, any noise has already built up into turbulence.

As a matter of fact, the noise in our type of cold-cathode magnetron is the basis of its operation. Without noise, or some type of oscillation, no electron can reach the cathode to make secondaries, and except for gas collision, no electron can reach the anode. We may say that the violation of Hull's cutoff relation is the result of this turbulence. The exact nature of this turbulence is not known; however, many of its properties are known. What is certain is the presence of some fluctuation that transports electrons to the anode and the cathode randomly. The anode current, the cathode back bombardment, the equivalent temperature, the plasma oscillation, and the excess noise are all manifestations of the phenomenon. Some electrons

gain energy (in our magnetron, about a few kiloelectron-volts), which shows the presence of strong fluctuations in the interaction space. These fluctuations are so numerous that the statistical approach is the only practical way to attack the problem.

In most of our tubes a broadband noise from a few tens of kilocycles to the cyclotron frequency was observed (50 kc to 5000 Mc). In the following pages, some noise mechanisms that may exist in our cold-cathode, long-smooth-anode magnetron will be described. It is understood that not all of these noises may exist simultaneously, but that several of them may be present together.

B. END-TO-END OSCILLATION

The electric and magnetic field form a potential well in which some electrons move from end to end forming two beams, with opposite directions, intimately mixed, giving traveling-wave gain and oscillations. Because of the presence of many random-phase oscillators in the interaction space, some electrons gain energy and strike the cathode at the ends, where the curvature of the magnetic field causes flux to pierce the surface (Fig. 16), as is explained in Sec. II. In the case of a high-secondary-emission cathode, then, more secondary electrons come from the ends that build up the space charge and may cause arcing, but more properly start oscillations in the transverse drift beam, which in turn causes turbulent diffusion to electrodes.

C. RELAXATION OSCILLATION

Because of the impedance of the outside circuit, if any momentary increase due to some instability occurs in the anode current, the

anode voltage falls. This fall may amplify the instability and more current goes to the anode. This process may continue until a non-linearity or the space-charge limitation stops the process. The frequency of relaxation oscillation in our tubes varies from 50 to 500 kc. A capacitor between the anode and cathode reduces or stops this relaxation oscillation. The relaxation oscillation may be caused by: (1) end-to-end motion of electrons in the case of a high secondary-emission cathode; (2) P.I.G. discharge in the case of a low secondary-emission ratio and presence of gas; (3) the instability in plasma, explained in Sec. IV-H.

D. CIRCUMFERENTIAL OSCILLATION

If, somehow, the drifting space charge becomes bunched, this bunch, in rotation around the anode, produces the so-called circumferential oscillation. This bunch rotates around the anode with the drift velocity $v_d = E/B$, where E is the electric field and B is the magnetic field in the interaction space. Furthermore, there is always some eccentricity in the anode with respect to the cathode, and inhomogeneity in the magnetic field. Therefore, the electron bunch, in rotation around the anode, cannot remain exactly on an equipotential surface. Deviations induce a current in the external anode circuit. If there is just one bunch rotating around the anode, the frequency may be found easily. For the aluminum cathode, with a spacing of about 1 cm, anode voltage $V_a = 10$ kv, B = 1000 gauss, and the cathode circumference equal to 45 cm, the circumferential frequency is about 20 Mc. In our experiments, for different situations, this frequency

changes from a few megacycles to about 30 Mc. The amplitude of this oscillation is related to many different parameters, but usually it is in the range of a 100- to 500-v change in anode potential.

Some experiments have shown a close dependence between this oscillation and the voltage variation due to the relaxation oscillation. Figures 44 and 45 show the circumferential oscillations modulated on the relaxation oscillations. The interesting point is that the maximum of circumferential-oscillation modulation of anode voltage occurs when the anode voltage is changing most rapidly. The anode-voltage fall indicates the flow of some of the space charge to the anode, and at the same time the circumferential oscillations are observed.

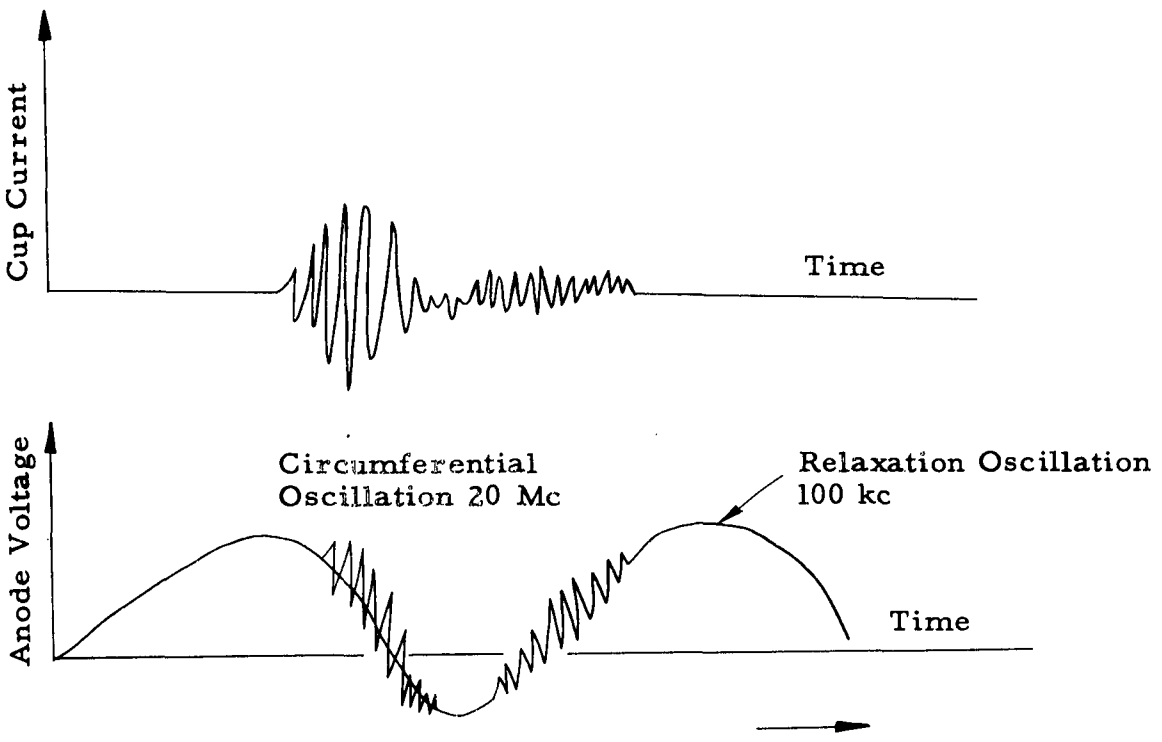

FIG. 44.—Sketch of the anode voltage and cup current variations against time.

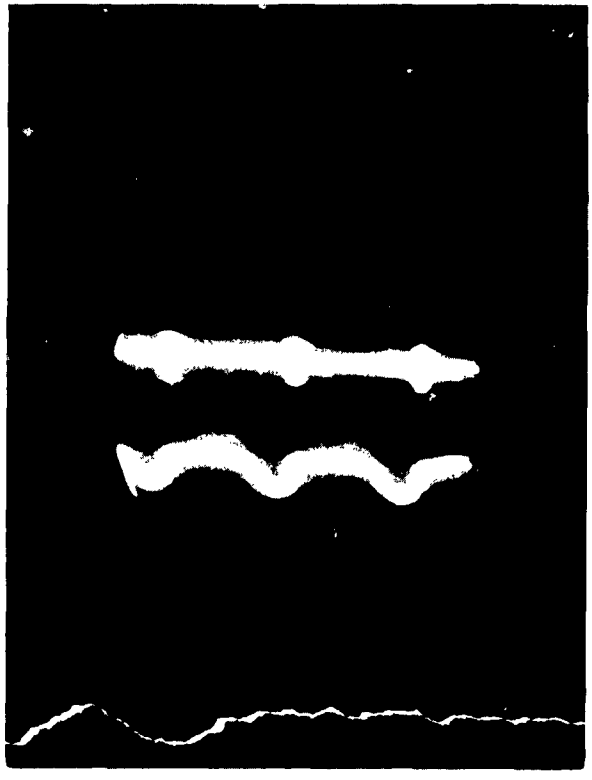

FIG. 45.—Photograph of the oscilloscope screen (2 μ sec/cm). Above is the cup current, below is the anode voltage; V_a = 30 kv, B = 625 gauss, p = 3 x 10^{-5} mm of Hg, d = 1 cm.

The oscillation of the cup current was also measured by oscilloscope. Figure 31 shows the location of cup, outside the cathode, to measure the collected energetic electrons. At the same time, the relaxation oscillation and the circumferential oscillation have effects on the cage current. In the top of Figs. 44 and 45 the cup current is shown, and the anode voltage variation is shown at the bottom. Figure 44 is a sketch from many tests. Figure 45 represents just one case. (The time changes from right to left in

Fig. 45.) It is seen that the cup current is a maximum in the time of the voltage fall. Sometimes the same cicumferential frequency, observed on the anode voltage (20 Mc), is observed on the cup current, too. This shows that, when the anode voltage is changing, probably some of the rotating bunch is driven toward electrodes; therefore, the circumferential oscillation makes bigger changes in anode voltage, and also more of the axially moving electrons are driven to the cathode ends and on into the cups, as well as adding secondary electrons to the total space-charge current.

E. CYCLOTRON FREQUENCY

An antenna was placed near the anode and the spectrum of the cyclotron frequency and some of its harmonics were observed. When the relaxation and the circumferential oscillations are coupled out stronger, the cyclotron oscillation appears stronger, too.

F. OSCILLATION DUE TO THE SPACE-CHARGE CURRENT

A space-charge density of about 10^{10}-10^{11} electrons/cm^3 exists in most of the cases in our experiments. The drift velocity, for the practical voltages and magnetic fields with the aluminum cathode, is about 10^9 cm/sec. Due to this rotational charge, usually a circulating current (Eq. 3.19) of about 50-100 amp is present. The magnetic field due to this circulating current, in our case, is about 5 gauss and in the direction of the original magnetic field. When, due to a turbulence, the space charge starts to increase, the circulating current and magnetic field increase. The increase of the

magnetic field compresses some of the space charge to the anode, so that the circulating current and, therefore, the magnetic field decrease. This process may cause an oscillation. The change of the magnetic field pushes the space charge back and forth between the anode and cathode, and may contribute to the relaxation oscillation discussed in Sec. IV-C.

G. PERIODICITY OF ELECTRON BUNCH: CYCLOTRON SYNCHRONISM

When space charge builds up, the Brilouin-flow state may almost be reached. From the discussions in Sec. I, it is understood that the ideal laminar flow of the Brillouin state is very difficult or impossible to reach, but in some circumstances, the flow may get close to the Brillouin state.

Figure 46 shows a situation close to the Brillouin flow, where electrons start from point N close to the cathode and get close to the anode in one cycloidal motion, but the length of the cycloidal trajectory is as long as the cathode circumference, so that the flow looks almost like a laminar flow. In this situation, when a bunch moves toward the anode and the cathode, in each drift rotation, it changes the anode current and causes current oscillation.

In general, it is possible that for some special electric and magnetic field, the electron bunch gets closer to the anode n times in each rotation around the anode. In this case the electrons rotate n + 1 times in their cycloidal motion around the anode. The one extra rotation is because of the one rotation around the anode. In Fig. 47, the point P will go to P' after one cyclotron rotation and go

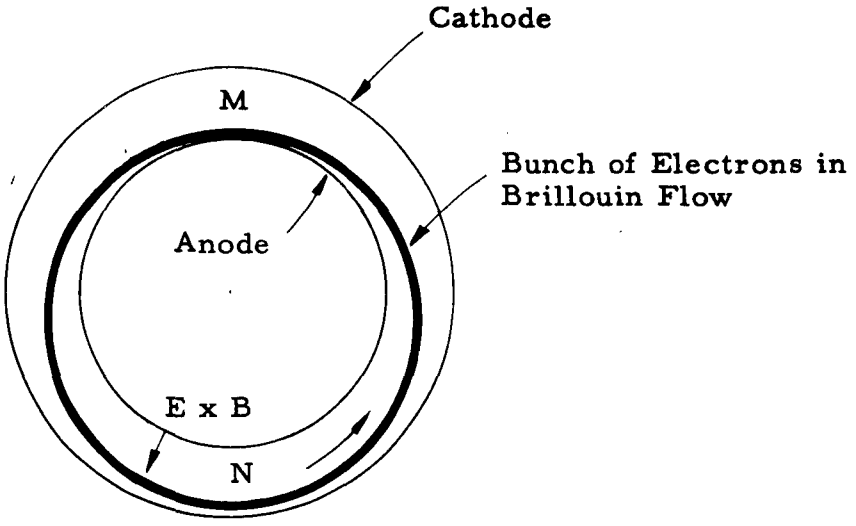

FIG. 46.—Electron motion in the "almost-Brillouin" flow.

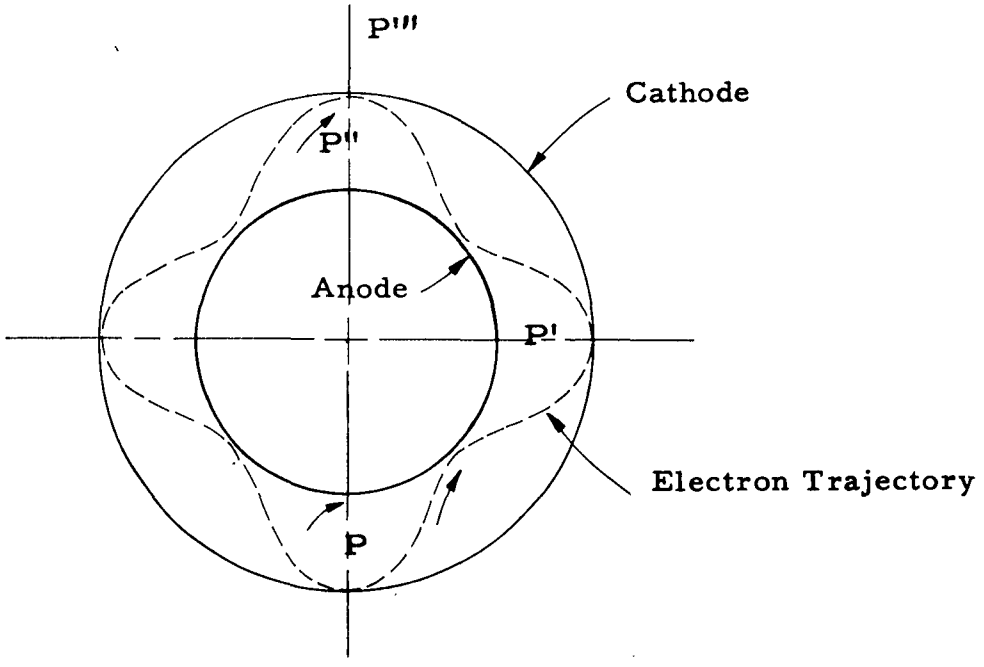

FIG. 47.—Electron trajectory with four fluctuations. This figure shows where electron flow gets close to the anode four times in each rotation around the anode. Integers from one to seven have been observed with a stainless-steel cathode.

to P" after two cyclotron rotations; then electrons at P" must rotate another 180° to be at the cathode at point P"' .

H. OSCILLATIONS DUE TO THE PRESENCE OF IONS

At low electric field, there is possibility of the accumulation of ions. At higher electric field, ions will go to the cathode almost in a straight line, because the radius of the ion gyration $2ME/eB^2$ is very large, where M is the ion mass. But at low electric field, near the cathode, some ions can have a radius small enough to stay in the interaction space. In Fig. 48, if an ion created at radius r happens to graze the cathode, then all those ions created at closer distances to the cathode have smaller radii and remain in the plasma. Therefore, the interaction space will be limited to the

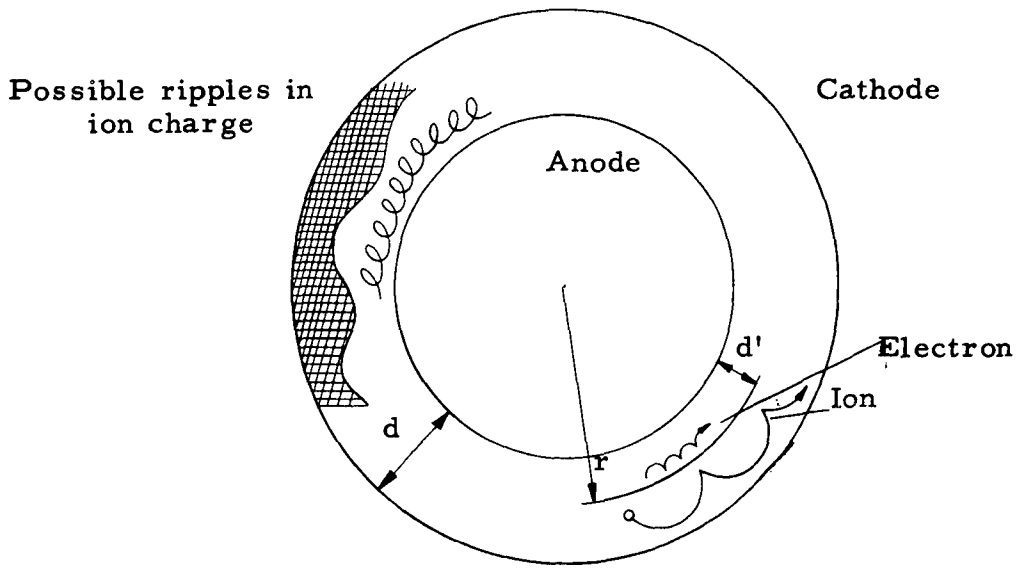

FIG. 48.—Showing the possibility of accumulation of ions and the predicted ion charge ripples.

new spacing d' which is smaller than d. The ion drift velocity is slower than the electron drift velocity in the interaction space, because the electric field acting on ions is smaller. The electron stream moves with respect to the ion stream similar to two beams with different velocities. Therefore, slipping-stream oscillations may result which make ripples in the surface of the ion cloud. When the surface of the ion cloud has ripples, the electron beam in the interaction space will be forced to get closer or farther from the anode, in its drift rotation. If a bunch or electron cloud is rotating around the anode due to these ripples, fluctuations result in the anode current and produce oscillation.

It is important to note that this process occurs when the Penning discharge has the dominating role, in which case the anode current is very small. Let us consider the three regions of the characteristic curve, Fig. 49.

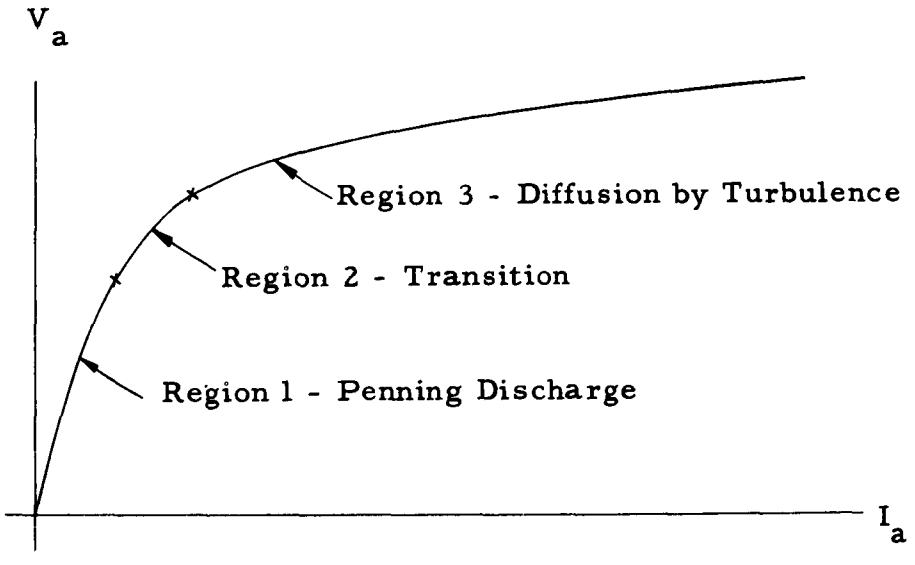

FIG. 49.—Three distinct regions of the V_a—I_a characteristics.

In region 1, electrons are produced by gas collision and by secondary emission due to primary-ion bombardment. The anode voltage and electric field are still small and the ion-cyclotron radius, especially near the cathode, is small, so that some ion charge might be present near the cathode. The ions and electrons in a layer near the cathode make a neutral plasma so that the effective spacing will not be d, from the cathode to the anode, but d' from the plasma surface to the anode (Fig. 48). The distance d' changes with various parameters, such as the magnetic field B, the anode voltage V_a, and the gas pressure p. The relationship between B and d' is Bd' = constant for any specified state of operation. Therefore, we may assume that d' changes as 1/B.

Electrons diffuse the distance d' across the magnetic field by gas-collision diffusion. An electron moves in a cycloidal trajectory with the cycloidal diameter equal to $2r = 2mE/eB^2$, and after each collision, it goes another step toward the anode. On increasing B and the step size get smaller proportional to $1/B^2$, and the electron flow toward the anode is reduced by $1/B^2$. Therefore, the diffusion coefficient[43,44] in the interaction region (spacing d') changes also. To show this fact, let us assume that B is increased; then d' decreases as 1/B, and with constant anode voltage, V_a, the charge density ρ increases proportional to $1/d' \sim B$, and the electric field E increases as $V_a/d' \sim (V_a B)$ or proportional to B. Therefore, the drift velocity $v_d = E/B$ remains constant and the circulating current $I_c = \rho d' v_d \sim B(1/B)v_d$ does not change. On increasing B, the circulating electrons and the number of their collisions with gas atoms of

constant density remain constant, but the diffusion coefficient decreases by a factor of $1/B^2$. However, the spacing d' is also reduced by a factor 1/B, and electrons have a shorter distance to go to the anode; or decreasing $d' \sim 1/B$, causes the anode current to tend to increase proportional to B. Therefore, by considering the reduction of d' and the diffusion coefficient $D \sim 1/B^2$, the anode current reduces as $B(1/B^2) = 1/B$. Then in this case, although the diffusion coefficient is proportional to $1/B^2$, it appears to change as 1/B because the distance changes also.

Noise in region 1 varies in randomness which decreases as region 2 is approached. Figure 50 shows the anode voltage for the top part of region 1 with dc anode voltage increasing from the top to bottom traces.

In region 1, the form and the frequency of the noise are related to the gas pressure. At higher pressure the periodic curves of Fig. 50 are sinusoidal and the frequency of sinusoidal oscillations changes with pressure as is indicated in Fig. 51. The frequency, according to Fig. 51, is linearly related to the pressure, but as is indicated in the figure, below and above a limited pressure range, the sinusoidal oscillations stop and other random types of noise with smaller amplitude start.

It is believed that the ion cloud exists near the cathode, in region 1, and as the anode voltage is increased, the thickness of the ion cloud decreases; in region 2, the ions have disappeared.

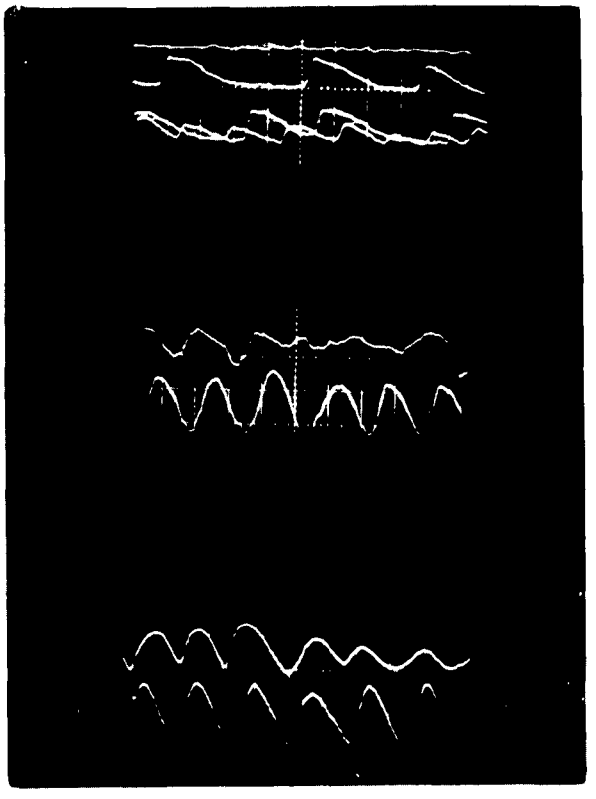

FIG. 50.--The anode voltage oscillation in the top part of region 1. (Scale: 1 cm = 5 sec.) Aluminum cathode, smooth long copper anode (d = 1 cm), B = 600 gauss, P = 10^{-4} mm of Hg.

With increase in gas pressure, in Fig. 51, the number of ions created by electron-gas molecule collision increase. The thickness of the ion cloud increases and, due to some instability, the plasma "blows up," charges travel to the electrodes and the process starts again. If the gas pressure is greater, the ion cloud builds up sooner and the frequency of instability is greater. This might be the reason for the linear dependence of the oscillation frequency in region 1 with pressure indicated in Fig. 51.

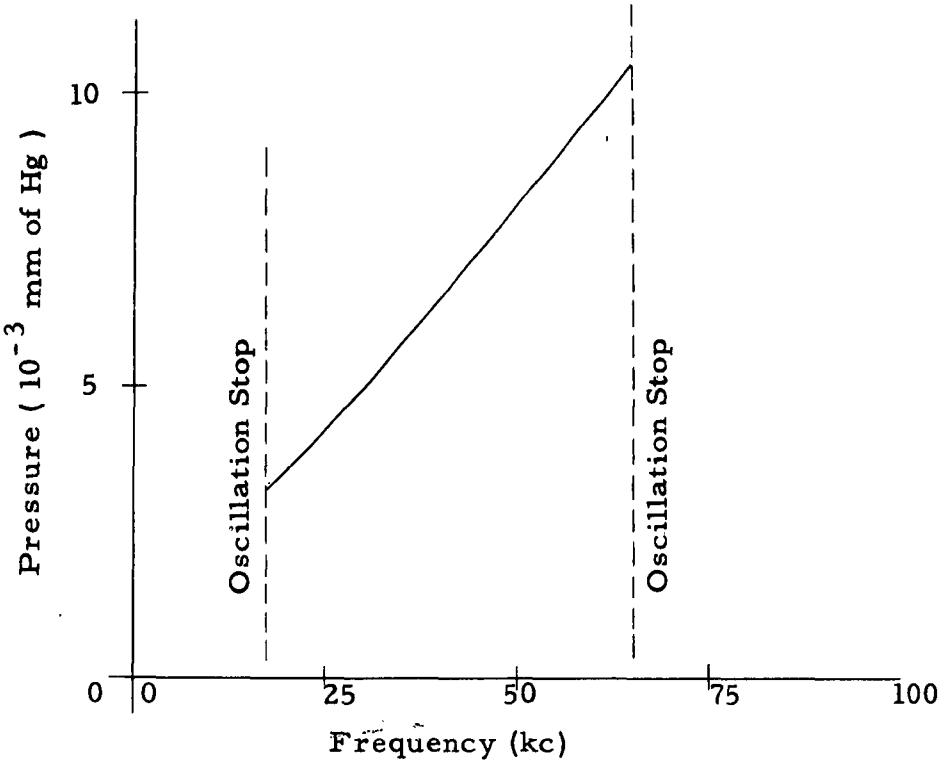

FIG. 51.—Variation of frequency with pressure in region 1.

The plasma instability explained might be the reason for the negative-resistance relaxation oscillation which was explained in Sec. IV-C by the effect of the secondary emission from the ends. When turbulence in the plasma starts to build up, more current is drawn to the anode, and due to the impedance of the outside circuit, the anode voltage falls. When the anode voltage decreases, the thickness of the ion cloud or the thickness of the neutral plasma increases, which helps the turbulence to grow more, so that more anode current and anode voltage fall results. The process continues until most of the charges go to the electrodes and the turbulence stops. The frequency of repeating this turbulence is proportional to

the gas pressure. When the turbulence is finished, the anode voltage starts to rise according to the time constant of the outside circuitry. Figure 52 (similar to Figs. 44 and 45) shows the anode oscillation with respect to time. In time τ_1 turbulence builds up and the anode voltage falls continuously; τ_1 depends on gas pressure and anode voltage. In time τ_2, the anode voltage rises, and τ_2 depends only on the impedance of the outside circuit. Reducing the impedance of the circuit shortens the time τ_2.

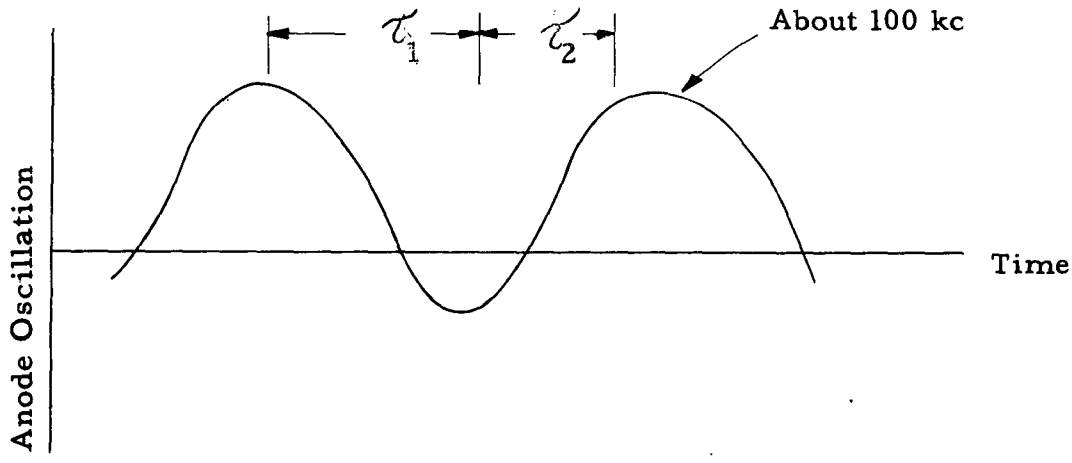

FIG. 52.—Rising and falling of the anode voltage due to the relaxation oscillation.

The instability probably grows from one point in the plasma. This instability, which is similar to a bunch, rotates around the anode with the drift velocity $v_d = E/B$. The frequency of this rotation, as mentioned before, is about 20 Mc. Therefore, the growth of the instability in the plasma is associated with the voltage fall of the

relaxation oscillation (about 100 kc) and the circumferential oscillations (see Figs. 44 and 45). When a convenient capacitor is connected between the electrodes, the relaxation oscillation disappears and the circumferential oscillation is reduced; however, the noise due to the plasma instability still exists, and noise from about 20 to 50 Mc is observed.

When the anode voltage is increased, region 2 of the $V_a - I_a$ characteristic curve (Fig. 49) is reached. This region is a transition between regions 1 and 3. In this region, it is believed that the ions disappear and the thickness of the neutral plasma is zero. Electrons are produced by collision with the gas molecules and by secondary emission at the ends. If the secondary-emission ratio δ is large, then longitudinal electron motion and secondary electrons at the ends are important. In this case a relaxation oscillation (Figs. 44 and 45) may build up on the end-to-end motion of electrons. Contrariwise, if $\delta \leq 1$, the end effect is not important, electrons are produced just by collision, and the Penning discharge is important.

When the anode voltage is further increased this transition region 2 and the turbulence of the region 3 starts. In this region the space charge is large, and the energy of the plasma oscillation in the interaction space is large enough to produce secondary emission. The noise in this region is random, the relaxation oscillation and the circumferential oscillation disappear, Penning discharge is no longer important, and effects related to the drift motion of charges around the anode have the dominating role. Some turbulence starts in

the space charge, electrons diffuse very easily across the magnetic field, and a large anode current is drawn. At the beginning of region 3 the amplitude of noise is small, but it grows with the increase of anode voltage and reaches sometimes to about 50 per cent of the anode voltage. Increasing the anode voltage still further causes an arc and stops the operation. In region 3, electrons diffuse very fast across the magnetic field, which may be explained by the presence of turbulence. Electrons diffuse across the magnetic field according to the buildup time of turbulence, which may be a few tens of times of the cyclotron period $2\pi m/eB$.[21,22,26] In Eq. (3.15), the diffusion coefficient D was defined as

$$D = \frac{\langle \Delta y \rangle^2}{\tau}$$

where Δy is the random step walked by an electron after each collision which is a fraction of the cycloidal diameter $2mEv/eB^2$, where $0 < \nu \leq 1$. Therefore, the diffusion coefficient in region 3 is

$$D \sim \frac{E/B^2}{1/B} = \left(\frac{E}{B}\right)^2 \frac{1}{B}$$

But E/B = constant for a given cathode material, according to many data, and the diffusion coefficient in region 3 is

$$D \sim \frac{1}{B}$$

In region 1, the diffusion coefficient is proportional to $1/B^2$, but because the spacing d' changes, it varies as $1/B$. Therefore, if we double (for example) the magnetic field the over-all diffusion coefficient is sufficient for the whole V_a-I_a curve, as far as its functional relation to B is concerned.

J. SLIPPING-STREAM OSCILLATION

This type of oscillation is suggested by many authors; MacFarlane and Hay[20] and Buneman[21,22] are perhaps the most important ones. They have shown theoretically that any perturbation grows in a laminar flow or Brillouin state. The spectrum of possible noise is also found. The frequency of the turbulence due to slipping-stream instability is a broad band of about 1/5 to 1/150 of the cyclotron frequency. In this band of frequency, also, strong random noise is observed, which is probably due to the random recurring of the slipping-stream oscillations.

K. PLASMA OSCILLATION

In Sec. III, it is assumed that the space-charge distribution is linear, from the cathode to the anode, when instabilities or space-charge fluctuations exist in the interaction space. On the assumption of the linearity of the space-charge distribution, it is unlikely that the plasma frequency f_p and the cyclotron frequency f_c should be equal, because the space charge is distributed all over the interaction space and the charge density is perhaps nowhere sufficient to make $f_c = f_p$. However, just before the turbulence starts, when the electron flow is close to the Brillouin state, the charge density in the Brillouin layer might be enough to make the plasma frequency ($\omega_p = \sqrt{e\rho_0/m\epsilon_0}$) very close to the cyclotron frequency ($\omega_c = eB/m$).

It is experimentally observed that when the plasma frequency gets close to the cyclotron frequency, the amount of noise grows. This suggests some type of relationship between the cyclotron and plasma frequencies. Some mechanism may be found to explain the relationship. It is possible that the plasma oscillation along the magnetic field increases resonance exchange of energy with some bunch of electrons in their cyclotron motion. This resonance exchange of energy between plasma and cyclotron oscillations causes the gain of energy by electrons from the dc field. As increased electron density causes ω_p to approach ω_c the waves grow faster and reach larger amplitude before breaking, and new wave growth starts again, quicker. Thus electrons are randomly displaced in all directions across the B flux, at a rate than increases fast enough to prevent ω_p from becoming equal to ω_c.

L. MINIMUM STARTING VOLTAGE AND CROSS-FIELD SPACE CHARGE

It is found that the space charge in the interaction region bunches most easily when the space-charge wavelength is approximately equal to the electrode spacing, as division of the space into these proportions gives greatest freedom from image charges and neighboring bunches. If the spacing between the cathode and anode is d, and λ is the preferred wavelength of a bunch, then $\lambda \approx d$, independent of velocity. Electrons drift through these square regions with drift velocity $f_d = E/B$ and random drift frequency $f_d = f_d/\lambda$. For the minimum starting voltage (MSV), $f_d = f_c$, where the f_c is the cyclotron frequency, and the size of bunch fits almost in a cycloidal trajectory. In this case, a special situation may occur: the plasma frequency f_p is uniform throughout and gets close to the cyclotron frequency f_c. As a result $f_d = f_c = f_p$. For this MSV situation, the Hull cutoff radius and the maximum current boundary both occur close together, and the ratio E/B can not be increased. On the other hand, $v_d = E/B$ can not be decreased because the necessary minimum of back bombarding energy is assumed in this lowest case. Bombarding energy varies with $(E/B)^2$ which changes only to meet the requirements of various δ. For aluminum and magnesium cathodes, δ is quite high and the MSV condition may happen easily. If the δ for some cathode materials is not high enough, a higher gas pressure may help to provide electrons for the MSV condition $f_d = f_c = f_p$.

There is another condition, Bd = constant, for any specified state of operation; B and d are tied together by this condition and

by the relation $f_c = f_d$. Therefore, many conditions must be satisfied in order that the MSV situation $f_d = f_p = f_c$ is satisfied. In Fig. 53, the V_a—I_a characteristic curves for different magnetic fields B are sketched. For a value of B below B_H, Hull's cutoff magnetic field for

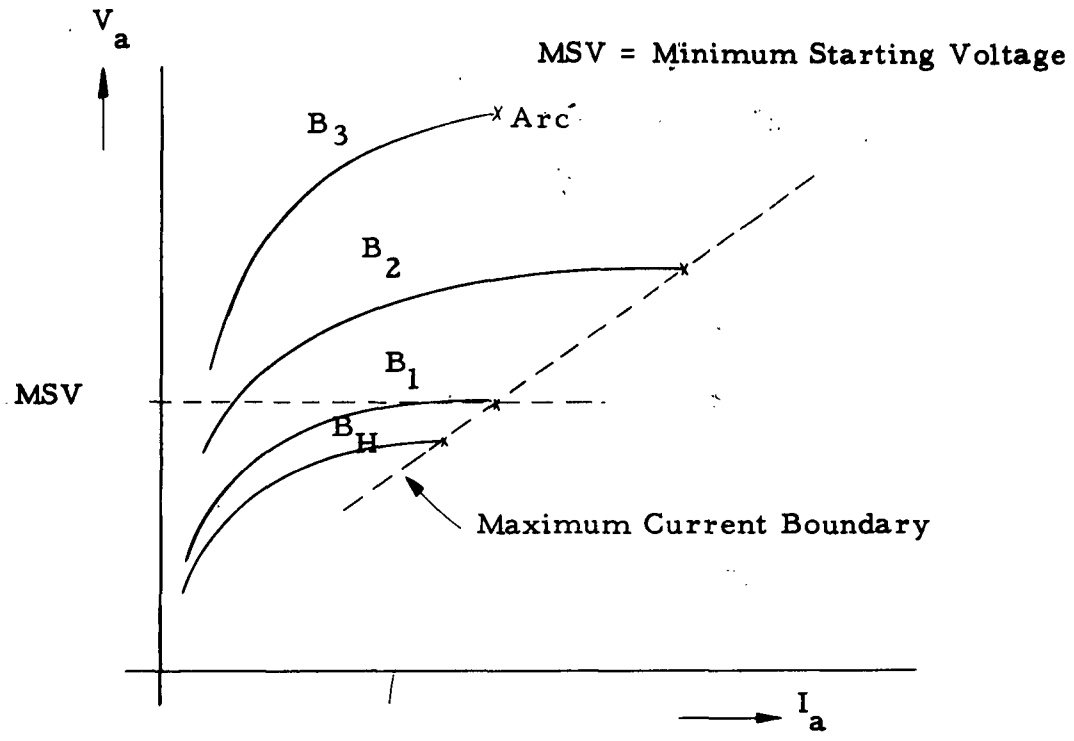

FIG. 53.—V_a—I_a characteristics and MSV.

some voltage V_a, the tube does not start, because E/B is large, and $f_d > f_c$. When B reaches B_1 in Fig. 53, $f_d = f_c$ and B_1 is almost equal to B_H, and the tube starts to oscillate. While the tube is oscillating, it is possible to decrease the magnetic field to B_H and operate at $f_d > f_c$.

When the magnetic field is increased to B_2 and B_3, f_c increases, but because E/B is almost constant there, f_d remains constant and the tube operates easier with $f_c > f_d$, because of slower diffusion and more adequate space charge. In this case, however, most of the charge is compressed near the cathode, and due to increased end bombardment, the tube arcs at lower anode current.

In all cases $\lambda = d$ is conserved. In our experiments with smooth anodes, we have generally worked in the range of $f_c = 1$ to $10f_d$ and the condition $\lambda = d$ satisfies our data. Aström[45] has also investigated this problem, and, with $f_c \approx 20f_d$, he reached the conclusion that $\lambda = d$.

In the rf case with a slow-wave structure, the situation is a little different. This difference is shown in Figs. 54 and 55. In Fig. 54, bunches fill the space and they repeat at each $\lambda = d$. The smooth anode, in this case, appears to have an equivalent circuit frequency of f_d, and when $f_d = f_c$, then MSV conditions exist and the system is more efficient; however, for $f_c > f_d$ the tube works easier.

In Fig. 55, a bunch is split: one half is retarded by the rf field and joins the succeeding bunch, and the other half is accelerated and reaches the preceding bunch. Then, in this case, the location is vacant, resulting in $\lambda \approx 2d$.

In slow-wave-structure anodes, f_d, the frequency of drift through bunches, should synchronize with f_s, the frequency of the slow-wave structure. The most efficient case is when $2f_s = f_c = 2f_d$; however, at $f_d > 2f_s$ the tube works easier if it depends upon secondary

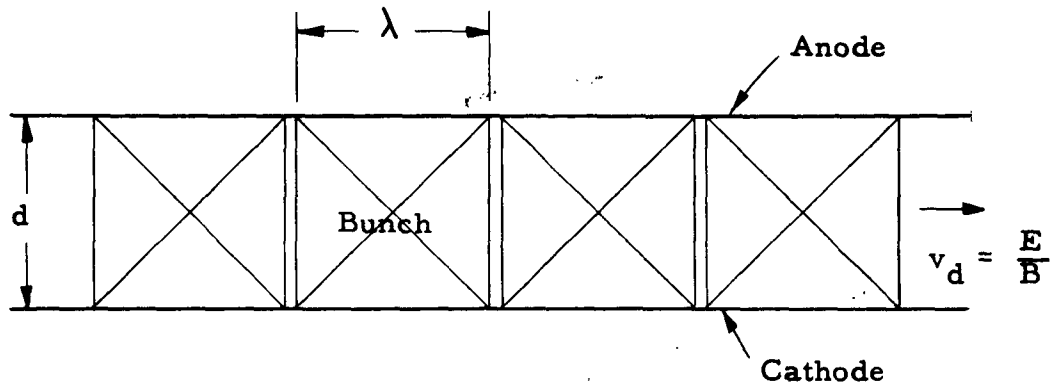

FIG. 54.—Bunches in a smooth-anode configuration, where $\lambda \approx d$.

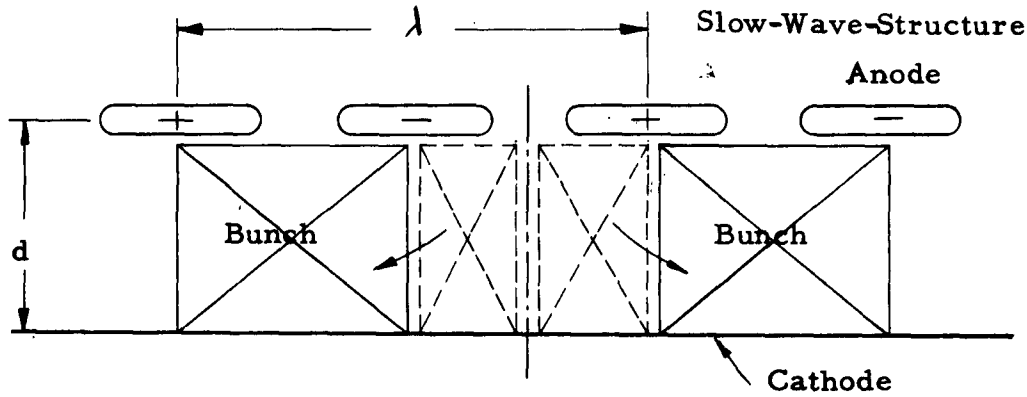

FIG. 55.—Bunches in a slow-wave-structure anode configuration, where $\lambda \approx 2d$.

emission. In our rf experiments, we have worked in a range of $f_c = 2f_s$ to $f_c = 20f_s$; some of the results are given in Sec. V.

M. BUNCH SIZE WHEN ONLY A LIMITED NUMBER OF ELECTRONS ARE AVAILABLE FROM GAS

The oscillation wavelength explained above is suggested also in an entirely different group of experiments of which the following is one example. Gas electrons are used instead of secondary electrons. In a long smooth-bore copper cathode and copper anode tube with 2.23 cm spacing, pressure about 10^{-4} mm of Hg, B = 1600 gauss, and anode voltages of 16, 20, and 25 kv, strong noise was observed such that neon bulbs located a few feet distant from the anode lead were lighted by the high-frequency field radiated. Below $V_a = 14$ kv, the space charge was probably not sufficient to make a sufficient rotating bunch for strong oscillation. Above $V_a = 30$ kv, this type of oscillation could not be detected because of the presence of many other types of noise and oscillation. The voltages 16, 20, and 25 kv are proportional to reciprocals of 6, 5, and 4. Furthermore, the noisy bands of oscillations observed at these voltages have about the same frequency and all occur within a narrow voltage range (about 1 kv). All of these results suggest some type of periodicity of beam trajectory in the system, where the periodicity changes inversely proportional to the voltage, V_a, or the drift velocity, $v_d = V_a/Bd$.

There is negligible secondary emission from copper, and insufficient space charge to make slipping-stream gain greater than unity except by a re-entrant chain of waves. Moreover, the frequency of drifting through these wavelengths appears to be the same as some fixed structural resonance of rather low Q, and about 100 Mc.

Turbulence diffusion can occur only if it does not seriously deplete the available supply of space charge. This diffusion requires more than the above quantity of available gas atoms ionized and striking the cathode and returning to be re-ionized. Voltages above 300 kv caused sputtering so intense that the gas intensity was increased without limit and plenty of electrons became available to sustain turbulent diffusion, until an arc occurred.

This turbulence destroyed the weak oscillations that might have appeared at several higher voltages, extending the series (6, 5, 4 wavelengths, as seen above) to 3, 2, and finally 1 wavelength around the tube. To extend the series the other way, to lower voltage, the same frequency requires shorter wavelength and $\lambda < 2d$, so that turbulence easily occurs instead, aided by the resonance, and dissipates the limited available space charge by diffusion to the anode so quickly that nothing is observed. Although this tube has a unipotential anode, the same criterion, $\lambda < 2d$, for easiest circuit oscillation starting agrees with that developed for segmented anodes. Turbulent diffusion or random bunching, without resonator interaction, starts most easily at $\lambda = d$.

V. RF STRUCTURES

A. INTRODUCTION

The first four sections are concerned with smooth-bore anodes (static magnetrons) and the understanding of the plasma problem in a magnetron, with a view to producing a high-power electron beam. In addition, several rf anodes were made in this Laboratory and tested. A short description and result of each rf anode is given in the present section. The aim is to understand the action of rf anodes whose segments have a pitch p from gap to gap. Although the operation of many of these rf anodes was not satisfactory, we have learned much regarding their operation. We have learned that strongest smooth-bore bunching action occurs within $\lambda = d$. We have learned why the best rf configuration has a spacing d equal to one half of the circuit wavelength 2p (or $p = d$) and bunch wavelength $\lambda = 2d$. It is well known that, for this spacing, the best efficiency is highest when the beam velocity makes a cyclotron trajectory also equal to 2p, or $f_c = 2f_s$ (where f_c is the cyclotron frequency and f_s is the frequency of rf anode); and that the efficiency decreases with departure from the above conditions. If $p = 3d$, the number of bunches must be tripled and $f_c = 6f_s$. All important interaction occurs within a square section distance ($p = d$) measured from the gap centers between anode segments, which in this case includes only a third of the total number of squares that could be drawn in a cross section of the space through which the beam drifts. If $p = n\lambda$ and n is not an integer, the bunches are wider or narrower but an integral odd number must be

associated with a pair of segments.

In our cold-cathode magnetron, the secondary emission and beam velocity are very important. With a low voltage or a low beam velocity, the tube does not start, because of the lack of secondary emission. In a high-voltage beam, the energy of electrons is so high that, due to decreasing secondary emission, the process stops at the maximum current boundary. Therefore, in a cold-cathode magnetron, velocity may be varied only over a smaller range than in a hot-cathode magnetron. In the design of an rf anode, the most favorable beam velocity for the material of cathode, and the conditions of $f_c = 2f_s$ and $\lambda = 2d$, should be met simultaneously for maximum efficiency. Furthermore, we have learned that the back bombardment necessary for secondary emission should be caused by the rf oscillation, not by random fluctuations that excite many other modes simultaneously. To meet this requirement, the starting voltage should be designed such that the synchronous velocity would be reached near the top of the first (straight) part of the V_a—I_a characteristic curve.

The most efficient rf anode, tested here, is the 150-Mc anode. Although we could not measure the absolute power of rf radiation, we could compare the powers and efficiencies for a fixed load.

A mode problem existed in our tubes; several tubes failed because the π mode was close to other complicated modes. Our aim, in all tubes, was operation in the π mode. The calculation of the π mode (or other modes) was very difficult, because of the complicated

configurations. Therefore, cold-test measurements were used to determine the frequencies of different modes.

The rf anodes were also used as probes in studying space charge. By such a probe, and by measuring the rf frequency in the cold test, we could find $\alpha = E_{eff}/E_{ave}$, where $E_{ave} = V_a/d$ and E_{eff} is the effective electric field acting on the beam. This coefficient in our tubes was about 50 to 90 per cent in most cases.

By these probes, we could study the number of bunches within 2p, the wavelength of the rf circuit. In some tubes with suitable dimensions ($\lambda = 2d$), we could sometimes have three bunches and the efficiency was then low. But if the rf bars are wide and flat and close to the cathode, the three bunches within 2p may be very efficient. In most cases, for p = d and one bunch within 2p, $\lambda = 2d = 2p$ is the best situation.

B. THE 150-Mc RF ANODE

The dimensions of this anode are shown in Fig. 56. The anode structure is shown in Fig. 57, and Fig. 58 shows the rf arc produced from a single electrode into space.

The anode has 12 bars, each made from two parallel 3/8-in. copper tubes, flattened and silver soldered together in the 10-cm center part. The bars are watercooled. The cathode is a short magnesium cylinder, continued by two other copper cylinders, and watercooled.

The V_a---I_a characteristic curves are shown in Fig. 59 for various values of magnetic fields. The starting rf oscillations are shown by circles in the figure.

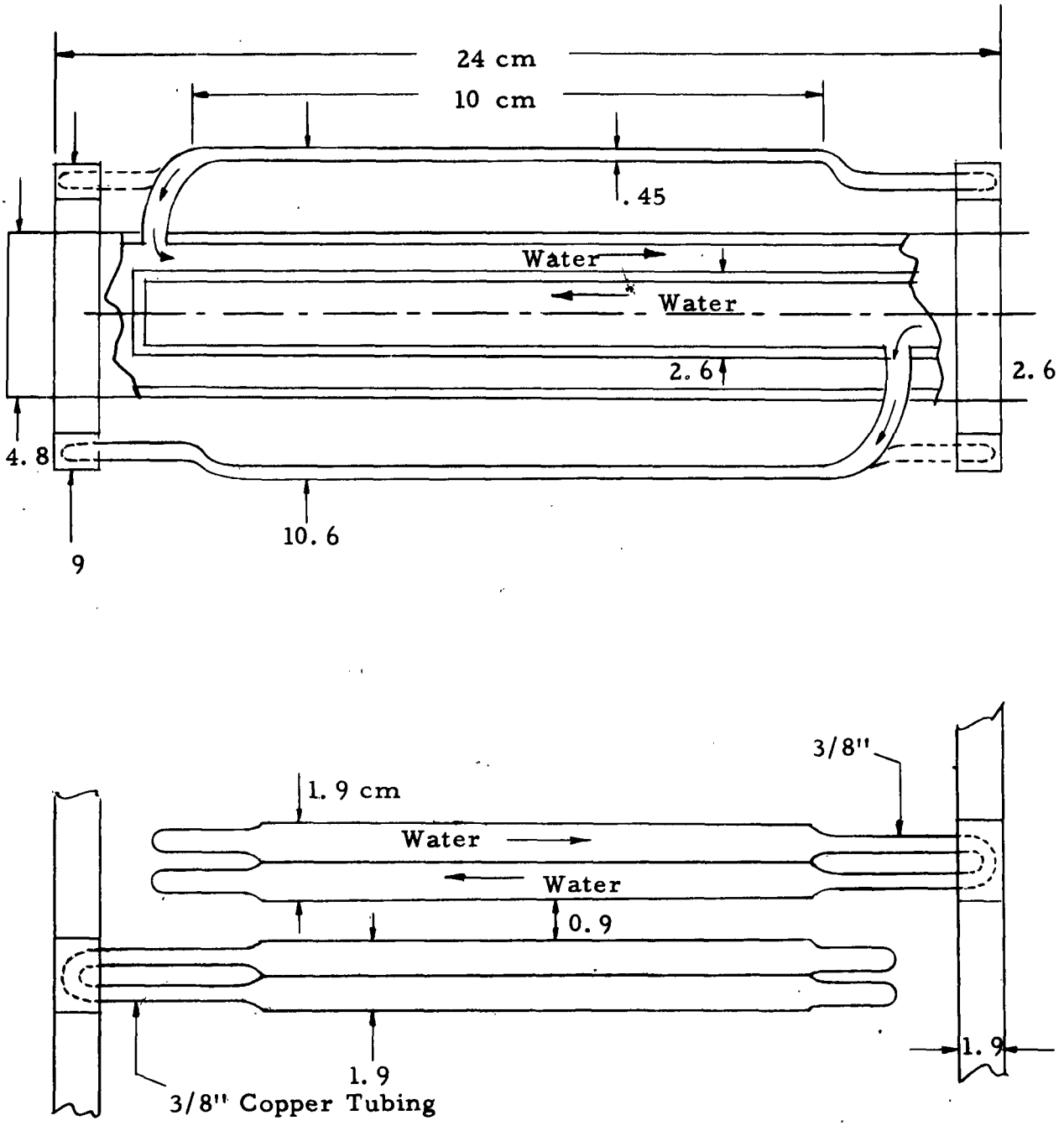

FIG. 56.—The important dimensions of the 150-Mc anode. Each bar has two copper pipes, one connected to the 2.6-cm-diameter outlet water pipe and the other to the 4.6-cm-diameter inlet water pipe. Cathode diameter is 12.6 cm and d ≅ 1 cm.

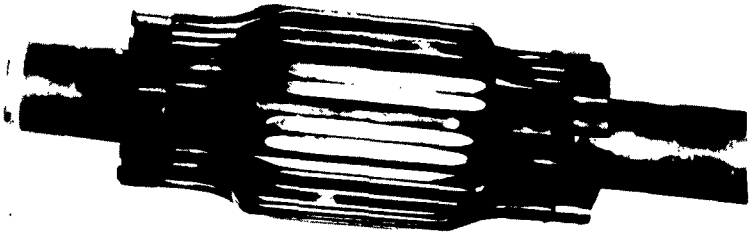

FIG. 57.—The 150-Mc rf anode, 12 bars, water-cooled copper cathode, diameter = 10.6 cm, length in the interaction space = 10 cm.

FIG. 58.— Arc from the top of the 150-Mc anode, sometimes as high as 3 m. The diameter of the rf shield is about 70 cm.

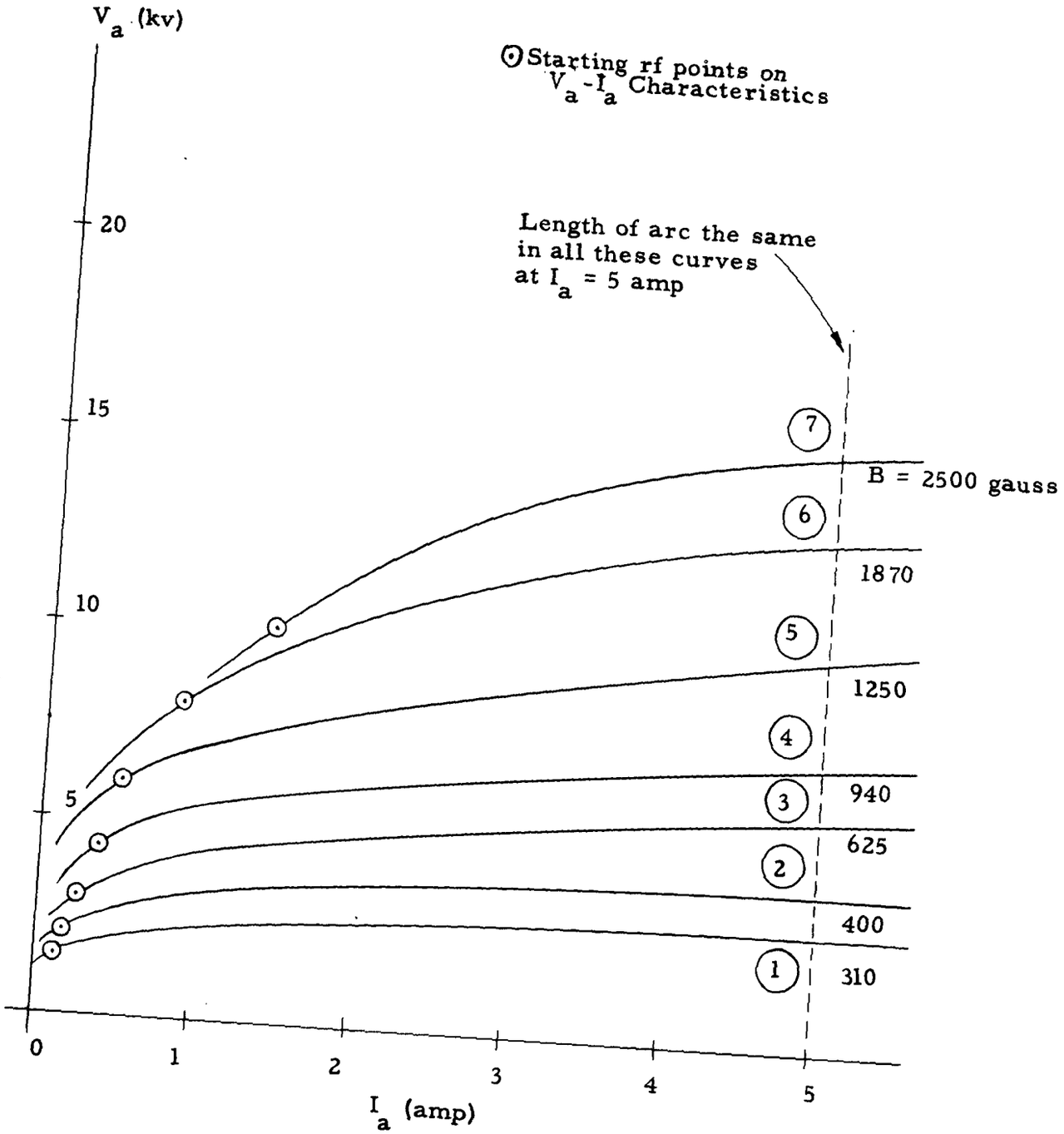

FIG. 59.—V_a-I_a characteristic curves of the 150-Mc rf anode.

This tube worked the best and had no mode problem. As the anode voltage was increased, the rf power was dissipated in an arc into space from a graphite bar, installed at the top of the anode. The length of arc was sometimes more than 3 m, until it reached the ceiling and the anode dc supply was shorted. The diameter of arc was sometimes as great as 5 to 10 cm. The magnesium secondary-emission ratio is large enough to produce high current; however, we could not go higher than $I_a = 8$ amp because of the rectifier limitation (about 100 kw, dc power). It is believed that the tube could work with much more than 100 kw. A pure magnesium cathode has a secondary-emission ratio less than unity and, in order to have a high secondary-emission ratio, it is necessary to make a thin layer of MgO on the cathode surface. It took a few days of operation, in the presence of air and oxygen, to prepare a good layer. Aluminum develops an oxide layer much quicker, but requires more energetic primary electrons, and has lower total yield.

C. VARIATION OF EFFICIENCY WITH MAGNETIC FIELD

We could not measure the rf power directly but, with a constant length of arc above the top of the anode, we could compare the dissipated rf power for various values of magnetic fields. At about $I_a = 5$ amp, the length of the arc was the same for a wide range of magnetic fields; hence we may assume that the output rf power is the same for a wide range of magnetic fields. The circuit automatically matched the impedance in each case. From this experiment, an important

result is obtained, that the efficiency of the tube varies as $1/V_a$ at a fixed current ($I_a = 5$ amp). We could not measure the best efficiency of each curve, for each magnetic field. The best efficiency of the curve for B = 310 gauss is close to the maximum current boundary (I_a of the order of a few tens of amperes). Therefore, the best efficiencies of each magnetic field cannot be directly compared; however, at $I_a = 5$ amp the efficiency at B = 310 gauss is the best, because in this case all bunches are moved outward by rf only and rf reaches deep in the space charge. But in the case of B = 2500 gauss, at $I_a = 5$ amp, most bunching is made by random oscillations and rf field works just on the outside of space charge. Therefore, rf bunches are very small, in this case, and rf efficiency is also small.

In Sec. IV-L, it is explained that in a smooth-anode magnetron, optimum space-charge bunching occurs when the space-charge wavelength approximately equals the electrode spacing, because of the influence of walls on fields due to charges. If a lengthwise section of the drift space were divided into square divisions having length equal to d, the separation distance between electrodes, then for the conditions of lowest starting voltage, each square would contain one bunch. Electrons drift through one of these square regions with drift velocity $v_d = E/B$ and drift frequency $f_d = v_d/\lambda$, where $\lambda \approx d$. But the minimum starting B occurs when $f_d = f_c$, for the required bombarding energy and its associated fixed v_d. With a slow-wave structure of pitch p, however, it was shown that the space-charge bunches again form most easily so that they would fit within square cross sections, but now

alternate squares become empty as the rf increases strength, if $p = d$.

The configuration of the 150-Mc anode is not the best, because $2p \approx 5.6$ cm and $d \approx 1$ cm and $2p/d \approx 5.6$ (instead of 2, which would be optimum for highest frequency). But the beam still drifts through a unit square with a velocity that makes $f_d = f_c$, and presumably $\lambda = d$ for each part of the bunch as it interacts with the circuit electrodes by crossing a gap in one cyclotron period. This occurs within a square centered at a gap. In this case, $f_c \approx 5.6\ f_s$, where f_c and f_s are the cyclotron and the slow-wave structure frequencies, respectively.

We believe that the curve B = 310 gauss, in Fig. 59, corresponds to the best efficiency, because $f_c = 870$ Mc for B = 310 gauss, and $f_c/f_s = 870/150 = 5.8$ which is close to $\lambda/d \approx 5.6$. When starting, in this case a cyclotron trajectory traverses the same part of a bunch at each successive wavelength. If the tube is already oscillating, B can be reduced to about half of 310 gauss, with similar decrease in V, but power output approaches zero.

In the curve B = 2500 gauss (Fig. 59) each bunch occupies alternate distances, p, but $f_c/f_s = 43$ and about $43/2 = 21$ cyclotron trajectories occur in a bunch, where cyclic repetition is meaningless, the bunch cannot be narrow, and efficiency must be less.

D. THE 150-Mc TUBE USED AS A PROBE

There is a problem of measuring electric field inside the interaction space without probe disturbance. In our experiments, the rf tubes were used as probes with a known type of interference with space charge. The probe fixes a frequency f_s and the electron beam

synchronizes with f_s. The effective electric field E_{eff} can be found from the synchronized velocity $E_{eff}/B = f_s \lambda$, and is compared with $E_{ave} = V_a/d$. We designate $E_{eff}/E_{ave} \equiv \alpha$; the variation of α with magnetic field is shown in Fig. 60, for the starting points of characteristic curves of Fig. 58 and the flat parts at $I_a = 5$ amp. At the starting points E_{eff} is about 60 per cent of the average electric field.

More importantly, the starting points are at just 1/2 of the voltage of the flat part of the curves, showing that the action starts when the outer edge of the beam is synchronous, but develops full strength when the middle of the stream reaches synchronism, where E is down to half value. The excess velocity of the outer edge now allows electrons to travel along the longer path around the contour of waves that are set up in the full depth of space charge.

E. THE 105-Mc RF ANODE

The 105-Mc rf anode was used as another probe with a copper cathode. The structure was very similar to the 150-Mc tube. It also had 12 bars, made from 3/8-in. copper tubing. Figure 61 shows the bars when they are cut from one end but still connected to the ring. The dimensions are shown in Fig. 62. This anode was used with several kinds of cathode materials.

The secondary emission of a copper cathode is very low, 1.3 maximum, and to run the tube, it was necessary to let gas in, to have enough electrons from the gas collisions. A graphite rod was installed on the top of the anode structure from which an arc in air

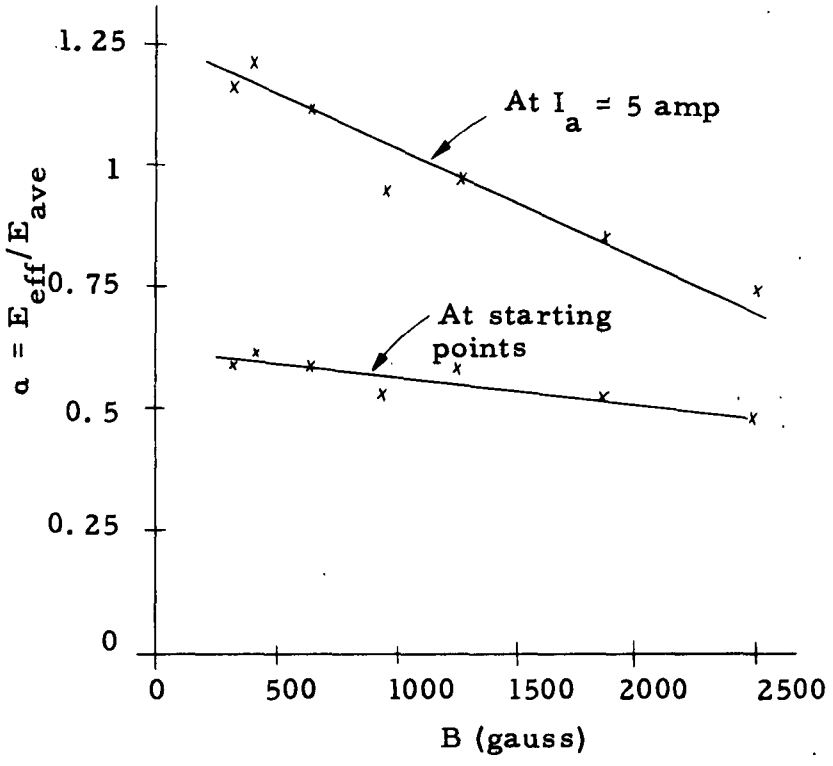

FIG. 60.—The variation of E_{eff}/E_{ave} with B, at rf starting points, for the flat parts of characteristic curves (Fig. 58).

could dissipate rf energy. The maximum length of arc in this tube was about 1 m. The electron source in this case was hydrogen gas with pressure about 10^{-4} - 10^{-3} mm of Hg.

Figure 63 shows the range of voltages for which the beam synchronizes with the slow-wave structure. The mark points in the voltage indicate the average voltages for each magnetic field, when the radiation is maximum. The drift velocity is almost the same in all these indicated points; $E_{eff}/E_{ave} \approx 0.55$ for these curves.

There was no mode problem in the 105-Mc tube, but inadequate cooling-water supply and the low secondary-emission ratio of copper cathode limited a higher rf power operation.

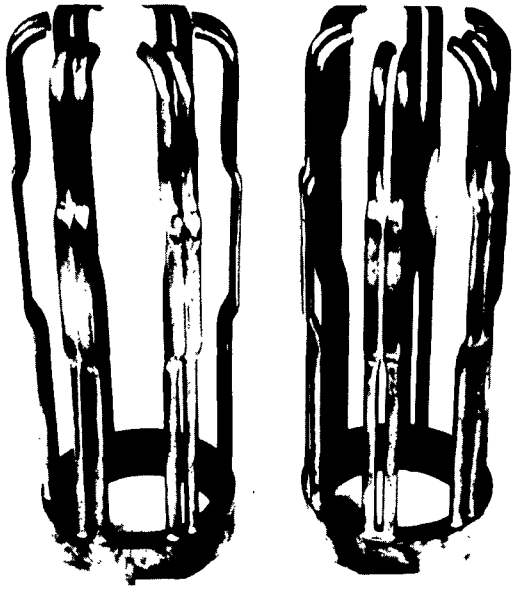

FIG. 61.—Bars of the 105-Mc anode when separated from the central pipe. Each bar is made from two pipes 3/8-in. copper tubing and flattened and silver-soldered in the center part. Two melted points are shown on the bar.

F. THE 400-Mc RF ANODE WITH COPPER CATHODE

The 400-Mc rf anode is shown in Fig. 64, and the dimensions in Fig. 65. This tube did not work well with the copper cathode, because of insufficient secondary emmision. Most of the electrons were created by collision with gas molecules at pressure about 10^{-4} mm of Hg. Radiation at 400 Mc was observed at 16 kv, 24 kv,

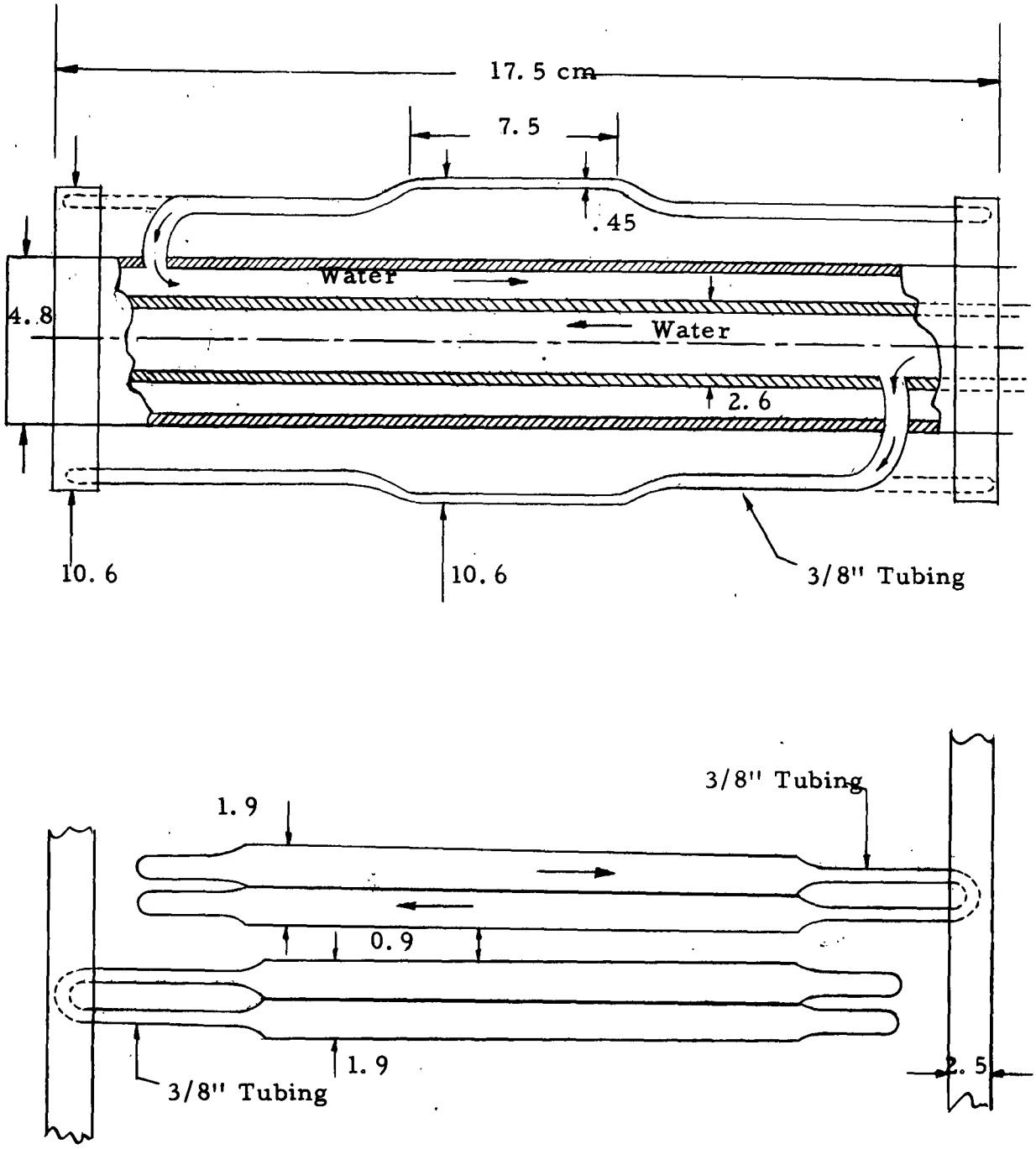

FIG. 62.—Dimensions of the 105-Mc anode. Water circulation is similar to Fig. 56. Tube has 12 bars, each made from two pipes of 3/8-in. copper tubing; $\lambda = 5.6$ cm, $d = 1.75$ cm, and the copper cathode diameter is 14.1 cm.

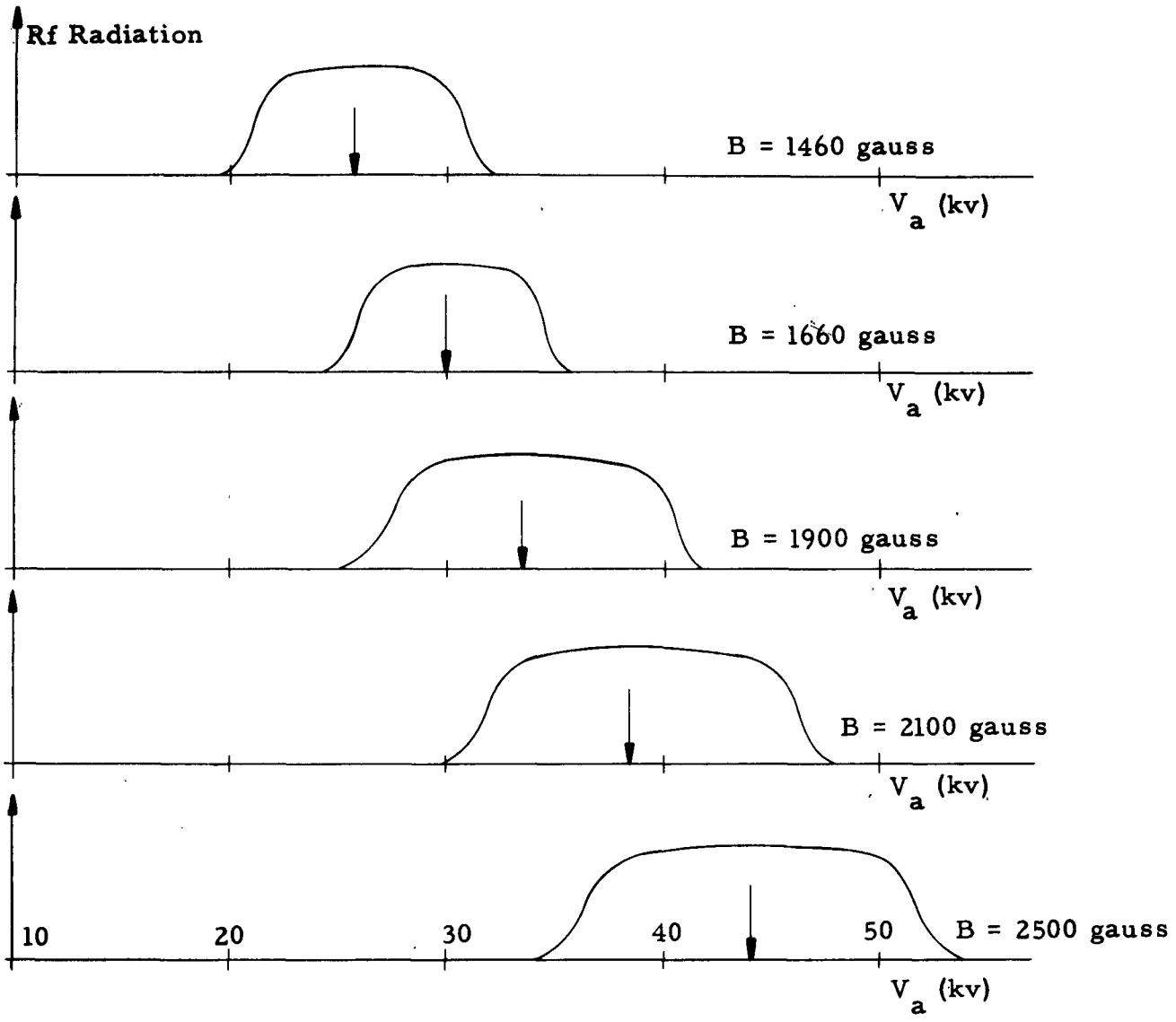

FIG. 63.—The rf radiation of the 105-Mc anode with different magnetic fields. Arrows show the average anode voltage for each magnetic field.

and 38 kv·$\alpha = E_{eff}/E_{ave}$ may be assumed to be about 60 per cent in comparison with the previous tubes. The drift velocity E_{eff}/B should synchronize with 400 Mc. But at V_a = 38 kv, B = 1700 gauss, α = 0.6, and d = 1.75 cm, the drift velocity is

$$v_d = \frac{\dfrac{38000}{1.75 \times 10^{-2}} \times 0.6}{1700 \times 10^{-4}} = 7.65 \times 10^{6} \text{ m/sec}$$

FIG. 64.—The 400-Mc anode.

and with 2p = 5.7 cm, this drift velocity synchronizes with 400 Mc of the slow-wave structure, only if there are three bunches within 2p, because

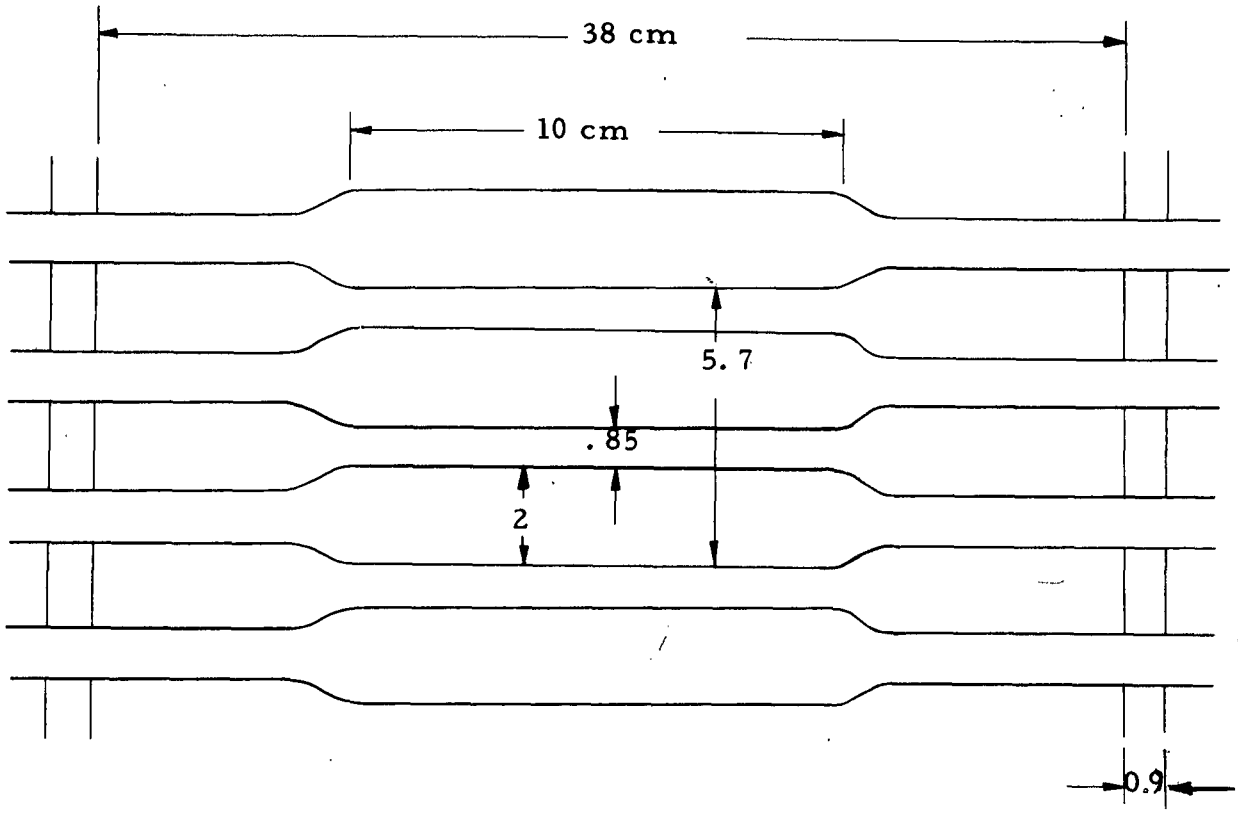

FIG. 65.—Dimensions of the 400-Mc anode. There are 12 flattened bars from 5/8-in. copper tubing. The diameter of the anode is 10.6 cm, the copper cathode is 14.1 cm, the spacing d = 1.75 cm, and 2p = 5.7 cm.

$$3\,\frac{v_d}{\lambda} = 3 \times \frac{7.65 \times 10^6}{5.7 \times 10^{-2}} = 400 \text{ Mc}$$

For V_a = 24 kv and B = 1700 gauss, there are five bunches within λ, in order to synchronize with 400 Mc. There are also seven bunches within a wavelength for V_a = 16 kv.

In these cases, bunches are very small, just on the top of the space charge, so that the rf power is very small. In order to have one

large bunch within λ, the anode voltage should be increased to about 110 kv which was not feasible in our experiment.

G. THE 400-Mc ANODE WITH MAGNESIUM CATHODE

The magnesium cathode was used with the 400-Mc anode to provide more current and more rf power. With the magnesium cathode, there was more anode current, but a new problem of mode interference arose. Figure 66 shows the V_a — I_a characteristic curve of the 400-Mc anode with the magnesium cathode. Two modes at 395 and 440 Mc were observed.

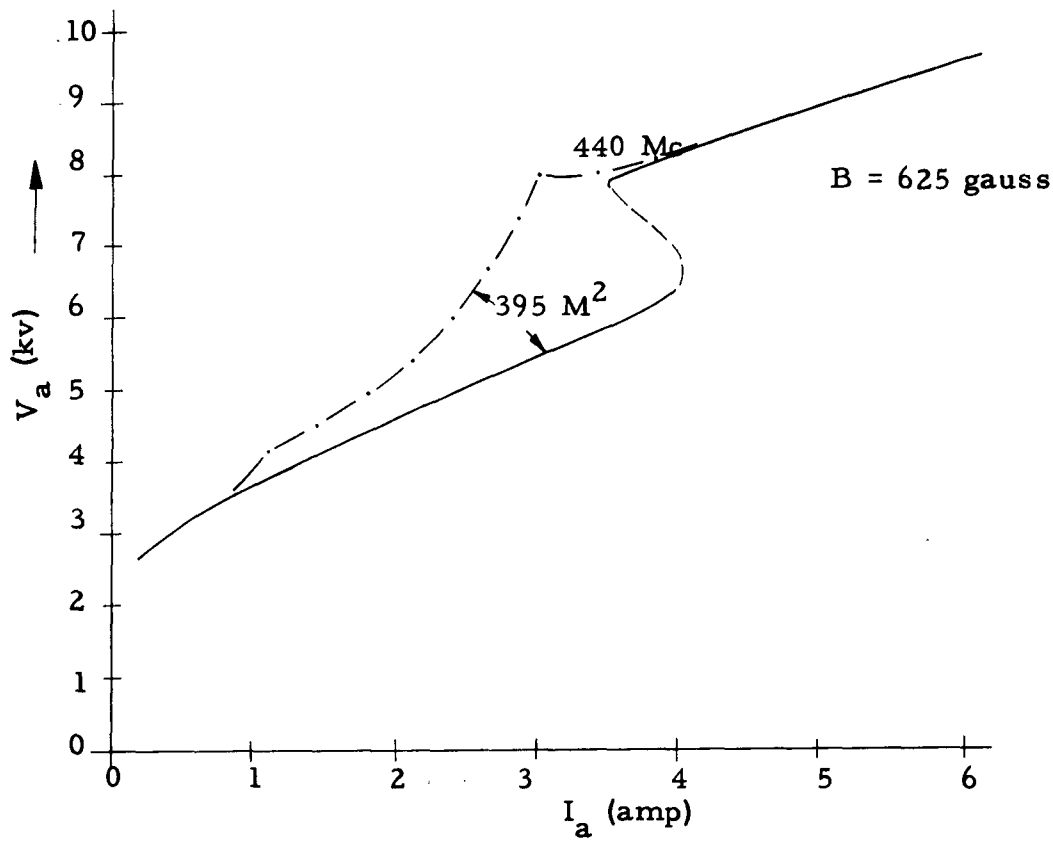

FIG. 66.—V_a — I_a characteristic curve of 400-Mc anode with magnesium cathode. Two modes are observed, at 395 and 440 Mc. The external resistance of dash-dot line curve is three times greater than the solid one.

The jump from one mode to the other is related to the circuit resistance and the rectifier voltage. In Fig. 66, the solid curve corresponds to a power-supply-circuit resistance of about 3000 ohms; the dash-dot line, about 10,000 ohms. The required anode voltage to synchronize the beam with the 440-Mc mode, is more than that for 395 Mc, and when the tube is operating at 395 Mc, with 4-amp anode current, the voltage drop in the rectifier voltage is about 4 amp x 3000 ohms = 12 kv. In other words, the rectifier voltage at I_a = 4 amp is about 12 + 6.5 = 18.5 kv, where 6.5 kv is the voltage applied on the anode. For the 440-Mc mode at I_a = 3.5 amp, 8 kv applied voltage, and 3000 ohms circuit resistance, the rectifier voltage is 8 kv + 3.5 amp x 3000 ohms = 18.5 kv which is the same as the other mode. Therefore, at this point, the tube oscillates at both frequencies. (Two independent curves require a low-resistance power supply.)

The rf power of 400 Mc with the magnesium cathode was very small because of (1) the mode interference and (2) the presence of three small bunches within λ. This result can be seen from the following calculation. Assume $\alpha = E_{eff}/E_{ave} = 0.75$, with V_a = 10 kv, B = 625 gauss, and 2p = 5.7 cm; then:

$$f = 3\,\frac{v_d}{2p} = 3\,\frac{\dfrac{10\text{ kv} \times 10^3}{1.75 \times 10^{-2} \times 625 \times 10^{-4}}}{5.7\text{ cm} \times 10^{-2}} = 400\text{ Mc}$$

To have only one bunch with 2p, it is necessary to increase the anode voltage about three-fold, or decrease B. Neither was possible because

the magnesium surface gave more emission current than the power supply could carry.

H. THE 400-Mc ANODE WITH ALUMINUM CATHODE

As explained in Secs. V-F and G, the 400-Mc anode was used with copper and magnesium cathodes. The secondary-emission ratio of copper was so low that the current was not sufficient and the secondary-emission ratio of magnesium (with a thin layer of MgO) was so high that the tube arcs at moderately high voltages. Therefore an aluminum cathode, which has a secondary-emission ratio between those of copper and magnesium, was tried. This combination did not work well either, because of mode interference and a high voltage requirement for one bunch within λ. Figure 67 shows the V_a—I_a characteristic curves of the 400-Mc anode with the aluminum cathode. Much noise was observed, but 400 Mc and 450 Mc were dominating modes in curves for B = 250 gauss and B = 312 gauss. In curve B = 156 gauss, although weak noise was observed, it works as a smooth anode, especially because f_s = 400 Mc and f_c = 435 Mc, and then $f_c < 2f_s$. For B = 285 gauss, the cyclotron frequency f_c = 800 Mc and $f_c = 2f_s$, and it is the best situation for efficient rf oscillation. This is why, probably, around B = 300 gauss, the rf oscillation is observed to be stronger. And, if there were no mode problem, around B = 300 gauss high rf power could be obtained. For higher magnetic fields (B = 625 or more), the bunches appear only as small ripples on the top of the space charge and their effect is very small.

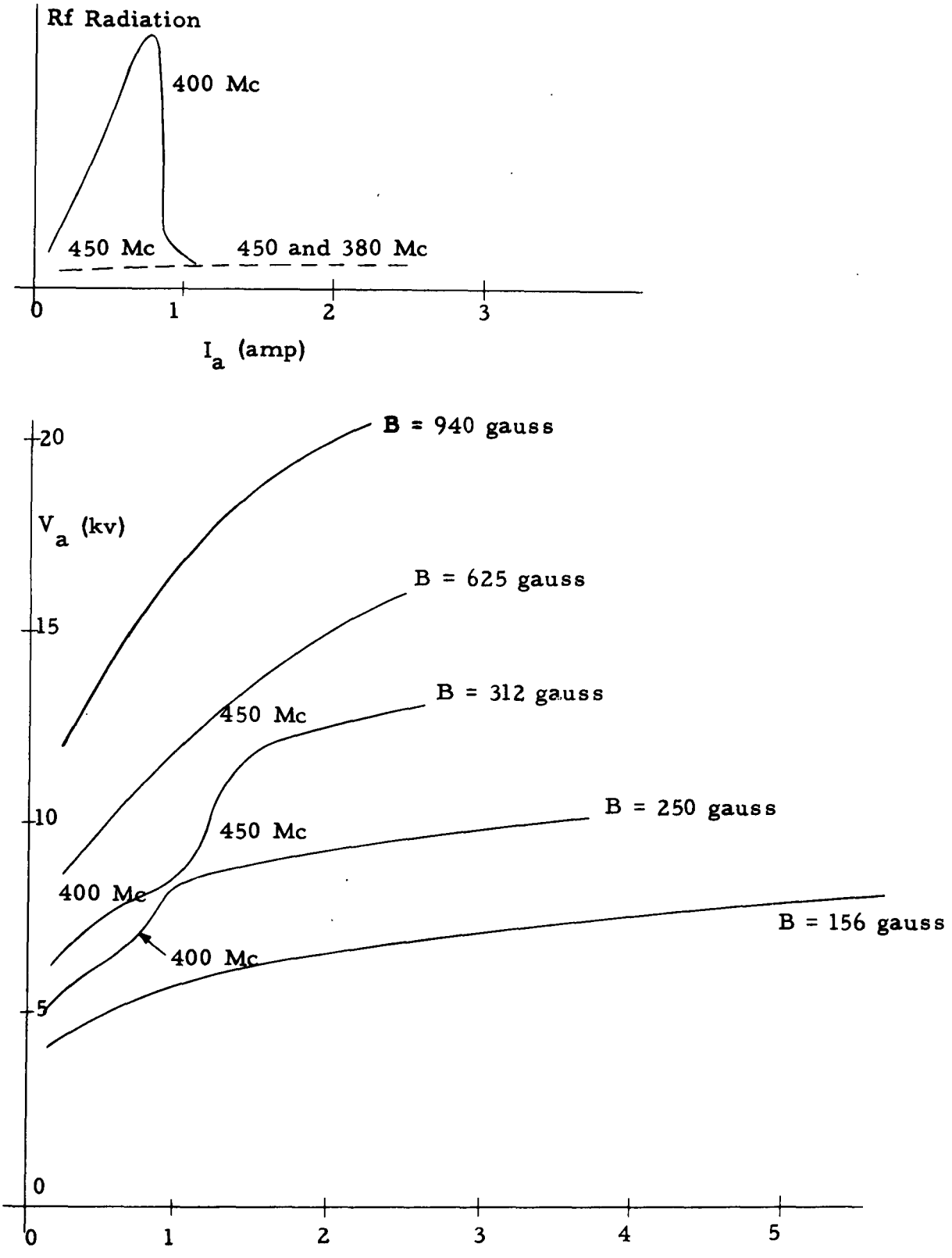

FIG. 67.—Characteristic curves of the 400-Mc anode with the 140 aluminum cathode (diameter 15.3 cm), d = 2.25 cm, and rf radiation.

In this test also, three small bunches existed within 2p. Assuming $\alpha = E_{eff}/E_{ave} = 0.725$, at $V_a = 7.5$ kv, B = 312 gauss, d = 2.25 cm, and 2p = 5.8 cm, it is shown below that three bunches are required to enable the beam to synchronize with 400 Mc.

$$f = 3 \frac{\frac{7.5 \times 10^3}{2.25 \times 10^{-2}}}{5.8 \times 10^{-2} \times 312 \times 10^{-4}} = 400 \text{ Mc}$$

This is also a reason for small rf output power.

At the top of Fig. 67, the rf output power is shown, measured with a small antenna and a receiver. The pattern of rf power is almost the same for all magnetic fields. At low currents, at anode currents below 1 amp, the π mode or 400 Mc is excited with the highest amount of power, but suddenly drops at about $I_a = 1$ amp. The reason for this result is believed to be the following. Electrons are created by P.I.G. discharge in the beginning of the curve, up to about $I_a = 1$ amp. After that, the diocotron random oscillations start, and the electron beam is produced only by these oscillations. Therefore the beam is excited already by many frequencies, and if any of these frequencies coincide with a mode of the tube it grows. This is the reason for so many observed frequencies if $I_a > 1$ amp. But below $I_a = 1$ amp, the beam has no particular frequency and is more likely to be excited by the π mode (400 Mc).

From this explanation it follows that it is best to calculate the voltage and the synchronous velocity such that the rf starts in region ($I_a < 1$ amp) where diocotron random oscillation has not

started; secondary electrons would be created by rf oscillation instead of by diocotron oscillations. In our experiments, the only tubes that worked well had rf designed to start at lower voltage than the diocotron oscillation. In Fig. 67, the 400-Mc π mode started before the diocotron oscillation, but because the bunches were very small, just on top of the space charge, the 400-Mc rf was overtaken by the diocotron oscillation at $I_a > 1$ amp.

J. THE 160-Mc ANODE WITH ALUMINUM CATHODE

A photograph and the important dimensions of the 160-Mc anode are shown in Fig. 68. This anode was one of the best earlier tubes that worked very well. An arc of about 80 cm long and 10 cm in diameter was produced by rf power, which was dissipated in air from the top of the tube. The characteristic curves and the variation of the arc length with current are plotted in Fig. 69. As shown, the anode voltage decreases with increase in anode current. This negative-resistance property of the curve may be explained by the extra gas at higher currents. In the joints, soft solder was used and often cracked due to thermal strains, so that higher power could not be obtained. The next mode to the 160-Mc π mode was about 500 Mc, which was very far from the π mode and the tube worked well.

In this tube, there was one bunch within λ, and this was a reason why it worked well. If we assume $\alpha = E_{eff}/E_{ave}$ about 70 per cent, $2p = 4.5$ cm, spacing $d = 0.7$ cm, $V_a = 6.8$ kv, and $B = 900$ gauss, we get

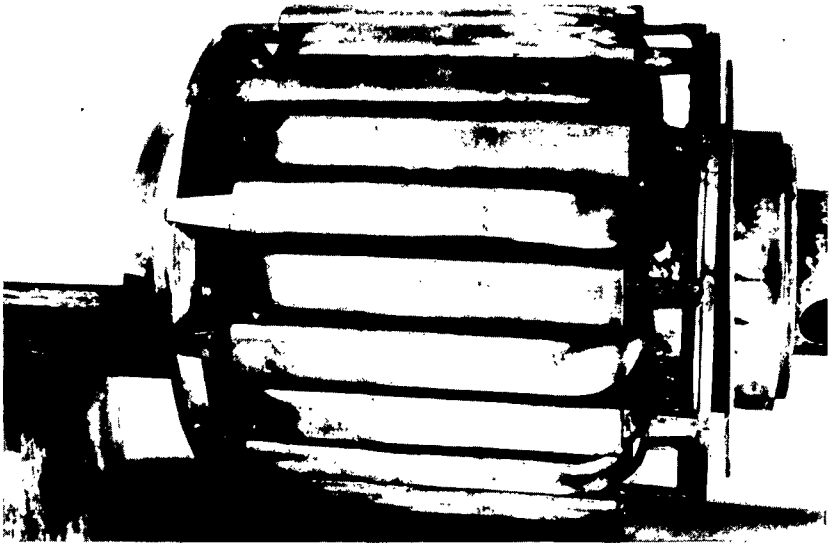

FIG. 68.—The 160-Mc anode. 24 watercooled bars, 2 cm wide; spacing between bars is 0.3 cm and 2p = 4.6 cm. The length of the bars, in the interaction region, is 12 cm. The diameter of the anode is 18.6 cm. The aluminum cathode is 20 cm long and spacing between the anode and the cathode is d = 0.7 cm.

$$f_s = \frac{\dfrac{6.8 \times 10^3}{0.7 \times 10^{-2}}}{900 \times 10^{-4}} \frac{0.7}{4.6 \times 10^{-2}} \approx 160 \text{ Mc}$$

for an ideal rf structure for this frequency and p = d, $f_c = 2f_s$, and

$B_c = 2B_s = 114$ gauss. For this structure, however, $2p = 6.5d$, requiring $B = 3.25\ (114) = 370$ gauss for minimum starting value; this was the value found experimentally.

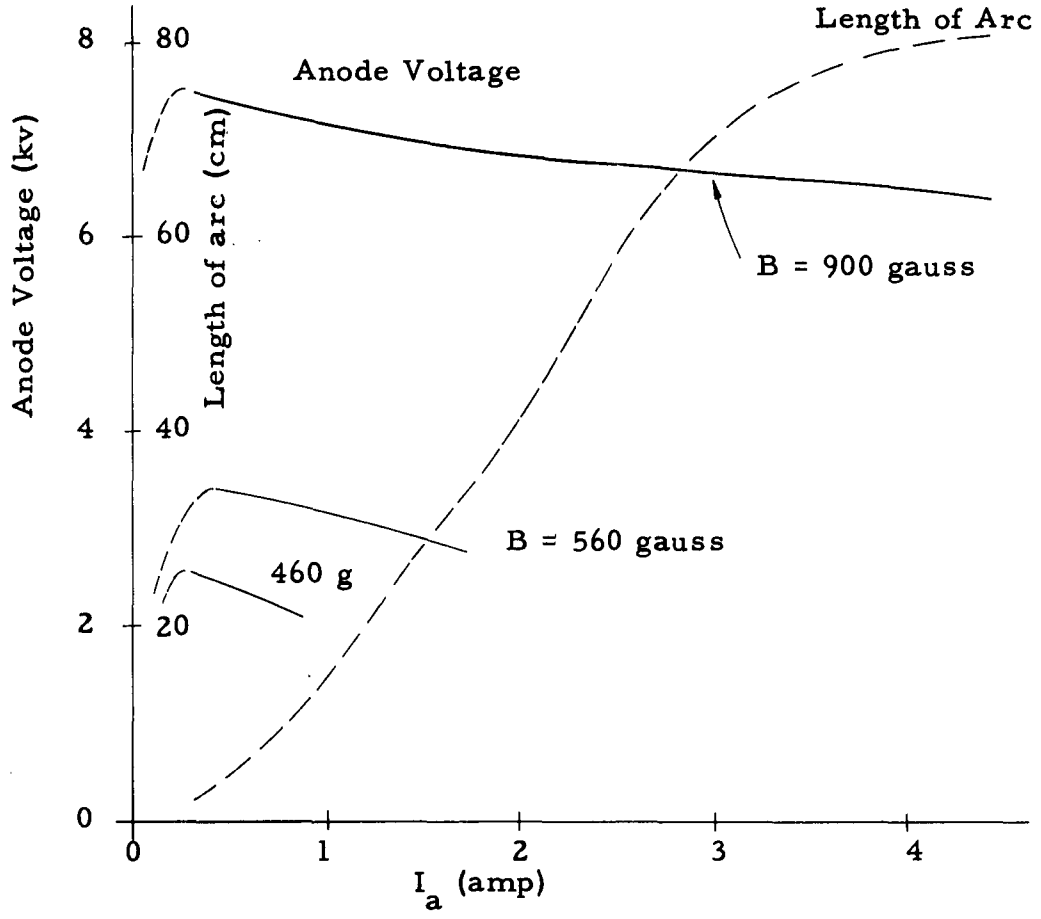

FIG. 69.—The $V_a - I_a$ characteristic curves and the length of the arc in 160-Mc anode.

K. THE 1240-Mc ANODE

This anode is made from a cavity resonant at 1240 Mc, shown in Fig. 70. The purpose is to excite the TM_{010} mode and by the help of two coupling channels, to produce π-mode electric fields on the bars.

FIG. 70.—The 1240-Mc anode. Two coupling channels are shown. The diameter of the cavity is 18.5 cm, and its height is 12 cm. 64 watercooled bars from 3/16-in. copper tubing are cut in the picture.

In each channel, the bars are connected alternately to the top and the bottom of the channel. This type connection makes a one-turn open loop at one edge of the channel; one end of the loop is connected to a bar and the other end of the loop is connected to the next bar. These bars are coupled to the circulating magnetic field of the TM_{010} mode and produce alternately positive and negative voltages on the bars. Besides the 1240-Mc π mode, many other modes were observed, and the operation was not satisfactory. The dc and pulse characteristic curves of this anode are shown in Fig. 71. There is only one bunch within 2p and also $2p/d = 2.4$, which is very close to 2, so that the geometric relationships are adequate and if there were no mode problem and no multipactors between the walls of the channels, probably it would work very well.

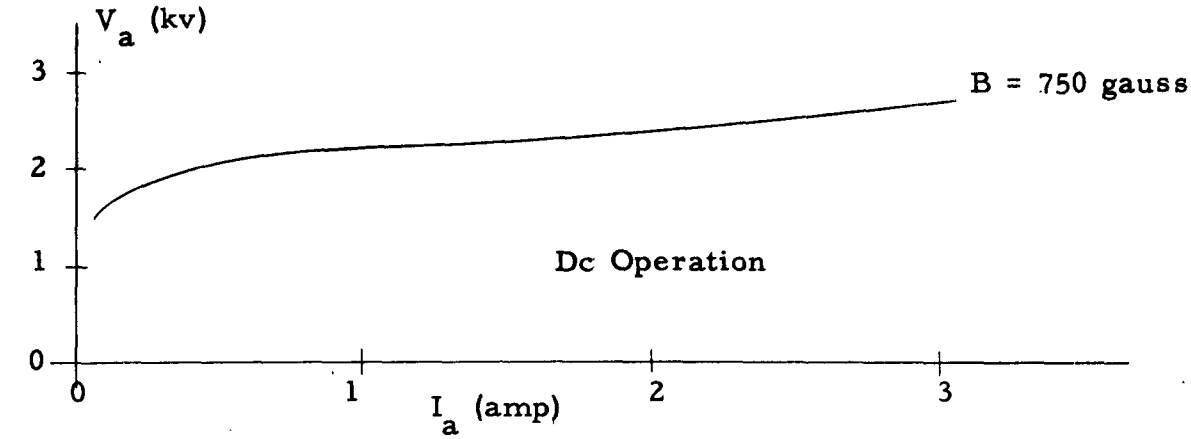

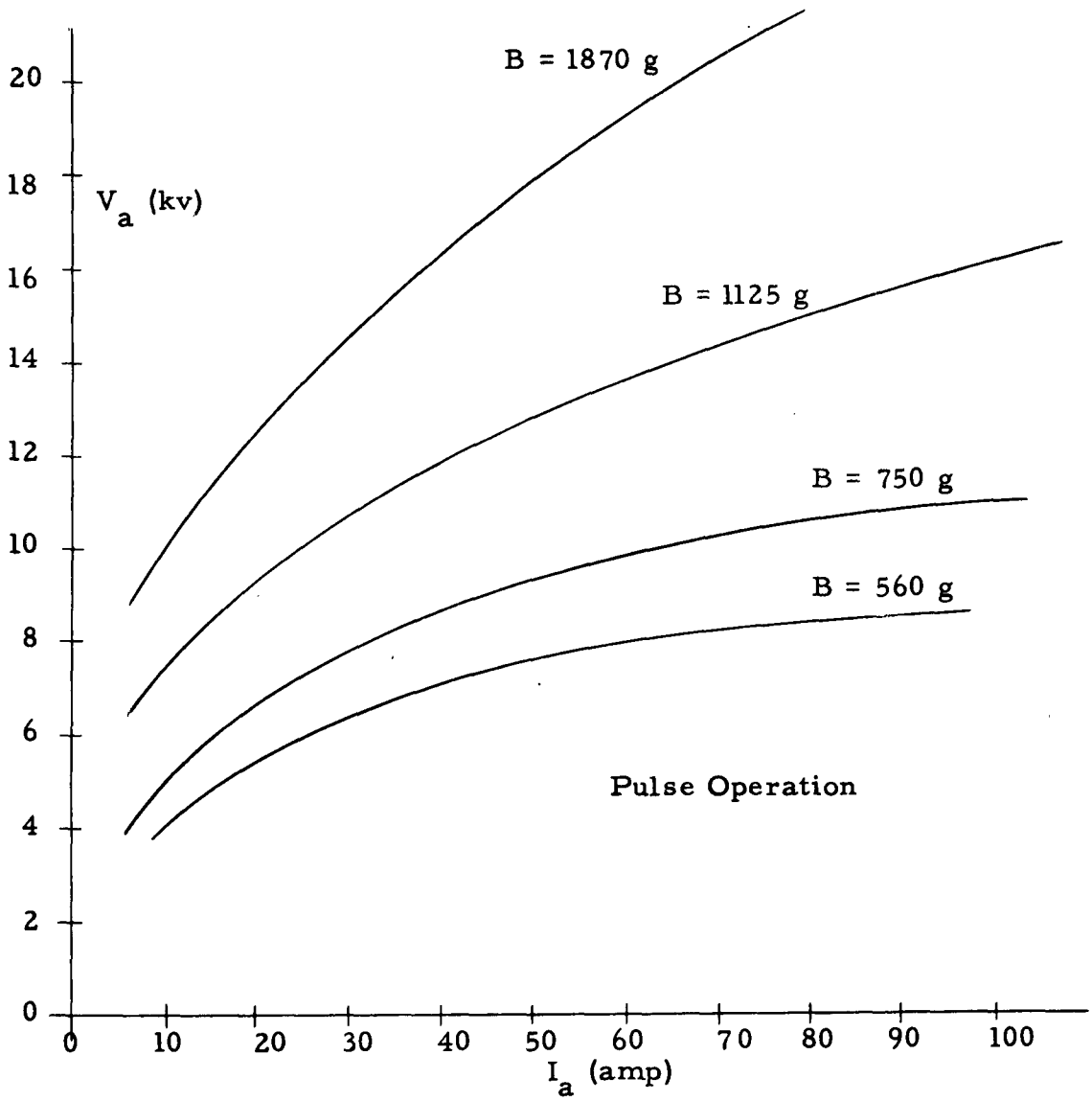

FIG. 71.—The 1240-Mc anode characteristics. The top is dc for keeping-alive operation and the bottom is the characteristic curves with 4-μsec pulses.

L. THE 1160-Mc ANODE WITH ALUMINUM CATHODE

This anode operates at the TM_{010} mode of a cavity. The top and bottom parts of this cavity are shown in Fig. 72. 100 bars, 5/32-in. copper tubing and water cooled, are soldered to the top and the bottom parts of the cavity, Fig. 73. On the top and bottom parts of the cavity, there are ridges and grooves alternately. The bars are soldered to the ridges. When the cavity is excited by the TM_{010} mode, the alternating current induced by the circulating alternating magnetic field inside the cavity goes from the center part of the bars (background is black in Fig. 73) to the top part of the cavity and returns. Those bars, which are soldered to the ridges, guide current to the wall through ridges. Those bars which are in the front of the grooves guide current to the end of the bars. From there, through the surface of the grooves, the current goes back toward the center to reach the end edge of the grooves. In this case the current path is longer, and therefore there is a voltage drop in those bars faced to the grooves with respect to the alternate bars. This voltage drop between two adjacent bars excites a π mode and interacts with the electron beam.

The V_a—I_a characteristic curve of the 1160-Mc anode with the 20-cm-diameter aluminum cathode is shown in Fig. 74. The best operation was obtained at B = 1000 gauss. Below 750 gauss, operation ceased; at more than 1000 gauss, the random fluctuations and other modes were stronger and the π mode operation was spoiled. The space-harmonic modes are a serious problem in this anode. Most of the input

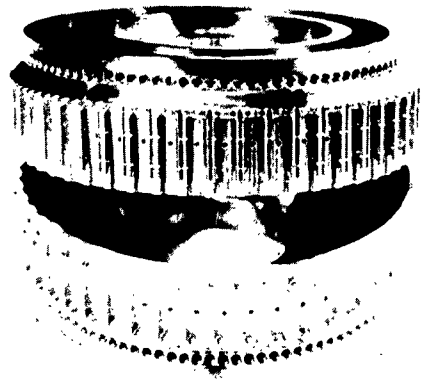

FIG. 72.—The top and bottom parts of the 1160-Mc cavity. There are alternate ridges and grooves in these parts. A bar or water-cooled tube is soldered to the ridge and the next bar faces a groove. The length of a ridge (or a groove) is 2.5 cm and the two parts of the cavity are separated by 1.6 cm. The holes for water connection to tubes are shown in the top and bottom.

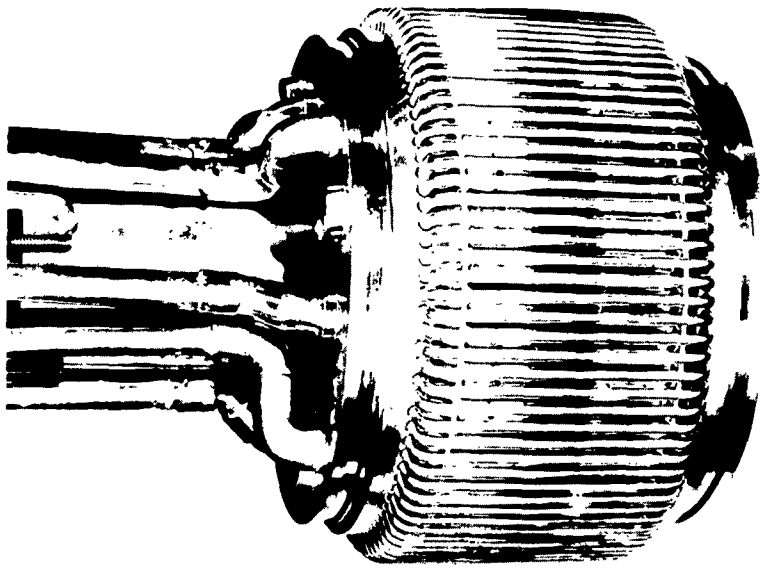

FIG. 73.—The 1160-Mc anode. 100 bars of 5/32-in. copper tubing connect the two parts shown. The length of the bars is 6.6 cm, but only the center serves as the interaction area. The bars are alternately soldered to the ridges for π mode excitation. The outside diameter of the cavity is 18.9 cm, and the spacing between the cathode and the anode is 0.55 cm. The cathode is aluminum with a 20-cm diameter surrounding this anode.

power was taken by undesired modes. There was no opportunity to install the dampers designed to damp the space-harmonic modes. (The best system to damp undesired modes is to use iron straps on the top and bottom of the bars. The iron strap does not affect the mode but kills others.)

In this tube, the wavelength of the slow-wave structure is 2p = 1.2 cm and the average spacing between the cathode and the anode is $d \approx 0.6$ cm; therefore, p = d and optimum rf configuration is obtained; it is believed that in the absence of the undesired modes, it works well.

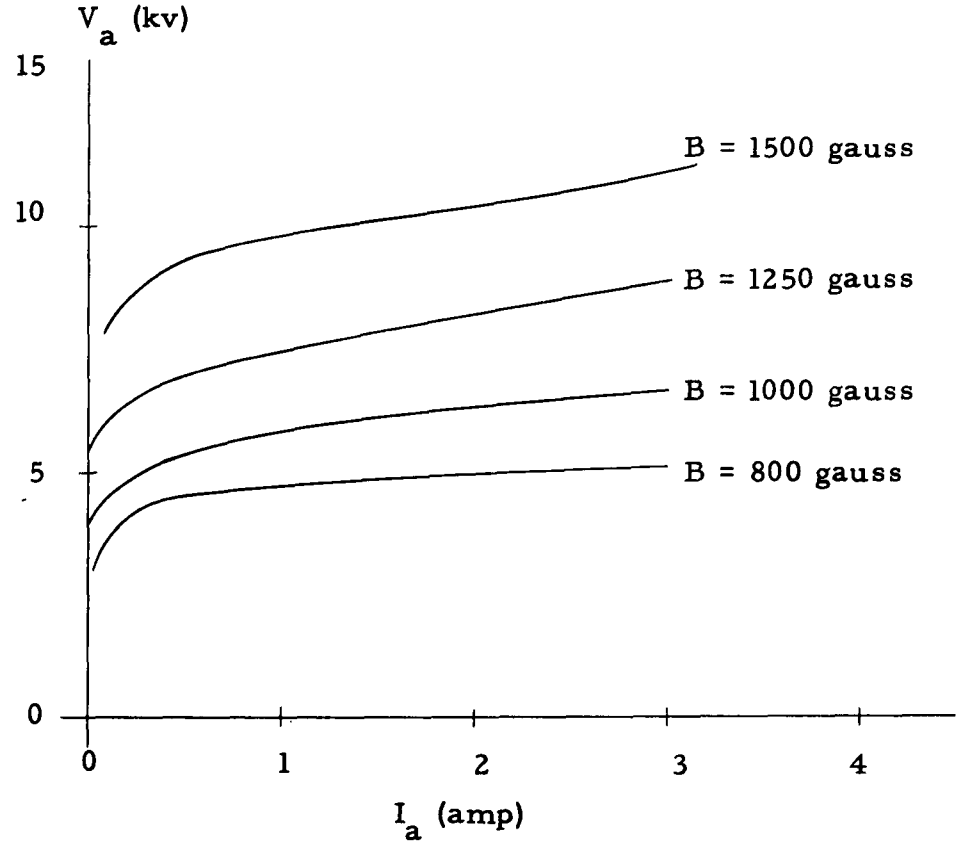

FIG. 74.—The characteristic curves of the 1160-Mc anode with the aluminum cathode (20-cm diameter), $p \approx 10^{-5}$ mm of Hg.

M. SPACE-CHARGE BUNCHING IN SMOOTH AND RF ANODES

It was explained in Sec. IV that the space charge bunches most easily within square cross section for which λ is the length of a bunch and d is the spacing, and $\lambda = d$. Consider Fig. 75, where the space-charge-free cycloidal trajectory (1) is shown to fit into the dimensions found to be most suitable for starting a bunch, namely a square.

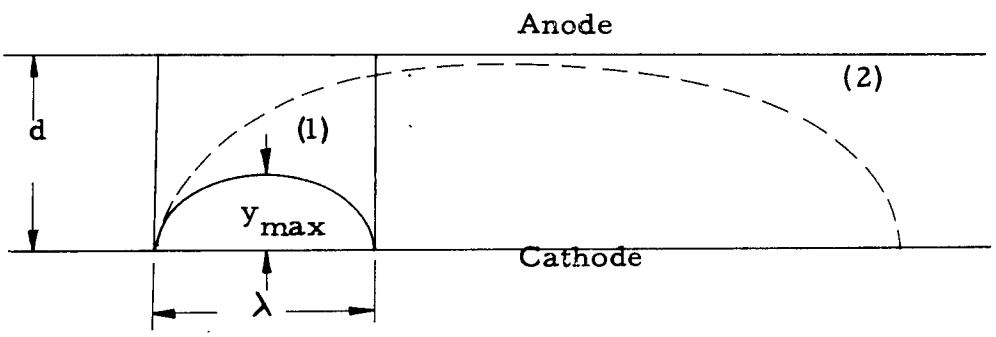

FIG. 75.—Trajectories relative to a square, $\lambda = d$.

The maximum excursion of space-charge-free electrons from the cathode is $y_{max} = 2mE/eB^2$ and the length of a cycloidal trajectory is $\pi y_{max} = 2\pi mE/eB^2$. In the case of trajectory (1) then, $\pi y_{max} = \lambda = d$, or $d/y_{max} = \pi$, and electrons drift through one of these square space divisions with the frequency $f_d = v_d/\lambda = E/Bd$. When an electron is passing through a square, it is also rotating in a cycloidal trajectory (ideally), and the cyclotron frequency f_c is equal to the drift frequency f_d for easiest starting, and therefore, $f_c = E/Bd$. However $f_c = Be/2\pi m$ also. In cold cathodes, according to our results, $v_d = E/B$ is constant for the particular δ of each

cathode material, because back bombarding energy is proportional to velocity squared. Therefore, there is a serious restriction on E and B and on frequency. However, in the hot cathodes or in the presence of gas, E/B is arbitrary.

In the case of trajectory (1), which is the most efficient case, the cold-cathode tube starts easily at a certain minimum voltage and minimum magnetic field. But after the tube is operating, it is possible to decrease B, to reach to the cutoff magnetic field B_H. This fact was shown by an experiment on the smooth-bore anode spacing d = 0.88 cm (Fig. 23). At B = 625, it starts to operate easily, when the voltage is $V_a \approx 7$ kv at $I_a = 100$ amp, and $y_{max} \approx 0.288$ cm; therefore, $d/y_{max} = 0.88/0.288 \approx \pi$, and this is the case where the cycloidal trajectories composing a bunch fit within a square. It will not start at any lower voltage, for any possible value of B, with this cathode material.

During operation the voltage and magnetic field were decreased to $V_a = 1$ kv and B = 130 gauss, which gives $y_{max} = 0.78$ cm close to d = 0.88 cm, and the tube was still working. The cycloidal trajectory in this case is similar to (2) in Fig. 75. It is necessary to note that these trajectories (1) and (2) are given just for comparing relative sizes and actually in the presence of space charge, they are quite different in shape. The electric field becomes very small near the cathode and it increases toward the anode but cycloids are formed only in uniform E. Therefore, the cycloidal diameter $y_{max} = 2mE/eB^2$ is replaced by some other relation giving greatly elongated trochoids

which are very small near the cathode and increase near the anode. Figure 76 shows the approximate configuration of a bunch with varying E and different sizes of cycloidal trajectories. Only on the top of the electron cloud, a true cycloidal trajectory could exist, and it fits $\pi y_{max} = d$, at the minimum starting voltage condition.

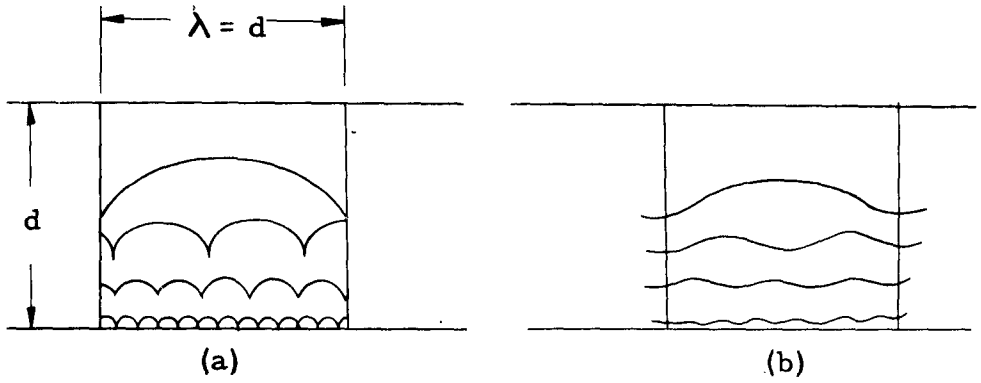

FIG. 76.—Electron cloud in a bunch: (a) the space-charge-free electron trajectories are shown for comparison in varied fields; (b) the electron motion is shown as ripples on the laminar flow.

Figure 76(b) shows that electron flow is getting close to laminar flow and the cycloidal trajectories remain only as ripples on the electron flow. Electrons on the bottom of the cloud do not contribute much to the rf interaction and only those on the top specify the synchronous velocity and the bunching within squares. These electrons did not start from rest in the fields in which they now exist, or they would have sharper cusps, as in Fig. 76(a).

In the case of trajectory (1) in Fig. 75, there is much freedom for electrons to move up and down and give energy to rf. But there is no freedom in the trajectory (2) in Fig. 75, because it strikes

the anode or cathode in any displacement and is lost. Therefore, trochoidal movements as large as trajectory (2) are not as efficient as (1), which is associated with the square cross section. With space charge, of course, these are merely ripples on very long trochoids, which approach Brillouin flow, where the electrons move almost parallel to the cathode.

There are good hot-cathode magnetrons that work with fields that could give ripples as long as the trajectory (2). In traveling-wave tubes and amplifier magnetrons, the electron trajectory is in the state of laminar flow, and arbitrary ripple lengths are possible, but a driving rf field is necessary. In the laminar-flow state the random diocotron (slipping-stream) instability occurs.[20,21,22] Figure 77 shows the configuration of the space-charge instability or the so-called diocotron oscillation.

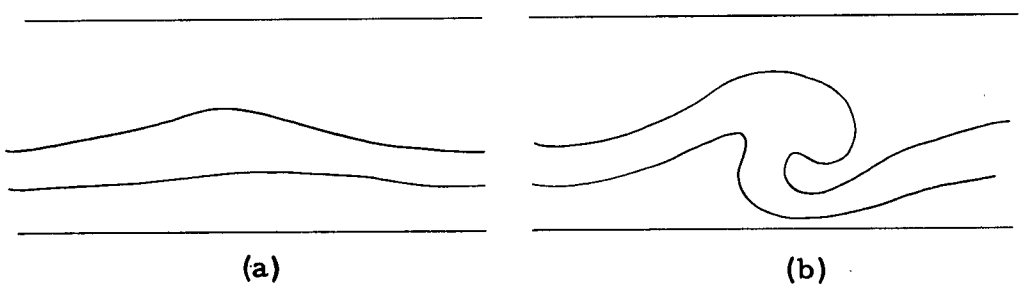

FIG. 77.—Slipping-stream instability: (a) the beginning of instability builds up; (b) turbulence.

The frequency of this instability, although on the average proportional to the magnetic field, is actually random. We have, however, found that the best is when rf starts before the diocotron oscillations start to make turbulence.

If we increase the magnetic field, the cycloidal size gets smaller and the space charge bunches very easily within a fraction of a square. Therefore, there is more freedom from wall effects and the tube starts to operate even easier, or quicker, than when a full square is needed.

With an rf anode, as with a smooth one, the space charge bunches most easily within a square cross section; however, only one bunch remains within 2p, the wavelength of the slow-wave structure. The missing bunch is divided and sent ahead or back, by rf fields to join the remaining ones. Therefore the best and most compact configuration for a π mode magnetron is $\lambda = 2p = 2d$. Again, in this case, the best magnetic field for starting with a tightly coupled load is the one that makes the cycloidal length equal to d, in order to make a bunch within a square. Therefore an electron travels the distance $\lambda/2 = d$ in one cycloidal motion, or $f_c = v_d/d = 2v_d/\lambda$. But $v_d/\lambda = f_s$ is the frequency of the slow-wave structure, so that $f_c = 2f_s$. An example of this configuration is the 1160-Mc anode. In this anode, $2p = 1.2$ cm and $d = 0.55$ cm, therefore; $p \approx d$ and the optimum configuration is obtained. It worked well with $B = 8000$ gauss and $V_a = 5$ kv; therefore, $\pi y_{max} = 2\pi(V_a/d)/(e/m)B^2 = 0.510$ cm, or the cycloidal length is about $d = \lambda/2 = 0.55$ cm. Figure 78 shows the ideal configuration and magnetic field.

Another example of square cross sections is the 150-Mc anode. In this anode $2p = 5.6$ cm and $d \approx 1$ cm; then $2p \approx 2.8(2d)$, which is not the best configuration—it is off by a factor of 2.8. It does work

very well at $V_a = 3$ kv and $B = 310$ gauss. Then, the length of a cycloidal trajectory $\pi y_{max} \approx 1$ cm. Therefore in this case, the space-charge bunches appear to be formed within square cross sections too. The bunch regions in the magnetron could perhaps be represented as in Fig. 79, with much longer retions nearly devoid of space charge, although λ includes both parts within the length 2p.

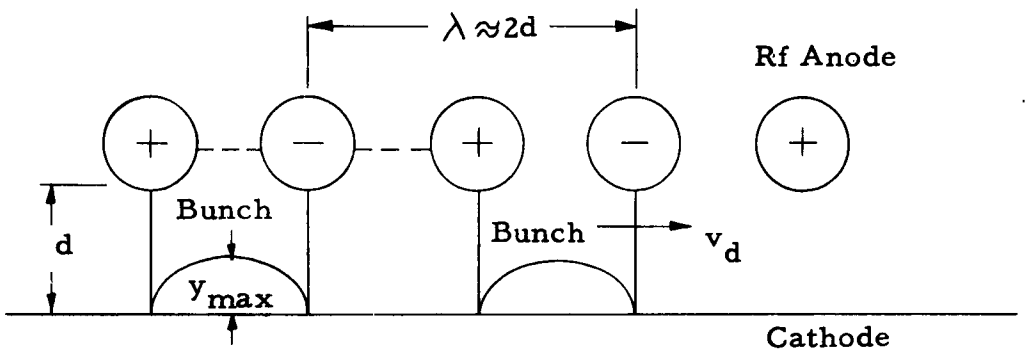

FIG. 78.—Bunch-fitting square spaces in 1160-Mc anode, where p = d and $f_c = 2f_s$.

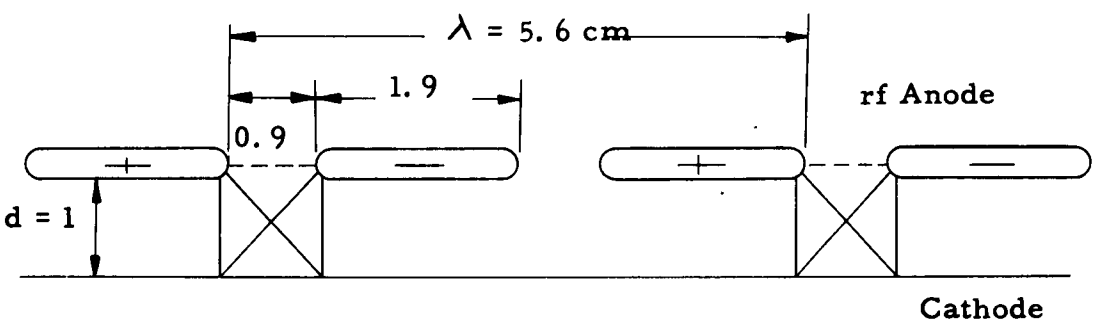

FIG. 79.—Bunch spacing in 150-Mc anode. There is one bunch within λ, but $\lambda = 2.8$ (2d) = 5.6 cm, and the length of the bunch is 1 cm and the 4.6 cm remainder of the λ is nearly empty. The actual total distribution of space charge could be a longer bunch formed by superposing many units that were bunched as shown.

In this anode, for B = 310 gauss, $f_c \approx 5.6\ f_s$, which means the electrons rotate 5.6 times in their cycloidal motion within one period of the slow-wave structure. The ideal case is when $\lambda = 2d$ and $f_c = 2f_s$, but here we have $\lambda = 2.8(2d)$ and $f_c = 2.8(2f_s)$ so that the length in which bunching action occurs remains equal to d.

The results of three rf anodes and a smooth anode are given in the table below. The minimum anode voltage and magnetic field for which the tube works well are given. It is shown that d/y_{max} is about π in all of them, which proves that the space charge tends to form a bunch within a length equal to spacing. In Sec. II it is also mentioned that the maximum of the sum of the average voltage gain by many randomly phased oscillators closely placed along the same magnetic field lines occurs for a value of V_a/Bd such that the space-charge-free height of a cycloid is d/π.

Table 1 is concerned with the minimum voltage and magnetic field for which the tube starts easily. Also, it has been observed that the space-charge bunching process occurs within square cross sections even at high magnetic fields, where $d/y_{max} \gg \pi$. In the 150-Mc anode, the tube worked well but with low efficiency at B = 2500 gauss, V_a = 15 kv, where $d/y_{max} = 37$ and $f_c = 47\ f_s$. If the space-charge bunching action occurs within a square through which the beam drifts in one cycle of the cyclotron frequency then in this case the squares are very shallow and likewise bunches are only slight variations in the density of upper edge. This would suggest that in this case the efficiency should be low, as the "empty" space between

bunch maxima would possess sufficient electrons to load the rf circuit.

On the other hand, if the only square of significance has a height d, the bunching is simply not well done if many cyclotron revolutions occur while passing through this region. Our experiments gave no clear choice, but perhaps both statements say the same thing.

Aström[45] tested in the range of $f_c = 20f_s$ and found that for extremely small space-charge density the bunches still form best with $\lambda = d$ as observed by the time to drift through a distance equal to d, although 20 revolutions occurred therein. The bunches, however, were very indistinct, barely recognizable.

Anodes	2p(cm)	d(cm)	2p /d	V_a(kv)	B (gauss)	f_c(Mc)	f_c/f_s	y_{max}(cm)	d/y_{max}
f_s = 1160 Mc	1.2	0.55	2	5	800	2240	2	0.162	3.4
f_s = 150 Mc	5.6	1	5.6	3	310	870	5.8	0.34	2.9
f_s = 160 Mc	4.6	0.7	6.4	2.5	460	1280	8	0.19	3.7
Smooth Anode	0.88	0.88	1	7	652	1830	1	0.285	3.10

Table 1. The minimum starting voltage and magnetic field for four efficient anodes.

VI. CONCLUSIONS

This report is concerned with magnetrons of the cold-cathode, secondary-emission type. Many cathode materials, such as aluminum, magnesium, copper, stainless steel and graphite are investigated and the results are given.

The space-charge distribution is found on the basis of simple diffusion and of statistical mechanics. The result of this distribution is very close to the experimental data given by other authors.

The bunches in the interaction region are examined and it is shown that, in a smooth-anode magnetron, the space charge bunches most easily when $\lambda \approx d$, if λ is the length of a bunch and d is the spacing between the cathode and anode.

In an rf anode with segment pitch p, although the initial space-charge bunching process occurs within square subdivisions, only one bunch exists in the best situation, within the wavelength 2p of the slow-wave structure, and this will be the length of λ. Therefore, the best configuration for a π mode magnetron is $\lambda = 2d$, with alternate natural bunches missing because of the action of the rf field. For this configuration still another condition exists for optimum operation: $f_c = 2f_s$, where f_c and f_s are the cyclotron frequency and the frequency of the slow-wave structure, respectively.

One of the disadvantages of a cold cathode is the interrelation of the magnetic field and velocity. In a low magnetic field, the back-bombardment energy is not sufficient to produce secondary emission; in a high field, the secondary-emission ratio gets smaller too.

Therefore, for each material, the beam velocity is limited. In our magnetrons, with diameters of 15-20 cm and spacings of 1 cm, beam power of 30 Mw in millisecond pulses is easily obtained. But the drift velocity is such that a distance of 1 cm is travelled at a 1500-Mc rate. Anodes of this size and frequency have complex mode properties. Good anodes for one tenth of this frequency, p = 10d, have no mode problems but if the bunching action occurs in a distance equal to the spacing, then most of the distance between bunch maxima is idle, and the power developed is no greater than with a smaller tube having p = d.

Noise is another important problem. In our tubes, the diocotron or slipping stream oscillations are the major factor for producing back bombardment, but they introduce a broadband noise to the tubes. Space harmonics are also troublesome in some ranges around 1000 Mc. Dampers might skillfully be used to kill these space harmonics. By our experiments, we have found that the best tubes are those which avoid this problem and operate around 200-300 Mc, far below the space-harmonic and the diocotron random-fluctuation frequencies.

Because it is the nature of bunches to form best within a drift distance equal to the spacing between electrodes, and to do this best if only one cyclotron period occurs while drifting through this distance, it seems unlikely that magnetrons can be designed better than those developed empirically many years ago.

REFERENCES

1. A. W. Hull, "The Effect of a Uniform Magnetic Field on the Motion of Electrons Between Coaxial Cylinders," Phys. Rev., Vol. 18, p. 13; 1921.

2. A. F. Harvey, High Frequency Thermionic Tubes, Chap. IV, John Wiley and Sons, Inc., New York; 1943.

3. E. G. Linder, "Effect of High Energy Electron Random Motion upon the Shape of the Magnetron Cutoff Curve," J. Appl. Phys., Vol. 9, p. 331; 1938.

4. E. G. Linder, "Excess-Energy Electrons and Electron Motion in High-Vacuum Tubes," Proc. IRE, Vol. 26, p. 346; 1938.

5. L. Brillouin, "Theory of the Magnetron I," Phys. Rev., Vol. 60, p. 385; 1941.

6. L. Brillouin, "Theory of the Magnetron II," Phys. Rev., Vol. 62, p. 166; 1942.

7. L. Brillouin, "Theory of the Magnetron III," Phys. Rev., Vol. 63, p. 127; 1943.

8. L. Brillouin, "Electronic Theory of the Plane Magnetron," Advances in Electronics III, p. 85, Academic Press, Inc., New York; 1951.

9. D. L. Reverdin, "Electron Optical Exploration of Space Charge in a Cutoff Magnetron," J. Appl. Phys., Vol. 22, p. 257; 1951.

10. W. Engbert, "Die Potential Verteilung im Magnetron," Hochfrequenztechnik und Elektroakustik, Vol. 51, p. 44; 1938.

11. L. Marton and S. H. Lachenbruch, "Electron Optical Mapping of Electromagnetic Fields," J. Appl. Phys., Vol. 20, p. 1171; 1949.

12. L. Page and N. J. Adams, "Space Charge in Cylindrical Magnetron," Phys. Rev., Vol. 69, p. 494; 1946.

13. H. C. Nedderman, "Space-Charge Distribution in a Static Magnetron," J. Appl. Phys., Vol. 26, p. 1420-1430; 1955.

14. D. Gabor, "Stationary Electron Swarms in Electromagnetic Fields," Proc. Roy. Soc., Vol. A, 183, p. 436; 1945.

15. R. Q. Twiss, "On the Steady-State Theory of the Magnetron," Advances in Electronics, Vol. 5, p. 247; 1953.

16. P. Fechner, "Étude sur le magnetron à l'état bloque," Ann. Radio Elect., Vol. 7, p. 83; 1952.

17. G. Hok, "A Statistical Approach to the Space-Charge Distribution in a Cutoff Magnetron," J. Appl. Phys., Vol. 23, p. 983; 1952.

18. G. Hok, Crossed-Field Microwave Devices, Vol. I, p. 235, Academic Press, New York and London; edited by E. Okress; 1961.

19. A. W. Haeff, "Space-Charge Wave Amplification Effects," Phys. Rev., Vol. 74, p. 1532; 1948.

20. G. G. MacFarlane and H. G. Hay, "Wave Propagation in a Slipping Stream of Electrons; Small Amplitude Theory," Proc. Phys. Soc., (London), Vol. B63, p. 409; 1950.

21. O. Buneman, "A Small Amplitude Theory for Magnetrons," J. Electronics and Control, Vol. 3, pp. 1-50; 1957.

22. O. Buneman, Crossed-Field Microwave Devices, Vol. I, p. 367, Academic Press, New York and London; edited by E. Okress; 1961.

23. L. E. S. Mathias, "The Space-Charge Distribution in the Preoscillating Magnetron," J. Electronics, Vol. I, p. 8; 1955.

24. P. A. Lindsay, "General Steady-State Theory of Linear Magnetrons, I," J. Electronics and Control, Vol. 8, No. 3, p. 177; 1960.

25. E. D. Hoag, "Glow Cathodes in Pulsed Magnetic Fields," Scientific Report No. 4, Electronics Research Laboratory, University of California; Series 60, Issue No. 239; 15 June 1959.

26. C. W. Hartman, "Production and Interaction of Electron Beams in Crossed Fields," Ph.D. Thesis, Dept. Elec. Eng., University of California, Berkeley; Series No. 60, Issue No. 325; 1 November 1960. Also, C.W. Hartman and D.H. Sloan, "Turbulence in Crossed-Field Electron Streams," (paper in preparation)

27. G. B. Collins, Microwave Magnetrons, McGraw-Hill Book Co., Inc., New York; 1948.

28. W. W. Peterson, "The Trajectron--an Experimental Dc Magnetron," TR No. 18, University of Michigan; 1954.

29. R. Q. Twiss, "On the Initial Space-Charge Distribution in a Cylindrical Magnetron Diode," J. Electronics, Vol. 1, p. 1; 1955.

30. R. L. Jepsen and M. W. Muller, "Enhanced Emission from Magnetron Cathodes," J. Appl. Phys., Vol. 22, p. 1196; 1951.

31. D. Gabor and G. D. Sims, "Theory of the Preoscillation Magnetron II," J. Electronics, Vol. 1, p. 25; 1955.

32. G. D. Sims and D. Gabor, "Theory of the Preoscillating Magnetron II," J. Electronics, Vol. 1, p. 231; 1955.

33. G. D. Sims, Crossed-Field Microwave Devices, I, Academic Press, New York, p. 179; edited by E. Okress; 1961.

34. G. Mourier, Small Signal Theory Crossed-Field Microwave Devices, p. 395, Academic Press, New York and London; 1961.

35. H.A.H. Boot and J.T.Randal, "The Cavity Magnetron," J. Inst. Elec. Eng., Vol. 93, Part IIIA, No. 5, p.928; 1946.

36. H. Bruining, Physics and Applications of Secondary Electron Emission, Pergamon Press, Ltd., London; 1954.

37. J. F. Hull, "The Internal Magnetron," Crossed-Field Microwave Devices, II, p. 291, Academic Press, New York and London; 1961.

38. H. A. H. Boot and J. T. Randal, "The Cavity Magnetron," J. Inst. Elec. Eng.,(London), Vol. 93, Part III A, No. 5, p. 928; 1946.

39. J. R. M. Vaughan, "The Cold Cathode Gas-Filled Magnetron," Crossed-Field Microwave Devices, II, Academic Press, New York and London; edited by E. Okress; 1961.

40. J. Backus, "Studies of Cold Cathode Discharges in Magnetic Fields," J. Appl. Phys., Vol. 12, p. 1866; 1959.

41. L. Spitzer, Physics of Fully Ionized Gases, pp. 68-81, Interscience Publishers, Inc., New York; 1956.

42. J. R. Whinnery and T. Van Duzer, Crossed-Field Microwave Devices, I, Academic Press, New York and London, pp. 332-333; edited by E. Okress; 1961.

43. W. Knauer, "Mechanism of the Penning Discharge at Low Pressures," J. Appl. Phys., Vol. 33, No. 6, p. 2093; 1962.

44. A. Simon, An Introduction to Thermonuclear Research, Pergamon Press, London, p. 160; 1959.

45. E. Aström, Proceedings of the Conference on Dynamics of Ionized Media, London; April 1951.

AF Cambridge Research Laboratories, Bedford, Mass.
Rpt. No. AFCRL-63-396. ELECTRON BEAM IN THE COLD-CATHODE MAGNETRON. Interim rpt. June 62.
149 p. incl. illus., tables, and 45 refs.

Unclassified Report

The cold-cathode magnetron with various cathode materials is examined. The kinetic energy of electrons in the direction of the magnetic field is found. The anode current and cathode back bombardment are formulated on the basis of statistical mechanics. Noise and bunching are studied. It is shown here for the first time that the space charge starts to bunch most easily when the length of a useful bunch is equal to the distance between cathode and anode in both smooth-anode magnetrons and in magnetrons with a slow-wave rf anode structure. Several rf anode configurations are discussed, and the results are given. It is found why the easiest starting configuration has the wavelength of the slow-wave structure equal to double the spacing between cathode and anode, and why the minimum starting value of magnetic field makes the cyclotron frequency equal to double the frequency of the slow-wave structure, when a specific energy of back bombardment is demanded by the cold-cathode secondary emitter.

1. Electron Tubes
2. Plasma Physics
I. Project No. 5634
Task No. 563402
II. Contract AF-19(638)-324
III. Univ. of Calif.
Berkeley, California
IV. M. Chamran
V. In DDC collection

AF Cambridge Research Laboratories, Bedford, Mass.
Rpt. No. AFCRL-63-396. ELECTRON BEAM IN THE COLD-CATHODE MAGNETRON. Interim rpt. June 62.
149 p. incl. illus., tables, and 45 refs.

Unclassified Report

The cold-cathode magnetron with various cathode materials is examinded. The kinetic energy of electrons in the direction of the magnetic field is found. The anode current and cathode back bombardment are formulated on the basis of statistical mechanics. Noise and bunching are studied. It is shown here for the first time that the space charge starts to bunch most easily when the length of a useful bunch is equal to the distance between cathode and anode in both smooth-anode magnetrons and in magnetrons with a slow-wave rf anode structure. Several rf anode configurations are discussed, and the results are given. It is found why the easiest starting configuration has the wavelength of the slow-wave structure equal to double the spacing between cathode and anode, and why the minimum starting value of magnetic field makes the cyclotron frequency equal to double the frequency of the slow-wave structure, when a specific energy of back bombardment is demanded by the cold-cathode secondary emitter.

1. Electron Tubes
2. Plasma Physics
I. Project No. 5634
Task No. 563402
II. Contract AF-19(638)-324
III. Univ. of Calif.
Berkeley, California
IV. M. Chamran
V. In DDC cbllection

AF Cambridge Research Laboratories, Bedford, Mass.
Rpt. No. AFCRL-63-396, ELECTRON BEAM IN THE COLD-CATHODE MAGNETRON. Interim rpt. June 62.
149 p. incl. illus., tables, and 45 refs.

Unclassified Report

The cold-cathode magnetron with various cathode materials is examined. The kinetic energy of electrons in the direction of the magnetic field is found. The anode current and cathode back bombardment are formulated on the basis of statistical mechanics. Noise and bunching are studied. It is shown here for the first time that the space charge starts to bunch most easily when the length of a useful bunch is equal to the distance between cathode and anode in both smooth-anode magnetrons and in magnetrons with a slow-wave rf anode structure. Several rf anode configurations are discussed, and the results are given. It is found why the easiest starting configuration has the wavelength of the slow-wave structure equal to double the spacing between cathode and anode, and why the minimum starting value of magnetic field makes the cyclotron frequency equal to double the frequency of the slow-wave structure, when a specific energy of back bombardment is demanded by the cold-cathode secondary emitter.

1. Electron Tubes
2. Plasma Physics
I. Project No. 5634
Task No. 563402
II. Contract AF-19(638)-324
III. Univ. of Calif.
Berkeley, California
IV. M. Chamran
V. In DDC collection

AF Cambridge Research Laboratories, Bedford, Mass.
Rpt. No. AFCRL-63-396. ELECTRON BEAM IN THE COLD-CATHODE MAGNETRON. Interim rpt. June 62.
149 p. incl. illus., tables, and 45 refs.

Unclassified Report

The cold-cathode magnetron with various cathode materials is examined. The kinetic energy of electrons in the direction of the magnetic field is found. The anode current and cathode back bombardment are formulated on the basis of statistical mechanics. Noise and bunching are studied. It is shown here for the first time that the space charge starts to bunch most easily when the length of a useful bunch is equal to the distance between cathode and anode in both smooth-anode magnetrons and in magnetrons with a slow-wave rf anode structure. Several rf anode configurations are discussed, and the results are given. It is found why the easiest starting configuration has the wavelength of the slow-wave structure equal to double the spacing between cathode and anode, and why the minimum starting value of magnetic field makes the cyclotron frequency equal to double the frequency of the slow-wave structure, when a specific energy of back bombardment is demanded by the cold-cathode secondary emitter.

1. Electron Tubes
2. Plasma Physics
I. Project No. 5634
Task No. 563402
II. Contract AF-19(638)-324
III. Univ. of Calif.
Berkeley, California
IV. M. Chamran
V. In DDC collection

AF Cambridge Research Laboratories, Bedford, Mass.
Rpt. No. AFCRL-63-396. ELECTRON BEAM IN THE COLD-CATHODE MAGNETRON. Interim rpt. June 62.
149 p. incl. illus., tables, and 45 refs.

Unclassified Report

The cold-cathode magnetron with various cathode materials is examined. The kinetic energy of electrons in the direction of the magnetic field is found. The anode current and cathode back bombardment are formulated on the basis of statistical mechanics. Noise and bunching are studied. It is shown here for the first time that the space charge starts to bunch most easily when the length of a useful bunch is equal to the distance between cathode and anode in both smooth-anode magnetrons and in magnetrons with a slow-wave rf anode structure. Several rf anode configurations are discussed, and the results are given. It is found why the easiest starting configuration has the wavelength of the slow-wave structure equal to double the spacing between cathode and anode, and why the minimum starting value of magnetic field makes the cyclotron frequency equal to double the frequency of the slow-wave structure, when a specific energy of back bombardment is demanded by the cold-cathode secondary emitter.

1. Electron Tubes
2. Plasma Physics
I. Project No. 5634
Task No. 563402
II. Contract AF-19(638)-324
III. Univ. of Calif.
Berkeley, California
IV. M. Chamran
V. In DDC collection

AF Cambridge Research Laboratories, Bedford, Mass.
Rpt. No. AFCRL-63-396. ELECTRON BEAM IN THE COLD-CATHODE MAGNETRON. Interim rpt. June 62.
149 p. incl. illus., tables, and 45 refs.

Unclassified Report

The cold-cathode magnetron with various cathode materials is examinded. The kinetic energy of electrons in the direction of the magnetic field is found. The anode current and cathode back bombardment are formulated on the basis of statistical mechanics. Noise and bunching are studied. It is shown here for the first time that the space charge starts to bunch most easily when the length of a useful bunch is equal to the distance between cathode and anode in both smooth-anode magnetrons and in magnetrons with a slow-wave rf anode structure. Several rf anode configurations are discussed, and the results are given. It is found why the easiest starting configuration has the wavelength of the slow-wave structure equal to double the spacing between cathode and anode, and why the minimum starting value of magnetic field makes the cyclotron frequency equal to double the frequency of the slow-wave structure, when a specific energy of back bombardment is demanded by the cold-cathode secondary emitter.

1. Electron Tubes
2. Plasma Physics
I. Project No. 5634
Task No. 563402
II. Contract AF-19(638)-324
III. Univ. of Calif.
Berkeley, California
IV. M. Chamran
V. In DDC collection

AF Cambridge Research Laboratories, Bedford, Mass.
Rpt. No. AFCRL-63-396. ELECTRON BEAM IN THE COLD-CATHODE MAGNETRON. Interim rpt. June 62.
149 p. incl. illus., tables, and 45 refs.

Unclassified Report

The cold-cathode magnetron with various cathode materials is examined. The kinetic energy of electrons in the direction of the magnetic field is found. The anode current and cathode back bombardment are formulated on the basis of statistical mechanics. Noise and bunching are studied. It is shown here for the first time that the space charge starts to bunch most easily when the length of a useful bunch is equal to the distance between cathode and anode in both smooth-anode magnetrons and in magnetrons with a slow-wave rf anode structure. Several rf anode configurations are discussed, and the results are given. It is found why the easiest starting configuration has the wavelength of the slow-wave structure equal to double the spacing between cathode and anode, and why the minimum starting value of magnetic field makes the cyclotron frequency equal to double the frequency of the slow-wave structure, when a specific energy of back bombardment is demanded by the cold-cathode secondary emitter.

1. Electron Tubes
2. Plasma Physics
I. Project No. 5634
Task No. 563402
II. Contract AF-19(638)-324
III. Univ. of Calif.
Berkeley, California
IV. M. Chamran
V. In DDC collection

AF Cambridge Research Laboratories, Bedford, Mass.
Rpt. No. AFCRL-63-396. ELECTRON BEAM IN THE COLD-CATHODE MAGNETRON. Interim rpt. June 62.
149 p. incl. illus., tables, and 45 refs.

Unclassified Report

The cold-cathode magnetron with various cathode materials is examined. The kinetic energy of electrons in the direction of the magnetic field is found. The anode current and cathode back bombardment are formulated on the basis of statistical mechanics. Noise and bunching are studied. It is shown here for the first time that the space charge starts to bunch most easily when the length of a useful bunch is equal to the distance between cathode and anode in both smooth-anode magnetrons and in magnetrons with a slow-wave rf anode structure. Several rf anode configurations are discussed, and the results are given. It is found why the easiest starting configuration has the wavelength of the slow-wave structure equal to double the spacing between cathode and anode, and why the minimum starting value of magnetic field makes the cyclotron frequency equal to double the frequency of the slow-wave structure, when a specific energy of back bombardment is demanded by the cold-cathode secondary emitter.

1. Electron Tubes
2. Plasma Physics
I. Project No. 5634
Task No. 563402
II. Contract AF-19(638)-324
III. Univ. of Calif.
Berkeley, California
IV. M. Chamran
V. In DDC collection

DISTRIBUTION LIST
Contract No. AF 19(628)-324

ORGANIZATION	NO. COPIES
AFMTC (AFMTC Technical Library-MU-135) Patrick Air Force Base Florida	1
AUL Maxwell Air Force Base, Alabama	1
OAR (RROS, Col. John R. Fowler) Tempo D 4th and Independence Ave. Washington 25, D. C.	1
AFOSR, OAR (SRYP) Tempo D 4th and Independence Ave. Washington 25, D. C.	1
ASD (ASNXRR) Wright-Patterson Air Force Base Ohio	1
RADC (RAALD) Griffiss Air Force Base, New York ATTN: Documents Library	1
Air Force Missile Development Center (MDGRT) Holloman Air Force Base, New Mexico	1
Hq. OAR (RROSP, Maj. Richard W. Nelson) Washington 25, D. C.	1
Commanding General USASRDL Ft. Monmouth, New Jersey ATTN: Technical Documents Center SIGRA/SL-ADT	1
Department of the Army Office of the Chief Signal Officer Washington 25, D. C. ATTN: SIGRD-4a-2	1
Commanding Officer Diamond Ordnance Fuze Laboratories Washington 25, D. C. ATTN: ORDTL-012	1
Redstone Scientific Information Center U.S. Army Missile Command Redstone Arsenal, Alabama	1
Defense Documentation Center (DDC) Cameron Station Alexandria, Virginia	10
Office of Scientific Intelligence Central Intelligence Agency 2430 E Street, N. W. Washington 25, D. C.	1
Scientific and Technical Information Facility ATTN: NASA Representative (S-AK/DL) P. O. Box 5700 Bethesda, Maryland	1
Director Langley Research Center National Aeronautics and Space Administration Langley Field, Virginia	1
Chief, Bureau of Naval Weapons Department of the Navy Washington 25, D. C. ATTN: DLI-31	1
Director (Code 2027) U.S. Naval Research Laboratory Washington 25, D. C.	1
Director, USAF Project RAND The Rand Corporation 1700 Main Street Santa Monica, California THRU: AF Liaison Office	1
AFCRL, OAR (CRXRA-Stop 39) L. G. Hanscom Field Bedford, Mass.	10
Aero Research Laboratory (OAR) AROL Library AFL 2292 Building 450 Wright-Patterson Air Force Base, Ohio	1
U.S. Army Aviation Human Research Unit U.S. Continental Army Command P.O. Box 428, Fort Rucker, Alabama ATTN: Maj. Arne H. Eliasson	1
Library Boulder Laboratories National Bureau of Standards Boulder, Colorado	1
Defence Research Member Canadian Joint Staff 2450 Massachusetts Ave., N. W. Washington 8, D. C.	3
Institute of the Aerospace Sciences, Inc. 2 East 64th St. New York 21, New York ATTN: Librarian	1
Massachusetts Institute of Technology Research Laboratory Building 26, Room 327 Cambridge, 39, Massachusetts ATTN: John H. Hewitt	1
Alderman Library University of Virginia Charlotteville, Virginia	1
Hq. ARCRL, OAR (CRTPM) L. G. Hanscom Field Bedford, Massachusetts	1
Hq. AFCRL, OAR (S. Herskovitz) CRDM-1 L. G. Hanscom Field Bedford, Massachusetts	5
Directorate of Development Planning DCS Research & Technology Hq. USAF (AFRDP-2, Michael Lorenzo) Washington, 25, D. C.	1
RADC (RALTP, A. Wiejek) Griffiss Air Force Base, New York	1
RADC (RALSR, Leonard Strauss) Griffiss Air Force Base, New York	1
ASD (ASRMPE, Mr. Richard Rivir) Wright-Patterson Air Force Base, Ohio	1
Advisory Group on Electron Devices (AGED) Office of the Director of Defense R&E 346 Broadway, 8th Floor New York 13, New York	4
Bell Telephone Laboratories, Inc. Whippany Laboratory Whippany, New Jersey ATTN: Technical Information Library	1
Technical Library General Electric TWT Products Section 601 California Ave. Palo Alto, California ATTN: Librarian	1
General Electric Advanced Electronics Center Tompkins County Airport Ithaca, New York ATTN: Mr. F. M. Perry	1
Eitel-McCullough, Inc. 301 Industrial Way San Carlos, California ATTN: Librarian	E 1
Sylvania Electric Products, Inc. Electronic Defense Laboratory 123 N. Whisman Road Mountain View, California ATTN: Library	1
Division of Sperry Rand Corporation Sperry Gyroscope Company Great Neck, Long Island, New York ATTN: Eng. Librarian	1
General Electric Company Power Tube Department Electronic Components Dvision Building 269, Room 205 One River Road Schenectady 5, New York	1
General Telephone & Electronics Laboratories, Inc. Bayside Laboratories Bayside 60, New York ATTN: D. Lazare, Mgr., Proj. Adm.	1
Eitel-McCullough, Inc. 798 San Mateo Ave. San Fruno, California ATTN: Donald H. Preist	1
Varian Associates 611 Hansen Way Palo Alto, California ATTN: Dr. Richard B. Nelson	2
Varian Associates 611 Hansen Way Palo Alto, California ATTN: E. W. Herold Vice President, Research	1
Lockheed Aircraft Corporation Missiles & Space Division Technical Information Center 3251 Hanover Street Palo Alto, California ATTN: W. A. Kozumplik, Mgr.	1
AVCO Manufacturing Company 2385 Revere Beach Parkway Everett 49, Massachusetts ATTN: Dr. A. R. Kantrowitz	1
Philips Laboratories Division of North American Philips Co., Inc. Irvington on Hudson, New York ATTN: William P. Arnett, Security Officer	1
Research Technology Associates, Inc. 100 Ladge Drive Electronic Park at Avon Avon, Massachusetts ATTN: J. Babakian	1
Raytheon Company Norwood Plant 415 Providence Highway Norwood, Massachusetts ATTN: L. C. Edwards	1
ARO, Inc. AEDC Library Arnold Air Force Station, Tennessee	2
Rocketdyne 6633 Canoga Avenue Canoga Park, California ATTN: Dr. R. H. Boden, Dept. 584-370	1
Aero Chem Research Laboratories, Inc. P. O. Box 12 Princeton, New Jersey ATTN: Dr. Calcote	1
Litton Systems, Inc. 336 N. Foothill Road Beverly Hills, California ATTN: Space Sciences Laboratory	1
Hughes Research Laboratories Malibu, California ATTN: Dr. M. R. Currie	1
Westinghouse Electric Corp. Box 284 Elmira, New York ATTN: D.C. Buck, Head Microwave Research & Development	1
Teledyne Systems Corp. 1625 East 126th St. Hawthorne, California ATTN: M.D. Adcock, Director Electromagnetic Systems Division	1
Linde Company 1500 Polco St. Speedway,24, Indiana ATTN: Dr. M. Stern	1
S-F-D Laboratories, Inc. 800 Rahway Avenue Union, New Jersey	1
F. J. Liberatore, Code 7420 U.S. Naval Research Laboratory Washington 25, D. C.	1

ORGANIZATION	NO. COPIES
New York University Institute of Mathematical Sciences 25 Waverly Place, Room 802 New York 3, New York ATTN: Dr. Morris Kline	1
Stanford University Stanford Electronics Laboratories Stanford, California ATTN: Dr. Dean A. Watkins	1
Stanford University Microwave Laboratory W. W. Hansen Laboratories of Physics Stanford, California ATTN: Dr. Marvin Chodorow	1
General Telephone & Electronics Laboratories, Inc. Microwave Physics Laboratory 1015 Corporation Way Palo Alto, California ATTN: Librarian	1

ORGANIZATION	NO. COPIES
California Institute of Technology 1201 E. California, Street Pasadena, California ATTN: Dr. S. S. Penner	1
Polytechnic Institute of Brooklyn Microwave Research Institute 55 Johnson Street Brooklyn, New York ATTN: Dr. N. Marcuvitz	1
The Ohio State University Department of Physics 174 W. 18th Avenue Columbus 10, Ohio ATTN: Prof. M. L. Pool	1
Cornell University Ithaca, New York ATTN: W. R. Sears	1

ORGANIZATION	NO. COPIES
University of Maryland College Park, Maryland ATTN: Dr. J. M. Burgers	1
Electrical Engineering Research Laboratory University of Illinois Urbana, Illinois ATTN: Dr. A. A. Dougal	1
Stevens Institute of Technology Hoboken, New Jersey ATTN: Dr. Bostick	1
University of Mississippi University, Mississippi ATTN: Mr. Thomas Tullos	1
Institute of Science and Technology The University of Michigan Post Office Box 618 Ann Arbor, Michigan ATTN: BAMIRAC Library	1

LIST OF SCIENTIFIC REPORTS PUBLISHED UNDER CONTRACT AF 19(628)-324

SR–No. 1: D. H. Sloan, C. Süsskind, and Staff, "Production and control of electron beams," Series No. 60, Issue No. 203, 15 June 1958.

SR–No. 2: V. Bevc, "Injection of space-charge-balanced electron beams for microwave tubes," Series No. 60, Issue No. 204, 15 June 1958.

SR–No. 3: A. J. Lichtenberg, D. H. Sloan, C. Süsskind, J. R. Woodyard, and Staff, "Electron and plasma beam dynamics," Series No. 60, Issue No. 238, 15 June 1959.

SR–No. 4: E. D. Hoag, "Glow cathodes in pulsed magnetic fields," Series No. 60, Issue No. 239, 15 June 1959.

SR–No. 5: J. N. Dukes, "A gaseous-conduction linear amplifier with magnetic focusing," Series No. 60, Issue No. 240, 30 June 1959.

SR–No. 6: B. N. Edwards, "A study of the Hall effect in gaseous conductors," Series No. 60, Issue No. 253, 30 September 1959.

SR–No. 7: J. W. Hansen, "Scheme for improving beam-tube performance by depressing collector potential," Series No. 60, Issue No. 260, 15 December 1959.

SR–No. 8: D. H. Sloan, C. Süsskind, A. W. Trivelpiece, J. R. Woodyard, and Staff, "Electron and plasma beams," Series No. 60, Issue No. 284, 15 June 1960.

SR–No. 9: R. E. Lundgren, "Extraction and modulation of electron beam from Philips ion gage," Series No. 60, Issue No. 306, 31 August 1960.

SR–No. 10: C. W. Hartman, "Production and interactions of electron beams in crossed fields," Series No. 60, Issue No. 325, 31 October 1960.

SR–No. 11: D. R. Noel, "Special deflection systems for cathode-ray tubes," Series No. 60, Issue No. 329, 2 December 1960.

SR–No. 12: B. E Dobratz, "A study of circuit-independent oscillations in a gaseous conductor," Series No. 60, Issue No. 344, 15 February 1961.

SR–No. 13: J. F. Fry, "The effects of rf energy on the pumping speed of a titanium sputter pump," Series No. 60, Issue No. 355, 18 April 1961.

SR–No. 14: B. Maxum and A. W. Trivelpiece, "Cyclotron-wave nonconvective instability," Series No. 60, Issue No. 379, 1 July 1961.

SR–No. 15: G. August, "Coulomb collisions in strong rf electric fields," Series No. 60, Issue No. 397, 24 August 1961.

SR–No. 16: G. August, "Plasma confinement of electromagnetic waves," Series No. 60, Issue No. 398, 24 August 1961.

SR–No. 17: Y. Ikeda, "Behavior of the space charge in a plasma magnetron," Series No. 60, Issue No. 433, 15 June 1962.

SR–No. 18: M. Chamran, "Electron beam in the cold-cathode magnetron," Series No. 60, Issue No. 453, 15 June 1962.

SR–No. 19: B. E. Dobratz, "Positive-column striations in gaseous conductors," Series No. 60, Issue No. 454, 19 June 1962.

SR–No. 20: Y. Ikeda, "Anode structures for cold-cathode high-power magnetron," Series No. 60, Issue No. 455, 30 June 1962.

SR–No. 21: L. Spinazze, "Dc electroluminescence in manganese-activated aluminum-oxide films," Series No. 60, Issue No. 482, 11 September 1962.